TRANSLATIONAL STUDIES INTO THE EFFECTS OF EXERCISE ON ESTIMATED BONE STRENGTH

Alyssa M. Weatherholt

Submitted to the faculty of the University Graduate School
in partial fulfillment of the requirements
for the degree
Doctor of Philosophy
in the School of Health and Rehabilitation Science,
Indiana University

September 2015

Accepted by the Graduate Faculty, Indiana University, in partial
fulfillment of the requirements for the degree of Doctor of Philosophy.

_____

Stuart J. Warden, Ph.D., PT, Chair

Doctoral Committee

_____

Alan E. Mikesky, Ph.D.

_____

Robyn K. Fuchs, Ph.D.

August 5, 2015

_____

Kara A. Egan, Ph.D.

ACKNOWLEDGEMENTS

Alyssa M. Weatherholt

TRANSLATIONAL STUDIES INTO THE EFFECTS OF EXERCISE ON
ESTIMATED BONE STRENGTH

Mechanical loading associated with exercise is known to benefit bone health; however, most studies explore exercise benefits on bone mass independent of bone structure and strength. The purpose of this dissertation is to explore the response of the skeleton to exercise across the translational divide between animal- and human-based studies, with a particular emphasis on exercise-induced changes in bone structure and estimated strength.

To explore the skeletal benefits of exercise, models were used wherein loading is introduced unilaterally to one extremity. Unilateral exercise enables the contralateral, non-exercised extremity to be used as an internal control site for the influences of systemic factors, such as genetics and circulating hormones.

In study 1, a dose response between load magnitude and tibial midshaft cortical bone adaptation was observed in mice that had their right tibia loaded in axial compression at one of three load magnitudes for 3 d/wk over 4 weeks. In study 2, the ability of peripheral quantitative computed tomography to provide very good prediction of midshaft humerus mechanical properties with good short-term precision in human subjects was demonstrated. In study 3, collegiate-level jumping (long and/or high jump) athletes were shown to have larger side-to-side differences in tibial midshaft structure and estimated strength between their jump and lead legs than observed in non-jumping athletes. In study 4, prepubertal baseball players followed for 12 months were shown to gain more bone mass, structure and estimated strength in their throwing arm relative to

their nonthrowing arm over the course of 12 months.

These cumulative data using a combination of experimental models ranging from animal to cross-sectional and longitudinal human models demonstrate the ability of the skeleton to adapt its structure and estimated strength to the mechanical loading associated with exercise. Study of these models in future work may aid in optimizing skeletal responses to exercise.

Stuart J. Warden, Ph.D., PT, Chair

TABLE OF CONTENTS

CHAPTER TWO: THE EFFECTS OF TIBIAL AXIAL

COMPRESSION LOADING MODEL ON TRABECULAR

AND CORTICAL BONE IN MICE

CHAPTER THREE: PREDICTIVE ABILITY AND SHORT-

TERM PRECISION OF pQCT ESTIMATES OF MIDSHAFT

HUMERUS MECHANICAL PROPERTIES

CHAPTER FOUR: THE EFFECTS OF UNILATERAL

JUMPING ON TIBIAL BONE MASS, SIZE AND

ESTIMATED STRENGTH

CHAPTER FIVE: THE EFFECTS OF ONE YEAR OF

BASEBALL ON HUMERAL BONE MASS, SIZE AND

ESTIMATED STRENGTH

CHAPTER SIX: SUMMARY AND FUTURE DIRECTIONS

APPENDIX

CURRICULUM VITAE

LIST OF TABLES

LIST OF FIGURES

LIST OF ABBREVIATIONS

μCT	Microcomputerized tomography
2D	Two-dimensions
aBMD	Areal bone mineral density
ANOVAS	Two-way factorial analysis of variance
BFR/BS	Bone formation rate
BMI	Body mass index
BSU	Bone structural units
BV/TV	Bone volume/total volume
$Ca_{10}PO_4OH_2$	Calcium hydroxyapatite
CNS	Central Nervous System
CSA	Cross-sectional area
CSMI	Polar cross-sectional moment of inertia
Ct.Ar	Cortical area
Ct.vBMD	Cortical volumetric bone mineral density
dL.Ar	Double label area
dl.Pm	Double label perimeter
DXA	Dual-energy x-ray absorptiometry
Ec.Pm	Endocortical perimeter
HR-MRI	High-resolution MRI
HR-pQCT	High resolution pQCT
HSA	Hip structural analysis
HSC	Hematopoietic stem cells

HU	Hounsfield units
ICC	Interclass correlation coefficients
I_{MAX}	Maximum second moments of area
I_{MIN}	Minimum second moments of area
I_P	Polar moment of inertia
Ir.L.Wi	Interlabel width
ISCD	International society of clinical densitometry
LSC	Least significant change
MAR	Mineral apposition rate
Me.Ar	Medullary area
MSC	Mesenchymal stem cells
pQCT	Peripheral quantitative computerized tomography
Ps.Pm	Periosteal perimeter
PTH	Parathyroid hormone
RMS-CV	Root mean squared-coefficient of variation
RMS-SD	Root mean squared standard deviation
SERM	Selective estrogen receptor modulators
sL.Pm	Single label perimeter
SSI_P	Polar stress and strength index
Tb.N	Trabecular number
Tb.Sp	Trabecular separation
Tb.Th	Trabecular thickness
Tt.Ar	Total bone area

Tt.BMC   Total bone mineral content

CHAPTER ONE: INTRODUCTION

1.1   Introduction

The musculoskeletal system consists of connective tissues: muscles, cartilage, tendons, ligaments and bones. Bone is a specialized connective tissue consisting of cells, fibers and ground substance. Unlike other connective tissues, its extracellular components are mineralized giving it substantial strength and rigidity. There are many functions in the body in which the bone participates, such as storing minerals, providing internal support, protecting vital organs, enabling movement and providing attachment sites for muscles and tendons. Bone is unique because its collagen framework absorbs energy, while the mineral encased within the matrix allows bone to resist deformation. Bone is a dynamic tissue that can undergo growth and remodeling in response to stimuli such as mechanical loading. Mechanical loading (exercise) is a common non-pharmacological way to maximize bone mass, structure and strength with the goal of preventing age-related bone loss and osteoporosis. Although there is vast knowledge gained from animal and clinical studies on exercise essential for preventing bone loss, there is still a void in the research. Most studies pertain to the benefits of exercise on bone mass independent of bone structure and strength. Since less is known on the bone structure and strength adaptations from exercise, there is a need for more research on this topic.

1.2   Bone anatomy

The human body comprises 206 major bones and includes an assortment of six different categories according to their individual shapes: long (i.e. humerus, femur and tibia), short (i.e. carpals), flat (i.e. scapula), sutural, irregular and sesamoid (i.e. pisiform) bones. The anatomy or morphology of these bones can be viewed hierarchically starting at the gross, macroscopic level and progressing microscopically down to the nanoscale level. Macroscopically, bones can be divided into two distinct types of bone tissue— cortical and trabecular (Figure 1.1 and 1.2A). These two tissue types have the same matrix composition; however, they differ substantially in terms of their structure and function, and relative distribution both between and within bones.
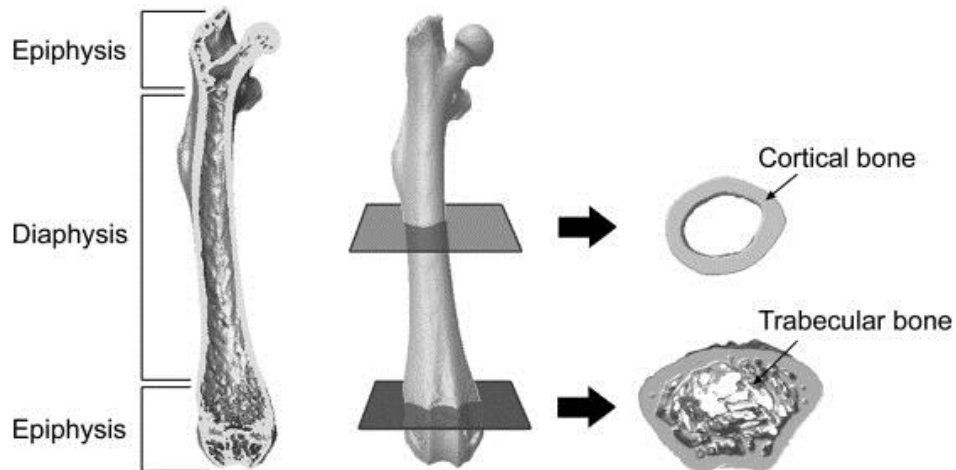
Figure 1.1. Macroscopic anatomy of long bone (Reproduced from Weatherholt et al. [1] with permission from Elsevier).
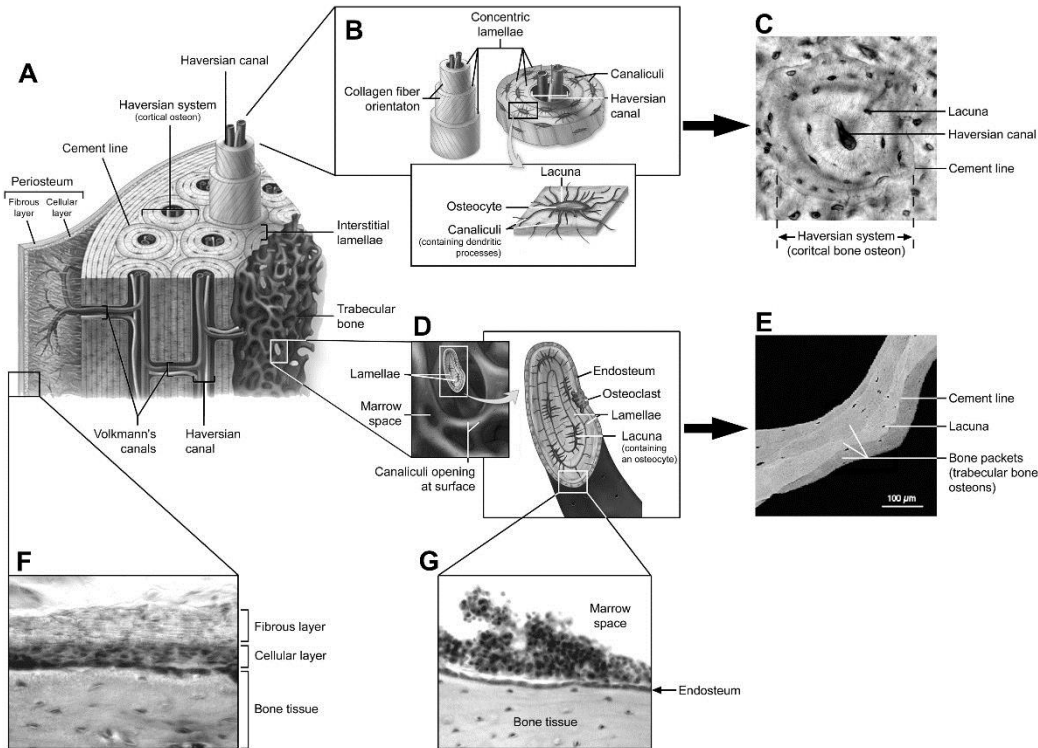
Figure 1.2. Microscopic anatomy of bone A.) Diagram of bone microstructure B.) Cortical bone osteon C.) Cross-section of cortical bone osteon D.) Trabeculae cross-section E.) Trabecular bone osteons viewed by backscattered electron imaging F.) Light microscope image of periosteum covering G.) Light microscope image of a trabecular bone endosteum lining (Reproduced parts A, B, D from O'Loughlin VD and McKinley[2]. Part E reproduced with permission of Elsevier Inc. from Roschger P, et al.[3]).

<u>1.2.1   Macroscopic bone structure</u>

a) Cortical bone

Cortical (or compact) bone makes up approximately 80% of skeletal tissue mass. It has a high matrix mass per unit volume and low porosity (microscopic pores constitute approximately 10% of total cortical bone volume). These features endow cortical bone with great compressive strength enabling it to prominently contribute to the mechanical role of bone. This is reflected in its distribution primarily within the cylindrical shaft (diaphysis) of long bones where it forms a thick shell (cortex) surrounding a medullary

canal (Figure 1.1). The tube-like design distributes bone mineral away from bending axes resulting in a substantial increase in bending resistance without a concomitant increase in bone mass. The net result is long bones with the strength and rigidity required for muscle action and weight bearing, yet lightness required for energy efficient motion. Cortical bone thins towards the expanded ends (epiphyses) and interposed developing region (metaphysis) of long bones where it plays a lesser, yet clinically significant mechanical role[4].

b) Trabecular bone

Trabecular bone has high porosity relative to cortical bone, with pores making up 50-90% of trabecular bone volume. The pores are interspersed among an orderly network of vertical and horizontal structural elements called trabeculae, which give trabecular bone a sponge-like appearance (Figure 1.1). The reduced matrix mass per unit volume and high porosity of trabecular bone reduces its compressive strength to approximately one-tenth that of cortical bone[5]; however, trabecular bone contributes to the mechanical role of bone by providing internal support. This supportive role facilitates the ability of bone to evenly distribute load and absorb energy, particularly in the vicinity of joints. It is also important during aging as trabecular bone is lost earlier and at a greater rate than cortical bone, which ultimately contributes to osteoporosis at trabecular rich sites[6].

c) Bone coverings

Bone surfaces are covered by specialized connective tissues. The periosteum covers external surfaces of most bones and is divided into two distinct layers—an outer

fibrous and inner cellular layer (Figure 1.2F). The cellular or 'cambium' layer is

positioned in direct contact with the periosteal surface and is of particular interest as it

contains mesenchymal stem cells (MSCs) which have the potential to differentiate into

osteoblasts and chondrocytes, and differentiated osteogenic progenitor cells. The

localization of these cell types has made the cellular layer a target for drug therapies and

cell harvesting for tissue engineering purposes.

The endocortical surface of a bone faces the medullary canal and is lined by the

endosteum, a single thin layer of bone lining cells (mature osteoblasts) and osteoblasts

which form a membrane over endocortical and trabecular bone surfaces to enclose the

bone marrow (Figure 1.2G). The endosteum contains osteoprogenitor cells, but does not

appear to contain either MSCs or hematopoietic stem cells (HSCs). However, a portion of

HSCs can be found next to the endosteum suggesting reciprocal communication between

cells within the endosteum and multipotent HSCs[7]. The close relationship between the

cells forms a so called 'stem cell niche' whereby the cells of the endosteum physically

support and influence stem cell activity[8].

1.2.2   Microscopic bone structure

Microscopic visualization of both cortical and trabecular bone reveals tissue that

is either woven or lamellar in structure. Woven bone has a disorganized collagen fibril

arrangement and is not typical in the adult skeleton, except in pathological conditions

(such as Paget's disease and osteosarcoma) or following injury (such as fracture). The

disorganization of woven bone results from the speed at which it forms, which precludes

the orderly deposition of collagen fibrils. The net result is bone tissue that possesses

enhanced flexibility at the cost of stiffness[9]. This is valuable following injury as rapid,

early formation of woven bone enhances early restoration of skeletal mechanical integrity

prior to its replacement by lamellar bone[10]. Lamellar bone is characterized by the

organized arrangement of collagen fibers into layers or lamellae. This arrangement gives

lamellar bone greater stiffness compared to the disorganized structure of woven bone.

Lamellae in cortical bone form osteons or bone structural units (BSUs) which consist of a

central canal enveloped in concentric lamellae of bone tissue. Outer lamellae form first

along the boundary of the osteon known as the cement line, with each successive lamella

being laid concentrically inside the preceding one (Figure 1.2 A-C). In trabecular bone,

lamellae are stacked into saucer-shaped bone packets that are separated by cement lines.

The first lamellae are formed towards the center of the trabeculae with each successive

lamella being stacked in parallel layers towards the bone surface (Figure 1.2 D and E).

Uniformly spaced throughout lamellae are cavities called lacunae from which branching

canaliculi radiate in all directions. The canaliculi penetrate the lamellae of the interstitial

substance to anastomose with canaliculi of neighboring lacunae to form a continuous

network of interconnecting cavities.

a) Bone matrix

Bone matrix is a composite consisting of organic and inorganic components. The

organic matrix makes up ~20% of bone wet weight and is comprised primarily of type I

collagen which gives bone its flexibility[11]. The inorganic matrix contributes

approximately ~65-70% of bone wet weight and serves as an ion reservoir. The ions form

crystalline structures predominantly in the form of calcium hydroxyapatite [$Ca_{10}PO_4OH_2$] that surround and impregnate collagen fibers to give bone the majority of its stiffness[12][13]. Without the addition of mineral to collagen, bone tissue would have properties similar to a rubber band, while without collagen, bone is brittle like chalk. Thus, varying the amounts and distribution of collagen and mineral provides bone with its ability to balance its flexibility and stiffness requirements. Alterations in the structure of collagen and/or its mineralization that occur from aging or genetic abnormalities such as osteogenesis imperfecta can compromise the structural integrity of bone tissue resulting in a weaker structure and a greater than normal susceptibility to fracture.

b) Cellular elements

Bone cells are derived either from HSCs or MSCs. HSCs and MSCs give rise to the principal cells that mediate bone resorption (osteoclasts) and formation (including osteoprogenitor cells, osteoblasts, osteocytes and bone lining cells), respectively.

<u>Osteoblasts-</u> Osteoblasts are bone forming cells and develop locally following proliferation of MSCs residing in the bone marrow stroma and periosteum. Mature osteoblasts express the matrix proteins type I collagen and osteocalcin, and alkaline phosphatase—a key enzyme in the mineralization process. Rows of active osteoblasts secrete unmineralized matrix (osteoid) before becoming either bone lining cells or incorporated into the bone matrix. Cells that become incorporated into the matrix gradually develop long cytoplasmic processes to remain in communication with surrounding cells and are considered immature osteocytes. As the matrix matures and

mineralizes, and the osteoid seam moves further away, the osteocyte becomes entombed in a bony matrix.

Osteoclasts- Osteoclasts are large, multinucleate cells that exclusively mediate the process of bone resorption. Osteoclastogenesis begins when a HSC is stimulated to generate mononuclear cells, which then become committed preosteoclasts and are introduced into the blood stream. The circulating precursors exit the peripheral circulation at or near the site to be resorbed, and fuse with one another to form a multinucleated immature osteoclast. Mature osteoclasts establish a microenvironment between themselves and the underlying bone by peripherally attaching to the matrix using integrins[14]. The attachment creates a compartment between the ruffled basal border of the osteoclast and the bone surface that is isolated from the general extracellular space[15]. An electrogenic proton pump transports in H^+ ions to acidify the compartment which acts to mobilize the mineralized component of bone. This exposes the organic matrix which is subsequently degraded using proteases. The end result is the removal of bone matrix and the development of characteristic shallow cavities known as Howship's lacunae.

Osteocytes- Osteocytes are the most numerous bone cells and are dispersed throughout the matrix where they occupy lacunae (Figure 1.2B and C). Lacunae are interconnected by an elaborate network of thin tunnels called canaliculi through which osteocytes pass cytoplasmic or dendritic processes[16]. These processes connect individual osteocytes with neighboring cells via gap junctions to facilitate both the transport of nutrients for osteocyte viability and the conveying of intercellular messages. Intercellular communication is also facilitated by the osteocytic release of signaling molecules into the extracellular fluid which flows through the lacuna-canalicular system[17 18]. Osteocyte

function remains unclear; however, their principal role appears to be the sensing of mechanical stimuli[19 20]. In addition, recent evidence has also found osteocytes have the capacity to regulate mineral metabolism and alter their surrounding matrix[20-22].

1.3 Bone physiology

Bone is a dynamic tissue capable of altering its structure and mass in order to adapt to changing requirements. The adaptation is achieved by different fundamental tissue-level activities, including growth, modeling, remodeling and healing.

1.3.1   Bone growth

Bones predominantly develop by endochondral ossification wherein condensations of mesenchymal cells differentiate into chondrocytes to form a cartilaginous template (or 'anlage'). Exceptions are parts of the clavicles and scapulae which form via intramembranous ossification which does not involve a cartilaginous precursor. In the anlage, chondrocytes hypertrophy and an ossification center forms by neovascularization of the initially avascular cartilaginous template. Osteoblasts associated with the newly developed vasculature begin secretion and mineralization of a type-I collagen-containing extracellular matrix. As development continues, the ossification center propagates towards the epiphyseal growth plates.

Epiphyseal growth plates are responsible for longitudinal bone growth. Toward the end of a developing bone, a resting pool of chondrocytes supplies cells to a

population of proliferating chondrocytes which in turn differentiate to form a pool of hypertrophic chondrocytes. Ultimately, the hypertrophic chondrocytes die by apoptosis and are replaced by trabecular bone. As long as the rate of chondrocyte proliferation within the growth plate stays ahead of the rate of hypertrophy, the growth plate remains 'open' and longitudinal bone growth continues. During this period, the growth plate is a site of relative weakness and susceptible to injury. This is no longer the case towards skeletal maturity when the final chondrocytes in the growth plate hypertrophy and become apoptotic resulting in cessation of longitudinal bone growth and growth plate closure.

1.3.2   Bone modeling

Modeling functions to move bone tissue through space altering bone cross-sectional size and shape, as opposed to bone length. It primarily occurs during growth, but continues to some degree throughout life as evidenced by lifelong periosteal expansion[23]. Modeling is accomplished by 'modeling drifts' whereby bone tissue is selectively added or removed from an existing surface[24]. The addition or removal of bone is achieved by the temporally and spatially independent actions of bone forming osteoblasts and bone resorbing osteoclasts, respectively. As formation and resorption during modeling do not occur at the same location, the two processes are said to be 'uncoupled.'

Modeling is influenced by stimuli including mechanical loading, administration of parathyroid hormone (PTH) and the withdrawal of estrogen, and is an important tissue-

level activity as it can alter bone strength without overtly increasing the overall mass of the skeleton. It does this by strategically placing bone tissue where needed most. For instance, periosteal apposition results in a bone with a larger diameter, which is useful as the ability of a bone to resist bending and torsional forces is related to the fourth power of its diameter. By adding material to the outer surface of a bone, there is a disproportionate increase in its ability to resist mechanical forces for the gain in mass.

1.3.3 Bone remodeling

Remodeling represents bone reconstruction wherein discrete, measureable 'packets' of bone are removed and replaced by new bone. It occurs continuously throughout life in response to stimuli including mechanical forces, microscopic bone damage (microdamage) and systemic hormones[25], and involves the temporally and spatially coordinated actions of osteoclasts and osteoblasts. These cells form teams collectively known as basic multicellular units (BMUs) (Figure 1.3). As osteoblasts always trail behind osteoclasts in BMUs and the entire structure moves as a unit, the resorption and formation processes are said to be coupled to one another. Coupling in remodeling is a strictly controlled process which ensures that where bone is removed new bone is deposited[26]. The process of this cycle includes four phases: 1) activation, 2) resorption, 3) reversal and 4) formation. Activation starts when a stimuli signals the process to begin. Once the activation begins it takes about 5 to 10 days to recruit precursor cells, differentiate and proliferate bone cells and then move them to the remodeling site. The subsequent phase is called resorption where osteoclasts take about 3

11

weeks to longitudinally resorb old bone. Following the resorption phase, is the reversal phase where osteoblasts cells appear on the resorbed surface. The final phase of the bone remodeling cycle is the formation phase where osteoblasts lay down new unmineralized (osteoid) bone to replace the resorbed bone followed by bone mineralization (this takes about 3 months). All together the remodeling cycle roughly takes about 5 months. The net amount of old bone removed and new bone restored in the remodeling cycle is a quantity called the bone balance[25].

Although coupling is rarely affected, bone balance varies in disease states. For instance, in osteoporosis, prolonged best rest, or hemi-, para- or quadriplegia, resorption and formation are coupled but there is a negative bone balance such that more bone is resorbed than is replaced by the typical BMU. The result is a net loss of bone mineral which can be assessed clinically by performing non-invasive bone mass assessments. Logically, many pharmaceutical agents for the treatment of conditions wherein there is a net bone loss attempt to create a positive bone balance whereby bone formation exceeds resorption in a typical BMU. The result is a net gain of bone mineral, which can be achieved either by inhibiting bone resorption (such as occurs with the administration of bisphosphonates therapies) or by stimulating osteoblasts to produce greater quantities of bone (such as occurs with the administration of PTH)[27].
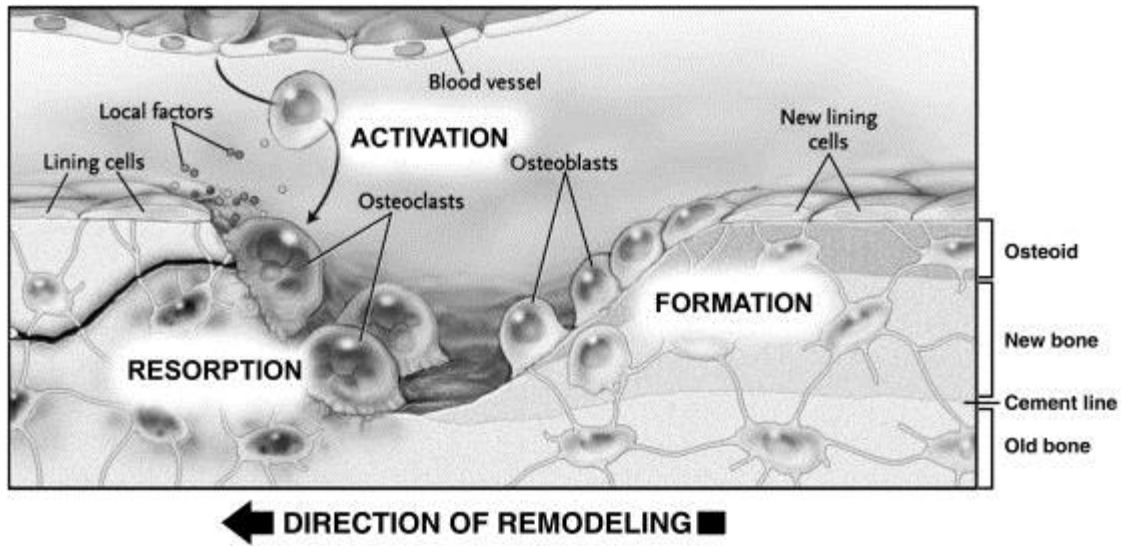
Figure 1.3. Bone remodeling by BMU (Reproduced with permission from Canalis E, et al.[28], Copyright Massachusetts Medical Society).

1.3.4   Bone healing

Bone is a frequent site for injury with the most common injury being a fracture. Bone heals in response to injury by regeneration, as opposed to repair. This is an important distinction as regeneration restores the native tissue and mechanical properties at the injured site enabling bone to meet its continuing mechanical demands.

The two major types of bone healing are primary and secondary. Primary or direct healing occurs when the fracture ends are rigidly fixed via early surgical intervention such that there is very little motion between the bone fragments. In this scenario, the need for an early stabilizing external cartilage callus is bypassed with healing occurring by direct synthesis of lamellar bone parallel to the bone's long axis[29]. In contrast, when macro- and micro-motion is permitted between the bone fragments, secondary or indirect

healing occurs which involves varying amounts of intramembranous and endochondral bone formation.

Secondary healing of bone fractures is more frequent and follows three overlapping phases: 1) inflammation, 2) reparation and 3) remodeling. Inflammation begins at the time of injury and initiates the complex cascade of events resulting in appropriate cellular recruitment, timed genetic expression, and the sequenced synthesis of numerous compounds. The subsequent reparative phase combines chondrogenesis and osteogenesis to initially form a bridge (or primary callus) which spans and surrounds the fracture site. This phase involves intramembranous woven bone being laid down underneath the periosteum slightly distant from the fracture gap, and the formation of a large cartilaginous mass both outside (external callus) and within (internal callus) the cortices. The cartilaginous callus serves to stabilize the fracture site which favors subsequent bone formation. The completion of this process results in clinical union. Following union, osteogenesis predominates with the cartilage formed during primary callus formation being replaced with new bone in a process of endochondral ossification that recapitulates bone development. The result is the formation of the secondary or definitive callus and consolidation of the fracture clinically. The final stage of the repair process involves transforming the woven bone to lamellar bone, resorbing the no longer required external callus, and remodeling the bone to form native tissue complete with osteons[29].

1.4   Bone biomechanics

Bone's major function in the body is to provide mechanical support. In order for

bone to provide mechanical support, mechanical integrity of the skeleton needs to be

achieved and maintained. The mechanical properties of bone are influenced by the

quantity, distribution and quality of the material. Since bone is a dynamic tissue, these

properties can change due to different stimuli. Principles of bone biomechanics can give

an understanding of the mechanical properties of bone and how different stimuli can

change those properties.

1.4.1   Load types

When an external or internal force is applied to a bone it is called a mechanical

load. There are several types of mechanical loads that the skeleton receives in a variety of

directions. In addition, loads can be applied in the laboratory setting to determine a

bone's mechanical properties. The loads that are placed on the skeleton are from forces

produced by body weight, gravity, muscle and other outside forces[30]. The loads that bone

receives due to those forces are tension, compression, shear, torsion and bending[30]. When

the forces cause bone to be loaded under tension, the two ends are pulled and results in

lengthening (Figure 1.4B). Opposite of tension, if the forces push the bone together and

cause it to shorten, the bone would be under compressive load (Figure 1.4A). If instead of

compressive loads, bone is loaded under shear, the forces are applied perpendicular to the

long axis causing parallel sliding of each layer over the other (Figure 1.4A). If instead of

shear loads, bone is under torsion, the ends of the bone are twisted (Figure 1.4A). Finally, when the bone is under bending loads it produces tensile loads on the outside and compressive loads on the inside of bone (Figure 1.4A)[30]. In general, bones are subjected to mainly compressive, tensile and torsional loads from everyday activity[31-33].

1.4.2   Load-displacement curve

Bone's behavior under the above different loading conditions can determine its mechanical properties. When bone is under one of those loading conditions, there is an internal reaction. The relationship between the imposed external load and the internal reaction can be examined by a load-displacement curve to find out its mechanical properties: strength, stiffness, deformation and energy dissipation (Figure 1.4A).

When analyzing the curve there are several extrinsic mechanical features about bone that can be learned. The first part of the curve is linear, which is defined as the elastic region. Inside the elastic region, the bone can be loaded and unloaded with zero energy lost and no permanent deformation or damage. The slope in the elastic region measures the stiffness or rigidity of bone. Stiffness means deformation is resisted under a certain load. In general, if two bones had their mechanical properties measured, the bigger one would be typically stiffer[30]. Past the elastic part of the curve starts the plastic region, if bone loading continues, the bone begins to yield and the curve starts to become nonlinear. At the point where the curve becomes nonlinear, the bone deforms permanently and sustains damage. The ultimate load is the defined load to where its internal structure starts to fail and the load level drops off with further loading ultimately

16

leading to catastrophic failure. The ultimate load and failure load usually occur closer

together. Overall, the load-displacement curve calculates some of the whole bone

mechanical properties.
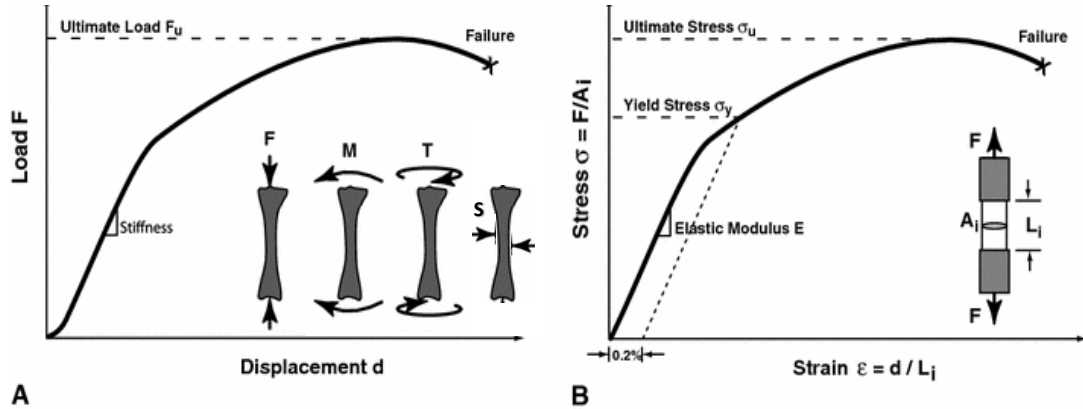
Figure 1.4. Load-displacement and stress-strain curves A.) Load-displacement curve- (F) compressive load, (M) bending load, (T) torsional load and (S) shear load B.) Stress-strain curve- (F) tensile load, (A_i) initial area and (L_i) initial length (Reproduced from Cole et al.[34] with permission by Springer International Publishing AG).

1.4.3   Stress-strain curve

To account for structural differences, the load-displacement curve can be adjusted

by dividing the load by the original cross-sectional area and deformation by the original

length. The resulting stress-strain curve provides information on the mechanical

properties of the bone's material independent of bone geometry/size. Stress (σ) is defined

as bone's internal resistance to an applied force which represents the intensity of force it

is receiving locally with the dimensions of force per unit area. Strain is defined by the

change in the bone length per original bone length. The units for strain in bone are small

so they are usually stated in units of microstrain ($\mu\varepsilon$). A typical strain in human bone is less than 1000 $\mu\varepsilon$ under tension and 2000 $\mu\varepsilon$ under compression[30 35 36].

Just as the load-displacement curve, the stress-strain curve is analyzed and plotted similarly (Figure 1.4B). However, opposed to the load-displacement curve which depends on the whole bone mass and geometry, the stress-strain curve provides information on material properties that are independent of the size and shape of the bone. The mechanical properties that are observed in this curve are strength, stiffness, deformation and toughness. Similar to the load-displacement curves, the stress-strain curve has an elastic region which is the area under curve from the point of yield stress down. This area of the curve measures the reliance of the material or the energy to yield. The linear slope in elastic region of the curve is called Young's modulus of elasticity. The Young's modulus of elasticity represents the internal stiffness of the material. In general, under normal loading conditions, bone can undergo some deformation and still remain in the elastic region[30 36]. In the elastic region, stress is proportional to strain. This is known as Hooke's Law which the equation is: $\sigma = E\varepsilon$. In this equation, E represents Young's modulus. Since strain is dimensionless, E has units of stress (Pa). When the sample of bone is stiffer, the slope is steeper and the modulus is larger. The larger modulus corresponds with larger stress for a given strain level. A typical modulus for a sample of cortical bone is in the range of 10-15 GPa[30 36], which compares to a modulus of 1200 GPa for diamond[36]. The ultimate strength and toughness of the material is represented on the curve at the point of ultimate stress. The total area under the curve from the point ultimate stress is the total absorption energy before material failure. The overall differences between the two curves on bone mechanical properties can be

observed between two types of athletes, one being a Sumo wrestler and the other a female gymnast[30]. First of all, the wrestler will have six times bigger bones than the gymnast which results in greater whole bone rigidity[30]. However, the intrinsic stiffness of their bones will be similar[30].

1.4.4 Mechanical testing

Mechanical testing is a laboratory method available to produce the two curves above in order to determine bone's mechanical properties. There are several different types of mechanical tests that have been performed in research which include: tension, compression, torsion and bending.

The first type of mechanical test is tensile loading, where a sample of bone is clamped at the wider two ends to a loading machine and the bone sample is then pulled at the two ends. During loading, force transducers at midsection of the sample measure the load, displacement, stress and strain. To get a direct measure of strain, a strain gauge can be placed on the sample at the midsection. Limitations to this test exist and include the bone samples needing to be large in order to ensure that the high stresses the sample receive at the grips are not contributing to the mechanical properties at the midsection of the sample[34 37]. Sample size is again another limitation for this test because trabecular bone samples need to be large enough to meet the continuum requirements for loading. The continuum requirements for loading trabecular bone samples are that the minimum dimensions must be five times larger than the subunits. For example, in human trabecular bone, the width of the sample needs to be 100-300 μm and spacing 300-1500 μm[36]. Even

though this mechanical test has limitations there are strengths which include the test being very simple and the most accurate way to get information on the mechanical properties of bone[34 37].

Another type of mechanical test used on bone is compressive loading, where a sample of bone is cut into the shape of a cube or cylinder. Once the bone sample is in the shape of a cube or cylinder, it is then placed between two loading platens and pushed together to shorten the sample. Just as tensile loading, compressive loading tests have transducers that can measure the load, displacement, stress and strain. Limitations to this mechanical test include an overestimation of the average sample strain due to the risk of the sample to come in contact with the platens[30 34 36]. Another limitation is the risk of premature failure and resultant underestimation of the sample's strength due to the sample not being positioned correctly[30 34 36]. Finally, a large error in calculating stress of the sample can happen due to improperly measuring and entering the samples cross-sectional area[30 34 36]. Even though there are limitations to compressive loading tests, there are strengths that include the use of smaller bone samples, with fabrication of those samples being easier, and an accurate test when comparing relative differences within a study[36].

To observe mechanical properties of bone in shear a mechanical loading modality such as torsion is used. When bone is under torsional loads, twisting forces are placed at the ends of the bone sample. The mechanical tests in torsion are performed by the bone ends being embedded in hard plastic and the plastic ends being placed in grips. Once the bone sample is placed in the grips, the machine twists the ends relative to one another. The torque measurement from this test is then converted to get shear stress and strain[38].

The conversions to get shear stress and strain have limitations because torsion also creates tension within the bone; therefore, it is not possible to measure and observe pure shear properties[30]. Another limitation to this test is the need for assumptions regarding whole bone geometry because bone diaphysis cross-section is simplified to a circle[39][40]. Since bone's actual shape is more complex and different along the length of the diaphysis, there can be a lot of assumptions when comparing bones that have different shapes and sizes[39][40]. This limitation was observed in a study by Levenston et al.[40] where there was 42% error in shear modulus and up to 48% error in maximum shear stress.

The last mechanical test and the most common method used to determine mechanical properties of whole bone and samples of bone are bending tests. Bending tests create compressive and tensile forces on bone. There are two types of bending tests which are the three point bending and the four point bending tests. The three point bending test is the most widely used[39]. During a three point bending test, the ends of the sample are placed on two supports and a load in the opposite direction with a single contact is placed at the mid-point of the sample. In contrast, in four point bending the sample is placed on two supports and compressive force is applied by a two-armed device. The area of interest in this test is between the two-armed devices. In order to receive accurate data, the two forces that are placed on the bone sample need to be done at the same time[39]. Force and displacement data can be recorded in both types of bending tests, and can be converted to stress and strain[39]. The three point bending test is typically used in rodent studies where their long bones are assessed to discriminate among the species and to observe any treatment effects on mechanical properties[37]. Another use for three point bending test was investigated by Jamsa et al.[41] which found differences in

mechanical properties between two body sites within the same mouse. Limitations to these tests exists. In order to ensure that the data is accurate, there are some precautions that need to be taken which include: the sample supports need to be smooth and rounded so there is minimal stress collected at the contact of the supports and the bone ends and the two arms in the four point bending test need to make contact at the same time. Another limitation to these tests are that if the ratio of bone length to thickness is not 20 the test can generate not only bending deformation, but shear deformation as well, which can lower the value of Young's modulus[39]. Regardless of these limitations, the strengths include no specimen preparation and the results are quite accurate when obtaining relative values within a study[39].

1.5   Determinants of bone strength

Unlike the individual loading states mentioned above, normal activities of daily living create complex loading conditions that are the combination of those modes. If the combined loading conditions exceed the overall strength of the bone, then it will fail with the result being a fracture. The overall strength of a bone is a function of three contributors which includes: bone mass, geometry (size and structure) and material properties (Figure 1.5). Therefore, to improve bone strength there are several ways which include increasing the bone's total mass, distributing the bone mass to where high loads are produced or enhancing the bone's material properties. The distinction between manmade structures and the skeleton are the metabolic activity levels of the bone cells which allows the skeleton to be dynamic by adapting and repairing bone properties

throughout life stages and various conditions such as exercise, injury and disease. For

example, in some studies using animal models, a reduction in material properties are

compensated by changing the geometry, resulting in similar material properties which

reduces the risk of fracture[42 43].

1.5.1   Bone mass

Of the three contributors to overall strength of the skeleton, bone mass is the most

studied. When bone mass is reported clinically, it is stated as bone mineral content and

measured by using a variety of imaging techniques[44]. In adults with healthy skeletons,

cortical bone mass directly reflects geometric measures, cross-sectional area. However, it

is different in trabecular bone, since its architecture is more complex and spatially

different, so mass is measured in small homogeneous tissue volumes. Trabecular bone

mass is measured as bone volume fraction which is the volume of bone present in the

total volume of interest (BV/TV) or apparent density which is the mass present in the

total volume of interest. Since trabecular bone has spatial variations in bone mass, there

can be as much as 100-fold differences in stiffness values within a single bone[45]. For

example in a tibial metaphysis, the range of stiffness values can be from 4 to 453 MPa[45].

However, assessment of bone mass only shows the total tissue quantity without reflecting

where the tissue is localized, which has an impact on fracture resistance.

Whole bone Strength

Total Bone Mass (BMC, BV/TV)

100%

0%

Geometric Distribution (geometry, architecture)

Material Properties (tissue composition)
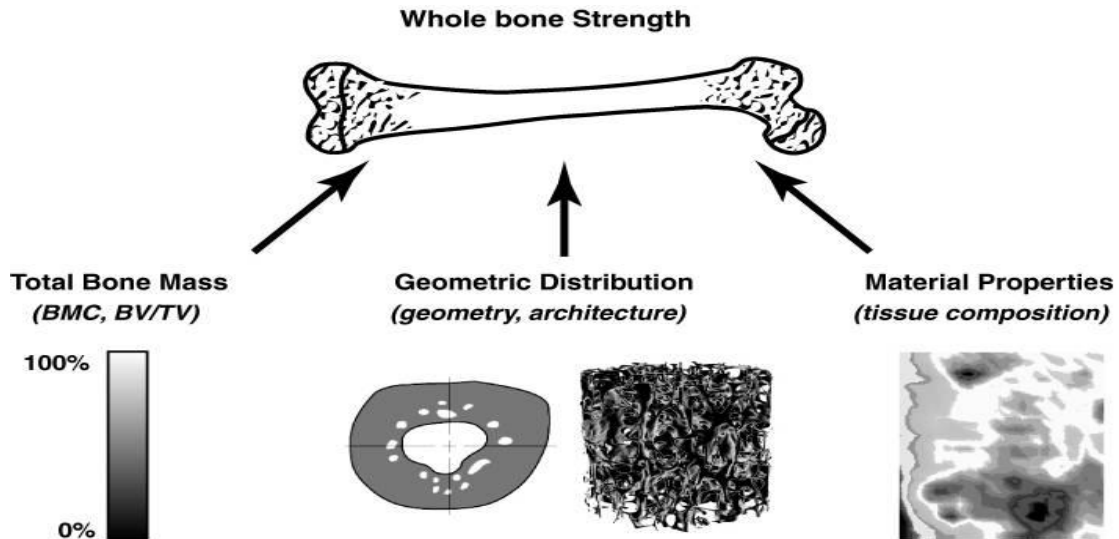
Figure 1.5. Determinants of bone strength (Reproduced from Cole et al.[34] with permission by Springer International Publishing AG).

1.5.2   Geometric properties

Fracture resistance in cortical bone is influenced by the area and distribution of bone under all the loading modes. If bone material properties were held constant, geometric measures that include cross-sectional area, moments of inertia, and the section modulus can quantify where the material is distributed as well as determine how the tissue responds to a given load. These measures are dependent on a particular loading type[46]. For example, when bone is under torsion or bending, there is more resistance to that applied load at the tissue located further from the bending plane or axis of torsion[34]. Bone strength will be different depending where the mass is distributed. For example in a solid cylinder, the resistance to a bending load is at the surface and not at the central core. So if the central core in this solid cylinder was removed, it would only have a 6% reduction in bending strength, even though 25% of the total bone mass was removed[46]. Similarly, a hollow and solid cylinder with the same bone mass will have different

24

bending strengths. The hollow cylinder will have 70% greater bending strength compared to the solid cylinder even though the hollow cylinder has 25% more diameter[46].

Fracture resistance in trabecular bone is influenced by the size and spatial distribution of the trabeculae. Similar to bone mass, the small homogenous samples are examined. In trabecular bone, there is up to 50% of differences in strength and stiffness with bones that have about the same bone mineral density (BMD) but different architecture[47 48]. Additionally, when bone is loaded at different locations, the architecture of trabecular bone will exhibit a preferred orientation for each location, resulting in varying strength values at different sites[49]. An example of this would be a human vertebrae, where it is twice as strong while loading it up and down compared to the left and right direction due to the trabeculae alignment[47 50].

1.5.3   Material properties

The final contribution to whole bone strength are material properties. As mentioned previously, bone has various levels of hierarchy with contributing structural elements that exist at those different levels. At tissue level, bone consists of cortical and trabecular bone which are lamellar tissue with differing microstructural organizations. At the material level, bone tissue consists of an organic matrix with primarily collagen that is Type I and an inorganic part with crystalline mineral. The characteristics of both combined and their interactions between each other will determine the material properties of bone tissue. The strength of bone tissue is greater when both the organic and inorganic parts are combined than that of each individual part. Additionally, the organic and

inorganic parts contribute to the mechanical behavior of the tissue differently. The inorganic part is related to material stiffness at the tissue and whole bone level by the amount of bone mineral content[51-53]. At the level of micro-and nanoscale, the inorganic part's characteristics such as crystallinity and carbonate substitution will contribute and determine whole bone strength and stiffness[54 55]. The organic part or the collagen contributes to the mechanical behavior of bone by the toughness and post yield deformation of the tissue. The characteristics of collagen that contribute to this behavior are the content, the maturity or crosslinking of collagen[52 56 57]. Micro damage can occur in response to daily activity; this can alter the amount of mineral and collagen structure[58-60]. In addition to collagen and mineral parts of the bone tissue, water inside the vascular-lacunar-canalicular spaces is thought to also impact strength and toughness of the bone, but has not been examined at the whole bone level[61].

1.6 Determinants of compromised bone strength

Since bone mass, material and structural properties determine bone strength, the clinical consequence of negative alterations to these properties can be weak bones and a resultant risk for fracture. The pathophysiology behind compromised bone strength is multi-faceted due to influences internally (i.e. genetics, hormones and immune system) and externally (i.e. mechanical loading, nutrition and medication) to the skeleton. These internal and external influences combine to alter bone mass, material properties and geometric properties which can weaken bone.

Internal factors that can contribute to compromised bone strength are genetic abnormalities that consequently leave bones either too thin or dense. An example of a genetic disease with an outcome of thin bones is osteogenesis imperfecta[62]. Osteogenesis imperfecta has a genetic abnormality in Type I collagen molecule which leads to a weak bone matrix and consequently compromised bone strength[62]. An example of a genetic bone disease with an outcome of dense bones is osteopetrosis. Osteopetrosis results in dense bones due to a dysfunction in remodeling. The remodeling dysfunction is a result of a decrease in bone resorption compared to bone formation which causes an accumulation of bone[63]. A decrease in bone resorption is caused by dysfunctional osteoclasts due to genetic defects. The pathophysiology behind the dysfunction is a decrease in the number of osteoclasts and, the osteoclasts that are available, do not resorb bone due the inability to acidify the ruffled border[63]. Unlike the osteoclasts being dysfunctional, the osteoblasts are working normally to form bone such that factors are being produced to allow bone to form normally. Due to bone formation working normally but not being offset by a normal rate of resorption, bone accumulates which decreases the medullary area.[63] There can be a number of problems that result when there is excessive bone accumulation, which include a reduction in blood cell production in the medullary canal and decrease in cranial nerve and vascular canals size[63]. These problems can lead to bones that have little blood supply which predispose them to fracture[63]. In the end, these genetic abnormalities leads to weak skeletal strength due to bones becoming too thick or thin.

1.6.2 Nutritional deficiencies

An external factor that compromises bone strength is not obtaining enough micronutrients, such as phosphorus, calcium and vitamin D. The lack of intake of phosphorus, calcium and vitamin D can result into a deficiency in the body which targets the inorganic part of the bone matrix. The most common nutritional deficiency in children is vitamin D deficiency which can result in the disease known as rickets. The main source of vitamin D comes from the skin absorbing ultraviolet light in band B (UVB)[64]. Other sources of vitamin D include fortified foods, fish and shell fish. Once inside the body, vitamin D acts as a hormone utilized for absorbing calcium from the intestine to promote healthy bone mineralization[64]. Without significant uptake of vitamin D, there is a decrease absorption of calcium, an increase bone turnover and decrease in mineralization of the bones, which consequently causes the skeleton to be soft and thus weak[64]. The weakened bones in children due to rickets can cause fracture and a deformity called bowing due to the cartilage without mineral overgrowth at the ends of long bones. This condition in adults which is known as osteomalacia has the same clinical outcomes as rickets.

1.6.3 Hormonal defects

Internal factors that can compromise bone strength are hormonal disorders, which can either cause overproduction or underproduction of the hormones that regulate bone growth, modeling and remodeling. The hormones involved in those physiological

processes are: sex steroids, parathyroid hormone, glucocorticoids, thyroid hormone, growth hormone and vitamin D. Hormones act on bone by effecting it either directly or indirectly. Direct actions on bones from hormones occur by binding to receptors on osteoblasts, osteoclasts and osteocytes which stimulates an action from the bone cells. Indirect actions from hormones on bone regulate mineral homeostasis of phosphorus and calcium at the intestines and kidney[27][64].

An example of an overactive hormone that decreases bone strength is hyperparathyroidism which secrets high levels of PTH into the blood with either low or high blood calcium concentrations[27]. Normally, PTH acts to maintain blood serum calcium concentrations in a very well regulated fashion[27]. The consequence of hyperparathyroidism is excessive bone resorption, with increased risk for fracture and deformities[27].

An example of lack of hormone production that decreases bone strength is insulin like growth factor-1 (IGF-1) deficiency which can cause a dysfunction in the bone remodeling and growth processes in children that result in inhibiting linear bone growth leading to short stature[65]. An additional example of lack of hormones or complete loss of hormones is hypogonadism where children or adults lack estrogen or testosterone hormones that regulate bone's remodeling process. Without these hormonal regulators, there is an increase in bone resorption and ultimately low bone mass and risk for fracture.

1.6.4 Medications

An external factor that can compromise bone strength is treatment in the form of medication for other diseases such as asthma, arthritis and epilepsy. The medications for those particular diseases target bone by abnormalities in calcium metabolism, reduction in bone formation, increase bone resorption and increase in osteocyte and osteoblast death which decreases skeletal strength[66][67]. An example of how medication can affect bone strength is the use of glucocorticoids which in excess stunt bone growth in children and cause thinner bones in adults, often leading to fracture[66]. Another example of how medication can affect bone strength, is the use of antiepileptic drugs which particularly causes a dysfunction in calcium metabolism that can lead to rickets in children and osteomalacia in adults[67]

1.6.5 Diseases

Internal factors that can compromise bone strength are diseases that affect intestinal absorption of calcium and infections that result in an immune response to the bone cells. Bone strength is reduced by these diseases because bone volume and mineral content become low[68-70].

Gastrointestinal (GI) disorders are a group of diseases that inhibit the intestinal absorption of calcium. GI disorders inhibit calcium absorption in the intestines by fats binding with both vitamin D and calcium and then are excreted in the feces[71]. Vitamin D

is then not available to upregulate calcium absorption in the intestines resulting in blood

calcium falling, bone turnover increasing and bone mineralization decreasing[70].

There are many infections in the body that can cause an immune response

targeting bone cells. The most common bone infection is called osteomyelitis. The

infection starts by bacteria entering at the bone metaphysis via the vascular network.

Once the bacteria is inside bone, it starts replicating and moving into the vascular tunnels.

The body's response to the bacteria inside the bone is an immune response that leads to

white cells producing local resorbing factors that target the osteoclast cells[72]. The

osteoclast cells then start resorbing bone's cartilaginous matrix[72]. The most common

location in the skeleton for this infection is long bones of the lower extremity; however,

all skeletal locations can acquire the disease.

1.6.6   Mechanical unloading

Given the anabolic and anti-resorptive benefits of mechanical loading, it fits that

mechanical unloading is detrimental to the skeleton. Muscles are considered a primary

source of mechanical stimuli that induce bone adaptation in the body. Consequently, it is

without surprise that a reduction in muscle loading due to motor paralysis presents a

significant disturbance to bone.

Bone changes resulting from motor paralysis in children have most commonly

been reported in association with cerebral palsy—a condition describing a group of

permanent, non-progressive disturbances in the developing brain that contribute to

disorders of movement and posture development. Cerebral palsy interferes with skeletal

growth and modeling leading to the development of bones with reduced length, mass and size.[73] For instance, Demir et al.[74] reported children aged 4-8 years with spastic hemiplegia resulting from cerebral palsy to have up to 4.5% shorter upper extremity bones compared to controls, while Golomb et al.[75] reported adolescents with severe hemiplegic cerebral palsy to have 39% less radial bone mass and 30% smaller projected bone area in their plegic arm compared with their non-plegic arm. The consequence of these bone deficits is an increase in the risk for low trauma fractures in individuals with cerebral palsy[76].

Bone changes resulting from motor paralysis in adults have most commonly be associated with stroke. Stroke refers to the interruption of blood supply to any part of the brain and frequently leads to hemiplegia, which particularly afflicts the upper extremity. In the adult skeleton, motor paralysis interferes with remodeling and stimulates new modeling to reduce bone mass and alter bone structure. For instance, in the first year following stroke bone loss in the proximal humerus of the hemiplegic upper extremity averages 17%, with values as high as 27% in those with severe paralysis[77]. The net result is an increase in the risk for low trauma fractures in individuals following a stroke.

1.6.7   Osteoporosis

Osteoporosis is the most significant and common condition influencing bone strength and fracture risk within the skeleton. It is a metabolic bone disease characterized by reduced bone mass and structural deterioration of the skeleton resulting in an elevated low trauma fracture risk. The most common sites regarding osteoporosis is focused on

fractures of the hip, spine, wrist and humerus. In the year 2005, the United States

accounted for 40% of the total incidence of fractures in the hips and spines as well as

over 75% of the total cost of fractures[78]. Fractures of the humerus and forearm accounted

for over one-quarter of osteoporosis-related fractures in the year 2005[78], with the lifetime

risk for osteoporosis-related fracture of the humerus and forearm in 45-year-old women

being 13.3% and 21.5%, respectively[79].

Osteoporotic fractures are multi-factorial, and generally result from excessive

loads placed onto a mechanically compromised bone. Excessive loads typically result

from falls that are sideways onto an lower extremity, outstretched upper extremity or

from significant height, with recent work suggesting falls are the largest risk factor for

osteoporotic fracture[80]. However, for a bone to break during an otherwise unremarkable

fall, the underlying mechanical properties of the bone must be compromised.

Bone strength is determined by the combination of its mass, material composition

and structure. As indicated earlier, there is negative bone balance in remodeling BMUs

during aging such that there is a net loss of bone mass. However, as bone loss within

single BMUs is small, the loss of bone during aging is determined more by the rate of

remodeling (i.e. number of BMUs) than by the magnitude of the negative balance in

individual BMUs[81]. The increase in the number of remodeling sites during aging

increases fracture risk independent of the bone balance within BMUs by: 1) replacing

densely mineralized bone with younger, less dense bone, thereby reducing material

stiffness; 2) creating regions of stress concentration susceptible to microdamage

formation due to the lag time between bone resorption and subsequent formation within a

BMU and; 3) impairing of collagen isomerization and maturation which increases bone fragility[81].

The combination of negative bone balance in BMUs and an increase in their frequency ultimately leads to mechanical degradation of the bone, which is particularly prominent following menopause. The estrogen deficiency associated with menopause increases the rate of remodeling, increases the volume of bone resorbed within BMUs by prolonging osteoclast lifespan, and decreases the volume of bone formed within BMUs by reducing osteoblast lifespan[82]. First estrogen loss at the cellular level increases osteoblastogenesis and osteoclastogenesis[83]. Osteoclastogenesis is increased due to both suppression of osteoblastic osteoprotegerin (OPG) production and the promotion of osteoblastic macrophage colony-stimulating factor (M-CSF) secretion[83]. Under normal conditions when there is sufficient estrogen, OPG is secreted by osteoblasts and binds to the nuclear factor-kappaB (RANK) on osteoclasts to inhibit interaction of RANK and RANK ligand (RANKL)[83]. RANKL is a cell-associated protein found on osteoblasts[83]. RANKL is a ligand for the receptor RANK that is found on the surface of osteoclast progenitors[83]. Under abnormal body conditions such as estrogen loss, RANK-L and RANK bind causing the receptor to activate the nuclear factor KB signaling pathway which stimulates the differentiation of immature osteoclasts into mature osteoclasts[83]. Additionally, M-CSF is secreted by osteoblasts and bind to immature osteoclasts to promote osteoclast differentiation[83]. Second, it causes an increase in the rate of new BMU's by increasing the activation frequency which results into an increase in bone turnover at the tissue level. Third, it causes a negative bone balance due to the resorption phase lasting longer than normal and the formation phase being shorter than normal[83].

These changes in formation and resorption phases are not normal due to reduced osteoclast programmed death and increased osteoblast apoptosis. Forth, the osteoclasts increase the time for recruitment which causes a longer progression of the BMU[83]. The results of these changes cause the number and depth of resorption cavities to increase.

Structural decay of the skeleton during aging presents at both trabecular and cortical rich sites. Since remodeling occurs on bone surfaces and trabecular bone has more surface than cortical bone, trabecular bone has more remodeling sites per unit volume than cortical bone. Trabecular bone is consequently lost at a higher rate than cortical bone during aging. The trabecular bone loss not only decreases mass, but also reduces trabecular connectivity which produces a greater deficit in bone strength than simple trabecular thinning[84]. Once trabeculae begin to disappear, remodeling continues on endocortical and intracortical surfaces resulting in trabecularization of the cortical bone. The net result is a decrease in cortical bone thickness and increase in its porosity, both of which are believed to contribute to osteoporotic fracture risk in the body[85]. Concurrent bone apposition on the bone surface during aging partly offsets the cortical thinning that occurs with aging; however, there is ultimately a net loss of bone compressive and bending strength, and consequent increase in fracture risk.

1.7   Imaging techniques for assessment of bone strength

Determination of bone strength *in-vivo* cannot be directly measured, therefore indirect evaluations are used. Indirect evaluations measure bone density and parameters of bone architecture by advanced imaging techniques. Imaging techniques include: bone densitometry techniques that measure bone mineral content and density such as dual-energy x-ray absorptiometry (DXA) and peripheral quantitative computed tomography (pQCT), bone macro-architecture techniques that measure overall bone geometry, shape and size such as DXA, pQCT and magnetic resonance imaging (MRI), and bone micro-architecture that measures trabecular and cortical bone geometry, shape and size such as high-resolution CT's and MRI's.

1.7.1   DXA

The first and most widely used imaging technique for measuring bone strength is the dual-energy X-ray absorptiometry (DXA). DXA measures bone strength by projecting two X-ray beams with varying energies through the body part or parts that are being measured[86][87]. The individual getting measured lies supine on the scanner bed and is positioned so the body part being measured is between the x-ray source (posterior to the body part) and the detector array (anterior to the body part). Reduction of the strength of the signal of the beam depends on how the tissues and x-rays interact[88]. From the DXA assessment, areal bone mineral density (aBMD) can be calculated which is the ratio of

bone mineral content (BMC) to projected bone area[88]. The software for commercial DXA's can assess hip, spine, forearm, and whole body.

DXA can extract bone geometry properties by the measurement bone area (cm^2), which is taken from regions of interest within the scans themselves. The methods that extract bone geometric properties at the hip and spine give information on bone shape, which provides the status of whole bone strength. The software that estimates hip geometric properties is called hip structural analysis (HSA), which uses the X-ray attenuation profile from the two-dimensional (2D) image DXA provides from the scan of the proximal femur[89 90]. In 2007, DXA scanners produced by Hologic Inc. (Bedford, MA,) had the HSA algorithms provided in the analysis software[88]. The geometric properties of the proximal hip can estimate total surface area, section modulus, cross-sectional (area) moment of inertia, cortical shell thickness, neck shaft angle and sub-periosteal width[91]. The validity of this software in predicting geometric proximal hip data and fracture risk has been provided by several large prospective studies[92-94]. The combined femoral aBMD and structural data provided by the HSA software are highly correlated to fracture risk and their independent contributions cannot be distinguished due to the same attenuation profile[95 96]. At the spine, geometric measures, shape and size of the vertebrae can be obtained from the DXA scans with semi-automatic analyzes of vertebral body heights[88]. A study investigating the effects of a 6 month home exercise program in postmenopausal women with severe osteoporosis of the spine used the DXA method to measure vertebral heights, finding that there was a slower rate of decline relative to non-exercisers[97].

DXA is currently the clinical method to diagnose low bone mass and osteoporosis[98]. The diagnosis is based off of aBMD T-scores that are calculated from the hip and lumbar spine[88]. Based on multiple studies on postmenopausal Caucasian women, these scores are good estimates of fracture risk[99]. A T-score is based on the number of standard deviations of the measure of aBMD on gender and race-matched young adults at peak aBMD[88]. Based on the World Health Organization, to be diagnosed with osteoporosis, a aBMD T-score of $\leq$ - 2.5 is the category[100].

DXA clinically is a very important tool because of its availability and low levels of radiation exposure. However, DXA has limitations such as the tool measures in 2D which makes it a poorly suited to observe bone adaptations to mechanical loading. Additionally, this tool's measurement outcomes only reflect the total amount of mineralized bone, which the rate of bone turnover is the direct relationship with magnitude of loading[101]. Over the long-term, changes in aBMD corresponds with bone turnover changes. However, over the short-term, changes in aBMD will not correspond with bone turnover changes due to each remodeling site and lag time that is required for mineralization[88]. Also aBMD is influenced by changes in the size of bone[102]. An example of this limitation are comparative images of the healthy and compressive fracture spine, BMC would not be different while the smaller area in the fractured one would result in an increase in aBMD[102].

The next group of imaging technique used to estimate bone strength are the CT-based methods which include whole-body CT, pQCT, and high resolution peripheral quantitative computed tomography (HR-pQCT). CT scanners that measure whole body, use spiral technology which allows synchronous rotation of the x-ray source. Additionally, these scanners have 64-256 multidetector rows that quantify in Hounsfield units (HU) the amount of attenuation photon energy that passes through the object being measured [88]. The index for amount of attenuation of photon energy that passes through an object ranges from -1000 for air and 0 for water with a standard pressure and temperature[103]. For bone, the total x-ray attenuation energy coefficient (μ) is calibrated for water (w) which calculates an HU value based on this formula = ([μ-μ_w]/μ_w) x 1000 with μ being the attenuation coefficient at the scanner's selected voxel and μ_w being the attenuation coefficient of water[103]. HU for bone is usually between 300-3000[104]. The inclusion of the HU units allows the conversion to bone density (g/cm^3) which is referred to as the QCT. The Hounsfield units available on CT scanners provides information on the amount of bone that is available without the added cost, radiation or the use of phantoms[103]. The measurement of volumetric BMD (vBMD, g/cm3) can be obtained using computer software packages available for clinical use (QCT Pro, Mindways Software Inc., Austin TX; Image Analysis Inc., Columbia, KY) or research-based computer software packages[105-107].

A research based tool for assessment of bone geometric properties is a pQCT which assesses bone at the peripheral skeleton[88]. The most commonly used pQCT models

in research are the XCT 2000 which measures lower leg and forearm and XCT 3000

which has a bigger gantry to accommodates more proximal sites of the peripheral

skeleton (both Stratec Medizintechnik, Germany)[88]. Another research based tool that

measures bone properties at the ultra-distal radius and tibia, is the XtremeCT (HR-pQCT,

Scanco Medical, Switzerland)[88]. Both the HR-pQCT and pQCT are equipped with

software that easily convert HU to vBMD values for long bone in the peripheral skeleton.

Unlike the pQCT and HR-pQCT's that measure bone properties at the periphery,

the whole body CT scanners are not limited to those locations. The peripheral devices are

limited to those specific anatomical locations due to the diameter of the gantry (pQCT

3000: 300mm, 2000L= 140mm & HR-pQCT=126mm) and the maximal way of travel (

pQCT 3000= 400 mm, 2000L= 400mm & HR-pQCT=150mm)[88 108]. All the CT

modalities are able to separately measure cortical and trabecular bone compartments at

any imaging site[88]. The typical bone property measurements obtained from the pQCT are

vBMD, BMC and cross-sectional area (CSA) of the total bone and of the separate

compartments (cortical, trabecular & medullary). In addition to those measured bone

properties, several bone geometric and strength properties can be estimated such as

cortical thickness, second area moment of inertia, polar moment of inertia, strength-strain

index and bone strength index[109-111]. In the whole-body CT images, these bone property

measurements can be extracted at lower resolutions and excluding the combined

estimates of vBMD by computer software such as BonAlyse (Oy, Jyvaskyla, Finland)

and OsteoQ reader service (Dundas, ON)[88]. Some additional bone property measures that

can be extracted using these software are trabecular thickness, spacing and connectivity

as well as pore size[88]. HR-pQCT also has software just like the other CT scanners to

measure those bone outcomes mentioned above as well as BV/TV in trabecular bone and trabecular number. HR-pQCT images can provide enhanced visualization of smaller-scale bone outcomes due to its spatial resolution of 82 μm^3 [88]. Additionally, the voxels of the HR-pQCT scanners are the shape of cubes compared to the rectangular prism shapes of the other CT scanners which allow this machine to measure bone properties consistently in not just axial plane, but other planes as well[88].

The whole body CT and pQCT imaging tools have been used in a variety of research studies to investigate changes in cortical and trabecular bone geometric properties at the proximal and mid-femur, proximal tibia, and distal radius from disease, age-related changes, medication, disuse and mechanical loading (exercise)[112-117]. The resulting data from these studies demonstrated how advantageous these imaging tools are for assessing cortical and trabecular bone geometric properties[112-117]. The geometric properties that were described in those studies above cannot provide critical information about the spatial distribution of the trabecular bone due to the limited resolution and the small size of the trabecular elements (trabecular thickness: 100-300 μm and trabecular spacing: 700-2000 μm), therefore the true measurement assessment of the trabecular architecture cannot be done by using CT and pQCT imaging techniques[88 118 119]. However, a few studies using CT and pQCT imaging techniques looked at marrow pore size and could distinguish between dominant and nondominant arms and arms with fracture and arms without fracture which demonstrates face validity for apparent structural measurements[120 121]. Additionally, age and gender differences in trabecular bone structure from the HR-pQCT scanner has been observed in a study by Riggs and colleagues and in a later study demonstrated the rate of loss in BV/TV and the pattern of

41

loss in each gender[6 122]. To date, there is not much research using HR-pQCT to detect

changes resulting from altered mechanical loading[123], however most of the research is

focused on fracture risk using this imaging technique[124-126].

The CT based imaging technique's abilities to observe trabecular and cortical

bone adaptations from mechanical loading is an important advantage compared to the

DXA. However, the CT based imaging methods are not without limitations. Some

limitations include: high equipment costs, operator trainings, physical dimensions of the

devices, image resolution, or effective radiation dose[88]. The last two limitations have a

trade-off so if there is improved resolution, there will be a reduction in error due to partial

volume effect, but with this improved resolution comes a higher radiation exposure. To

fix the partial volume effect without improving resolution, software has been developed

to minimize this as well as noise artifacts after the image was processed[127]. Currently and

the most likely in the future, CT is the method that most choose for determining effects of

mechanical loading on bone structure and estimated strength[88 128].

1.7.3   MRI

The final imaging technique that determines bone strength is the magnetic

resonance imaging (MRI). The MRI uses a magnetic field with a sequence of

radiofrequency pulses to encode the spatial frequency of protons within a gradient by

producing 3D images[88 129]. When bone is imaged by the MRI, the hydrogen molecule is

the most studied component[88 129]. An MRI image of bone cannot provide an estimate of

bone density because the tissue has low water content and the proton's T2 relaxation time

is short. An MRI assesses what the chemical environment of the protons are, therefore, bone does not give a good signal in a standard MRI and cannot get a measure of bone density[88 129]. However, the medullary cavity of bone has water and fat within the trabecular bone network, which provides a strong signal, therefore the MRI can give an indirect measurement in-vivo of trabecular bone[129]. Another type of MRI besides the standard one is an high-resolution MRI (HR-MRI) machine which can be used to assess peripheral bone sites at the heel, knee and wrist as well as at the proximal femur to quantify apparent structural measures[130].

Studies have been done to utilize either the standard or the HR-MRI method to detect femoral-neck geometry differences in athletes with varying loading environments relative to a reference group and radius geometry changes due to aging or osteoporosis[131-136]. The findings of these studies were changes in both cortical and trabecular geometry at the two bone sites compared to the reference group or baseline measures[131-136]. One limitation that was found from these studies were partial volume effects caused the overestimation of BV/TV and trabecular thickness (Tb.Th)[131-136]. Additional, to date, there are no longitudinal studies utilizing the MRI to detect changes in bone geometry and apparent structure of the trabecular bone in response to mechanical loading.

The MRI imaging techniques have advantages as well as some limitations compared to the other methods. A major advantage compared to the other methods mentioned were the ability of the MRI to evaluate the bone properties without the use of ionized radiation[88]. The major limitations to this method are the lack of access to use these scanners, since it is a fairly new method and the necessary equipment for the MRI

to assess bone properties as well as the amount of time required for imaging and analysis[88].

1.8   Therapies for osteoporosis

In the United States, osteoporosis affects about 10 million people over the age of 50 with the bone disease projected number to rise over 14 million by 2020[78]. About 80% of the 10 million people with osteoporosis are women[78]. Fractures related to osteoporosis occurs in about 1.5 million people annually[78]. Fracture results in an increase mortality and morbidity. The ultimate consequences of osteoporosis and osteoporosis related fracture are the estimated costs in health care which in the United States costs about 13.7 to 20 billion dollars annually[78]. The annual healthcare costs are distributed to hospitals receiving 52%, nursing homes receiving 30% and outpatient centers receiving 13% of those costs[78]. The healthcare costs related to osteoporotic fracture are projected to rise to an estimated 25 billion dollars by 2025 due to more people living longer [78]. Although there is no cure for all osteoporotic fractures, there are ways to prevent the fractures such as taking prescribed drugs (i.e. anabolic and anti-catabolic) and adopting lifestyle behaviors (i.e. nutrition and exercise) that both address aspects of the bone remodeling cycle to increase bone mass and enhance bone structure for improved bone strength.

Drug treatments for preventing osteoporotic fracture have been available for over 20 years, however in the last five years there has been an increase in the development of new drug treatments[137]. There are currently two types of drug treatments available in the United States that target the remodeling cycle which include anabolic and anti-catabolic drugs.

The most common class of drug therapies to treat osteoporosis are anti-catabolic drugs that target osteoclasts. The most common prescribed anti-catabolic drugs are bisphosphonates. Studies have shown that bisphosphonates work positively in bone by reducing bone turnover and increasing bone mass and mineralization[137]. However, the use of bisphosphonates have some negative side effects that include: accumulation of microdamage[138 139], no change in bone strength[138 140] and long-term use has been associated with fatigue loading fractures[138 139 141]. These negative side-effects do not prevent all osteoporotic fractures. However, there are other types of anti-catabolic drugs that exist which include: calcitonin, estrogen, selective estrogen receptor modulators, and denosumab.

Estrogen has been one of the earliest therapies used for osteoporosis which has been found to reduce bone turnover and improve bone balance[83 142]. However, it was found in a longitudinal clinical study after use of estrogen for five years that it significantly increased risks of cardiovascular diseases in post-menopausal women even though it significantly reduced fracture risk[142]. This study was projected to last 8 years but was shut down by the Data and Safety Monitoring Board, due to the significant

cardiovascular risks from the estrogen treatment[142]. Since estrogen therapy's other health risks outweigh the bone benefits, physicians rarely prescribe this drug for treating osteoporosis; therefore, a different approach was developed to better isolate estrogen's favorable bone effects.

The therapies developed were selective estrogen receptor modulators (SERMs), which are similar to estrogen treatment, but does not produce the same negative side effects[143]. SERMs were studied extensively in a three year clinical trial, where it was found that it reduced vertebral fractures in post-menopausal women; however, it was found that it did not reduce fracture risk by significant increase BMD compared to bisphosphonates[143]. While SERM's act like estrogen by blocking bone's ability to resorb and thus reduce fracture risk, it however is less pronounced compared to estrogen[143].

Like the other anti-catabolic treatments, calcitonin a counter-regulatory hormone to PTH, acts on the osteoclasts to reduce its resorptive activity[144]. However, the effects of this drug compared to the bisphosphonates are less in BMD and resultant fracture risk[144].

The last type of anti-catabolic drug and a newer treatment is denosumab which works through a receptor ligand complex to target the RANK ligand in osteoclasts to inhibit bone resorption[145]. A clinical study called the Fracture Reduction Evaluation of Deosumab found that after at least a year taking this drug, post- menopausal women found a significant reduction in new fractures as well as bone turnover. However, there was contraindications of hypocalcemia, accumulation of bone microdamage, and the BMD levels declined towards pretreatment levels or even further if treatment was stopped[145].

Another class of drugs that can treat osteoporosis and resultant fracture is anabolic drugs. Anabolic drugs that treat osteoporosis target the osteoblast cells to increase and resultant increase in bone mass. In the United States there is only one type of approved anabolic drug on the market called teriparatide. Teriparatide is synthetic version of endogenous PTH, which is given intermittently so that its actions result into osteoblasts overfilling the resorption cavities causing a positive BMU balance[146-148]. The net actions of teriparatide is an increase in bone mass and improved microarchitecture with a reduction in osteoporotic fracture[146-148]. Even though teriparatide been known to benefit bone, there is some contraindications reported by humans which include arthralgia's, pain and nausea[148]. One contraindication that was observed in an animal study that consequently caused the surveillance of humans and limited the long-term use was osteosarcomas developed in one long-term animal study[149]. In addition to the contraindications, once a patient stops the drug bone formation decreases quickly as well as the additional bone during treatment decreases such that benefits of the treatment are gone.

While these drug treatments increase bone mass thru targeting the remodeling process, the extent and overall complete prevention of osteoporotic fracture does not occur. Additionally, some of these drugs cause an increase in risks of other diseases as well as complete cessation reverses treatment effects such that bone will become weak again. Since drug therapies are not completely treating and preventing osteoporosis and fracture, other methods are out there which include lifestyle factors such as nutrition therapy (i.e. calcium & vitamin D) and exercise. These therapies just as the previous therapies target bone remodeling as well as mineral metabolism however, unlike the drug

therapies which treat people who have been diagnosed with osteoporosis, lifestyle factors can be done not just after diagnosis but through- out life to prevent osteoporosis later in life.

1.8.2   Lifestyle therapies

Due the importance of calcium in the body as well as providing stiffness in the skeleton it is very important to get enough dietary calcium across the lifespan. Even though the public knows the importance of getting enough calcium into the body, there is still insufficient intake among the American population thus, it is not a surprise that calcium is used for osteoporosis treatment to prevent fractures[71 150]. Without sufficient dietary calcium intake, the remodeling rate increases such that bone resorption rates are higher than formation which results into bone loss in adult skeleton as well as insufficient mineralization in the growing skeleton [71 150]. Eating calcium rich foods as well as supplementing with calcium daily can return the remodeling rate to normal which will restore balance at BMU's[71 150]. While calcium supplements can help restore remodeling rate for deficient people with osteoporosis, individuals with osteoporosis who have sufficient calcium in the body will not need additional calcium supplements since this disease is multi-facet and other factors besides calcium intake can affect remodeling rate and bone mass[151]. Additionally, studies that used the combination of supplemental calcium and vitamin D as part of treatment for post-menopausal osteoporotic women have found that there was a minimal increase in bone density without any effect on fracture risk[151 152]. While both vitamin D and calcium supplements seem to not have a

significant effect on bone strength and fracture risk, both nutrients have been observed to reduce mortality rates in the older population[153].

As mentioned earlier, optimal vitamin D in the body is also important. In general, vitamin D acts on the intestine to increase calcium absorption. Vitamin D also acts on the kidney to increase calcium reabsorption, helping to maintain calcium concentration in the blood. Vitamin D plays an important role in calcium homeostasis and bone metabolism. When there is not sufficient vitamin D in the body, rate of remodeling increases which causes a negative bone balance. The negative bone balance results in a decrease in bone mass and resultant strength. In addition to vitamin D's actions on bone through the remodeling cycle and calcium metabolism, it is also acts on the muscles. It has been observed that vitamin D deficiencies also have negative side effects on the muscles as it targets the Type II muscle fibers. The negative consequences on muscles include a decrease in strength with an increase in risk of falling that has an potential for a bone fracture if the fall produces a significant load or the skeleton is already weak[154]. Since insufficiencies of vitamin D can compromise both the muscle and bone with resultant increase risk of fracture due to low bone mass, clinical studies have been done to determine how much vitamin D intake is needed to decrease the resultant negative effects on both systems[152][154][155]. Based on a meta-analysis of those clinical trials on how much vitamin D supplements is sufficient for preventing falls and fractures, the Institute of Medicine made the recommendation that people over 65 years need a 800 IU vitamin D per day to reduce the risk of negative consequences that insufficiencies cause on the musculoskeletal system[154][156].

In addition to optimal nutrition, exercise plays an important role in the prevention and treatment of osteoporosis. Exercise reduces the risk of osteoporosis, falls, and related fractures[157][158]. Exercise throughout the lifecycle is important in order to prevent osteoporosis. Optimal bone health can be achieved by exercising across a lifespan by providing resistance to age related bone loss and resultant fracture. Exercise during growth is principally anabolic stimulating modeling on the periosteal surface[159]. The net result is structural optimization of the skeleton whereby bone material is distributed in such a way that it is better positioned to resist external loads without excessively increasing the overall mass of the skeleton[159]. In the mature skeleton, loading may limit bone loss by reducing negative bone balance within BMUs by decreasing the amount of bone resorbed or increasing the amount of bone formed by each team of cells[158]. In addition to the direct bone health benefits on the mature skeleton, the overall benefits of exercise on the muscles may end up reducing the risk of falling[160]. Healthy muscles are thought to reduce the risk of fall, but can also cushion the fall which has the potential of preventing trauma to bone[161]. While studies support the notion that continued exercise and proper nutrition through-out life benefits bones by having the right amount of substrate available for optimal bone strength, however what is unknown is if prescribing exercise specifically in the growing years results into enhanced bone structure and strength long-term and ultimately reduction in rate of osteoporosis and fracture in the later years[162-165].

1.9   Mechanical loading

1.9.1   Wolff's law

Bone's ability to adapt to mechanical loading (exercise) has been studied over a hundred years ago. The first person to document bone's dynamic ability to adapt to mechanical loading is German anatomist, Julius Wolff who was influenced by the work of Wilhelm Roux (1885). This influence resulted in Wolff developing a theory in 1892, which stated bone can adapt to its environmental physical demands according to mathematical laws[166]. The law was based on studies investigating anatomical dissection which showed that bone mass increased where bone was predicted to receive high loads and low bone mass where low loads were received[166]. In addition to those anatomical dissection studies, Wolff incorporated previous work from anatomist Meyer and engineer Culmann, which he further studied their work and found that the trabecular bone in the femoral head and neck were orientated according to where the bone had high loads which allowed the head and neck to have reduction in bending stresses when it was repeatedly loaded at the same level[166]. All of these observations allowed Wolff to come up with Wolff's law that stated:

> Every change in form or function of bone or of their function alone is followed by certain definite changes in their internal architecture, and equally definite alteration in their external conformation, in accordance with mathematical laws[167].

William Roux who was an influence to Wolff expanded Wolff's law by suggesting that bone's adaptation to mechanical loading is a "quantitative self-regulating mechanism" which was thought to be regulated at the cell level[168].

1.9.2 Mechanostat theory

Wolff's law was than further developed in the 1960's by a scientist named Harold Frost whose additional hypothesizes form the current theory of bone adaptation which is the "mechanostat" theory[169]. Frost first recognized that the stimulus the bone cells receive from loading would be the production of strains as a result of the load[169]. The mechanostat theory recognized that bone has a negative feedback system[169]. This negative feedback system is the input of the outside mechanical loads engendered on bone that is transmitted inside to the bone cell by a local mechanical strain which results in an output of placing appropriate bone mass and architecture[169]. Bone cells output of appropriate bone mass and architecture is based on a strain set point, the set point is dynamic and varies according to location on bone. Bone formation occurs, if the strains experienced by the bone cells are higher than the set point, therefore, results in a stiffer bone with reducing the strains it receives and resetting the level of the strain set point[169]. Conversely to bone formation, bone resorption occurs if the strains experienced by bone cells are lower than the set point, therefore, results in a decrease in bone mass and resetting the level of the strain set point[169]. This is an important concept to understand in bone physiology as the mechanostat theory states it is a local phenomenon where the local strain environment changes and therefore adjusts by forming or resorbing bone mass locally[169]. In addition to this local phenomenon, mechanostat theory is also influenced by systemic circumstances which can regulate the operation of the local bone cell environment by modifying or overwhelming its ability to establish and maintain structural competence[170][171].

1.10   Animal Models

The question that both Wolff and Frost did not address in their theories were specific components of bone cells' strain environment that act as the controlling stimulus for bone modeling and remodeling. This question has lead scientist to address it in animal studies.

1.10.1 Exercise models

One of the easiest ways to increase the load received by the bone is to increase the level of exercise intensity undertaken. A variety of animal study techniques have been developed to observe a high level of exercise intensity, the exercise techniques are often in the form of forced treadmill running[172-174], swimming[175-177] or jumping[178 179]. In addition to these animal study techniques, other models can be done in rats who wear weighted packs on back or press weighted levers to get food rewards[180].

In these animal models mentioned above, the whole body received the load through muscular contractions and ground reaction forces that were higher than normal activity. These studies are very useful because there is no special equipment and they utilize what the animal does naturally to challenge the strength of the skeleton in which the mechanostat theory evolved from to address[181]. These animal models may seem like the easiest therapy to prescribe in order to regulate bone mass or structure, however they are not so easy because it involves a mixed stimulus loading environment which makes it difficult to interpret the results[181].

In addition to the limitations mentioned, the local strain environment is altered which engenders a lot of other physiological responses such as the oxygenation and tissue blood flow[182][183], changes in the endocrine environment[184] and muscular contractions that causes the local release of osteogenic factors from the muscle[185]. These limitations just make it more complicated to interpret the results of this intrinsic animal model as to the response of the loading as to be just bone alone. A further limitation to this model, is that the exercise engendered on the animal is a whole body phenomenon, therefore controls need to be used in the experimental design of the study for comparison of their exercise experience that mimic the experimental group, but without the modified exercise regime[181]. Lastly, the quantification of the local strain environment could only be estimated mathematically with no experimental validation. Such validation was introduced in the 1940's with the chronically implanted electrical resistance strain gage[186].

1.10.2 Strain gauge

Although the strain gauges were invented in the 1940's by Gaynor Evans[187], these were not used on live animals or humans, but freshly anesthetized animals after a short-term impact loading experiment. In the 1960's Lanyon and co-workers were the first scientists to attach strain gages on live animals and humans in a variety of different bones[186]. These scientists observed various components of the strain environment stimulus during a variety of physical activities[186][188-196]. Lanyon and co-workers found that in long-bones of animals and humans, the peak strain levels were similar and the

variety of physical activities engendered a peak strain of approximately 2-3,000με (2-3 x 10^{-3})[186 188-196]. In a horse, Lanyon and co-workers recorded the peak compressive strain levels in the third metacarpal bone while galloping to reach a maximum magnitude of 5,000 με (5 x 10^{-3})[196].

Lanyon and co-workers studies supported Frost's mechanostat theory of bone adaptation by observing similar peak strain levels in both animals and humans as well as in different bones which therefore suggested that the peak strain set-point is similar between species[186 188-196]. However, clarification of this similar peak strain levels between species and bones needs to be addressed, that this is not a single target strain at every skeletal site. Since the highest physiological strain in bone is engendered by a bending load, therefore the peak longitudinal strain will change around the bone's circumference depending on if the bending load is in compression, tension or passes through the neutral axis[181]. Additionally, studies have found lower strains engendered some weight bearing bones sites as well as other non-weight bearing bone sites[197]. An example of this is the skull, where doing activities such as chewing, smiling and hitting a ball resulted into varying strain levels of 80-200 με[197]. This suggests that the local strain set-point environment is not the same at different bones as well as different sites on the same bone[197].

In the early studies, scientists used a rosette gauge that was bonded to the bone of interest. The rosette gauge calculated strains in three directions, which were tensile, compressive and shear strains. These gages were then used to confirm a part of Wolff's theory that the trabecular bone were aligned such to receive loads in tension and compression strains[189]. In addition to the rosette gauges measuring the magnitude and

direction of strain, strain rate could be recorded by electrical resistance gages when bone experienced loading and unloading[189]. The highest strain rate ever recorded was during a sunfish striking a prey[198]. The measurement of strain rate in the sunfish was -615 x 10^8 με and was recorded on the operculum bone which is the bone covering the gills[198]. Despite the rosette gage being quite advantageous, there was some disadvantages that included the size of the gage and the number of extra channels that had to be monitored[198]. Due to these disadvantages, some studies that used small animals such as rodents, used a single element gage[199 200]. Unlike the rosette gauge, the single element gage could only measure strains in one direction in which the gauge was placed in, therefore magnitude and direction of strain could not be measured[199 200]. So when investigators use these gauges it is important to place the gauge correctly in the direction of where the measurement of strain of interest and to know that when there is a reduction of strain in the recording, it may mean changes to the direction and reduction in the magnitude of strain[201].

In-vivo strain gauges are considered the most widely used device to measure strains engendered to bones, however, it is not the only type of method to record strains in bone, especially *ex-vivo*. Another method is a digital image correlation, which requires a speckle pattern at the surface of the bone of interest[202]. Then multiple images are taken during the loading experiment to observe the movement of the speckle pattern[202]. Thus, calculating strains across varying bone surfaces[202]. In addition to the digital image correlation, another method called finite element analysis is used to calculate stresses and therefore, get strains from that calculation. This is a widely used method, but there are some limitations to this technique such as assumptions to where the load path was within the bone and the material properties, which are usually not the same along the length of

the bone[203 204]. Although this method has some limitations, it does have a major

advantage over the other techniques such as estimation of whole bone strain pattern in

which strain gauges cannot measure since they only sample the strain environment at the

surface of the bone. Therefore, finite element modeling can provide information on strain

environment inside the bone to where the trabecular in located, whereas the other

methods do not[205-207]. To reduce the assumptions that are made with finite element

modeling, the investigators can combine that technique with *in-vivo* μCT to allow more

accurate prediction of the bone formation and resorption after a loading experiment[207].

Whatever method is used to measure bone strain environment, it is very important

to have the strains and strain rates normalized between the groups that are being

studied[197]. It is also worth mentioning that the same load amount will not result in the

same strain on different bones with varying sizes, shapes or material properties[197 203].

Therefore, the amount of load and the rate of load need adjustment so the strains the

bones receive is the same across the same study[197]. The adjustments are needed in order

to directly compare the adaptive responses on the bones.

1.10.3 Invasive models

While the accessibility of the use of strain gauges for assessing the strain

environment the bone cells experienced have been validated, there was still a need to find

a suitable model for altering this environment in a controlled way and to observe the

adaptive response. One model that was developed to do this, was an invasive model

called osteotomy which is surgically remove a bone or parts of the bone to alter the strain

environment on the remaining bone[208]. The osteotomy model have three validated bones that use this model, such as radius, ulna and peripheral metatarsals[208]. In the ulna osteotomy experiments, part of a pig's ulna is removed which therefore increases the amount of strain the remaining radius receives during ambulation[208]. In response to this strain environment, bone formation occurs in the radius. In this model, after three months it was found that the strain environment returned to similar values of the intact control limb. The control limb makes this model advantageous compared to the whole body exercise models, since there is no control limb in the exercise model which allows comparison of bone's adaptive response to the loads[208]. Even though this model has an advantage over the exercise model, it has a limitation that includes an invasive surgery at the location being studied which makes it only possible to monitor rather than control the different components of the strain environment[208].

The first model to successfully attempt to control the mechanical load environment to observe bone's adaptive responses to it, was in the 1960's by a scientist named Jiri Hert who used a rabbit tibia surgical model[209 210]. This model applied different load magnitudes by an external device called electromagnetically machine to the bone of interest through transfixing pins[209 210]. By using this model, Hert and colleagues were able to find that bone's adaptive response to loading, (re)modeling is not controlled by the Central Nervous System (CNS)[209-211]. Even though Hert and colleagues findings were groundbreaking, they could not quantify the actual strain that was engendered to the rabbit[209-211]. This capability of quantifying the actual strain was not developed until Lanyon and colleagues combined this model with a strain gauge[212]. Although the sheep[212] was the first animal they used for the combination of the two techniques, the rooster and

turkey (avian model) ulna were the most successful large animals to utilize this combination of techniques[213-215]. The ulna was chosen due to the bone being large enough to place transfixing pins at the ends and three rosette strain gauges at the midshaft. Additionally, the animals were chosen because of being flightless, which the isolation of the bone's natural loading is not inconveniencing their normal daily living[213-215].

The avian surgical model involved performing an osteotomy on the proximal and distal ulna and placing metal caps on the ends of those locations with metal pins drilled in the caps to secure the bone. By doing this method, it isolates the external loadable bone which therefore makes this model advantageous to the previous models using long limb bones. By using this technique, questions were answered in regarding the effects of different components of the strain environment on bone mass and structure. Although this model had advantages, it also had some disadvantages which included a major one that involved the pins that were placed in the bone caused a local woven bone response to load that was engendered[213 214]. Woven bone formation prevents whole bone analysis. In addition to this limitation, another limitation is that trabecular bone could not be analyzed because it is located outside of the pins to where the bone is loaded[213 214]. To overcome these limitations, a new technique was developed by Chambers and colleagues using the surgical model approach, but loaded a rat tail vertebrae[216]. This approach was different to the other surgical models because the pins were placed adjacent to the vertebra of interest that underwent loading which allowed woven bone formation to be limited and full analysis of the bone of interest. In addition to eliminating woven bone formation on the bone being loaded, trabecular bone in response to loading is studied as well because tail vertebra contain a lot of trabeculae. These advantages over the other surgical models

allow this approach to be used today[217-219]. However, there is still limitations to this approach as well as the other approaches which include this woven bone formation outside of the pins location and also the body's inflammatory reaction to the surgery might affect the bones adjacent to the pins. Another limitation to this approach is that the tail vertebra do not normally receive high loads as to which this model engenders on them. Finally, the last limitation is that there needs to be a healing period where the bones and pins integrate before start of the loading experiments.

1.10.3 Non-invasive models

The first non-invasive animal model was developed by Turner and colleagues in 1991, where they loaded a rat tibia under four-point bending and observed there to be adaptive bone responses to this model[220]. This model's method used a device that had two contact points on the ends of the limb on the lateral side and two contact points just inside the other contact points on the medial side of the limb. A bending load was applied in the medial-lateral direction to where the lateral part of the limb was under compression and the medial side under tension[220]. In addition to doing the four-point bending loading arrangement stated above, a shame loading arrangement was added to the experiment as a control where the medial contact points were placed just under the lateral contact points so no force was produced during application of the load[220]. This model has its advantages over the invasive models mentioned above, however it also has some limitations that include the loading contact points are too close together that the loads are applied through the periosteum. Loads that are applied to the periosteum can result into woven bone

formation due to periosteal disturbance such as what this model's load provides and therefore, limits analysis to the endosteal bone surface, which may respond differently in response to the strain from the periosteum[221].

To address the limitations that the four-point bending model had, Gross and colleagues developed a new model that used cantilever bending in which a mouse's knee and the ankle were placed in these specialized cups and the ankle moved in the lateral direction from the knee to produce a bending load in the tibia/fibula[222]. This model eliminated what the four-point bending model could not do was allowing analysis of both periosteal and endosteal bone compartments. Even though the four-point bending model's limitations were eliminated, there was still concerns for this new model in that the bending load did not accurately translate into the axial load that was generated in humans and animals during ambulation. Additionally, this model only observed a response of loading at the diaphyseal area of the bone where the majority of trabecular bone is not located; therefore, observance of trabecular bone adaptation to loading could not be studied[222].

The rat ulna loading model was developed by Torrance and colleagues to address the concerns of the previous models[223]. In this model, the rat ulna is loaded axially at physiological relevant strains with loads introduced at the olecranon and flexed carpus[223]. Scientists used the ulna because axial loading of the tibia caused necrosis at the knee and ankle joints due to high strains[199 200 224 225]. However, this did not occur in mice when loading the tibia. So now the mouse is the animal of choice for using the tibial axial compressive loading model[199 200 224 225].

The mouse tibia loading model had its advantages over the other non-invasive models such as the loading program was controlled and it allowed long bones to have sufficient time for the adaptation response to be completed. An additional advantage of this model was that the whole bone can be analyzed in response to this loading regime. Further this models advantages were extended to studying the fibula as well as the tibia[225]. The models method for axially loading the mouse tibia/fibula is quite simple that cups are placed on the knee and tarsus. The cup that is placed on the knee is attached to an actuator arm from a hydraulic or electromagnet machine and the tarsus cup is connected to a load cell to which a load can be applied in a controlled manner. The strain that is engendered to the bone in this model is compression and bending which causes an increase in strain stimulus, resulting in an adaptation.

Due to the placement of the cups in tibia/fibula loading model, there are a number of strengths that include observing both trabecular and cortical bone adaptation and the reduction of the number of animals needed for the study[224]. Cortical and trabecular bone adaptation can be observed in tibia/fibula loading model because the bone does not have any contact with the loading cell. A final strength is along the length of the tibia there are regions where high and low adaptation occurs in response to this model which includes locations that are measured from the proximal end of the tibia with the highest adaptation at 37% site and the lowest adaptation at the 75% site[224]. Even though these two sites are complete opposite on the bone adaption, the strains engendered are similar in both locations however, the physiological responses to the strain at those locations are different such that bone formation is related to down-regulation of osteocytic sclerostin than to strain engendered[203 226].

Even though the axial loading models have their strengths, there are limitations to these models. The main limitation includes the external applied load needing to be higher than the previous models for an adaptive response because bone is stiffer in this loading direction. As a consequence to the high loads engendered in the axial loading models, young animals might develop early growth plate closer at the ulna or tibia and fibula[227] [228].

1.11   Knowledge gained from animal models

Bones adaptive response to mechanical loading has been studied through animal models extensively since the 1940's[181] [187]. The information that has been gained from these animal studies are optimal loading parameters that provide the most osteogenic response and benefit to bone. There are five loading parameters which include: strain magnitude, strain rate, rest period insertion, type of loading and strain duration.

1.11.1 Strain magnitude

The most important component of a loading program to which will engender an osteogenic response in bone is the peak strain magnitude. There has been multiple studies that support this claim by demonstrating with various peak loads, while keeping the other components of the loading experiment the same. The findings are a dose-response in relationship with peak loads engendered with more new bone formed at higher loads[220] [229-232]. In addition to these studies, other studies have claimed that there was a window of

bone adaptation to which bone mass and architecture would not change at a set range of strain stimuli. However, a few studies would contradict those findings about a set range of strain stimuli window of opportunity for bone adaptation. Those studies used the isolated turkey ulna and the axial tibia loading models with disuse in the first model and sciatic neurectomy the second model to support evidence that there was no window of bone adaptation[230][232]. In addition to these two studies, another study by Ellman et al. supported the two studies above by the use of a graded unloading model to which a finding of a linear relationship between a percentages of weight bearing to bone loss was found[233]. Since these studies were only a single type of loading modality, there could not be confirmation that it would occur in a natural loading situation. In a natural loading environment, all of the loading modes are combined together to provide a spectrum of strain magnitudes that have this set range of averaged strain stimuli which can cause little or none response to the loads that are engendered.

As stated in the mechanostat theory, bone's adaptation to mechanical loading is a local phenomenon[171][224][234]. As such, mechanical loads will cause varying peak strains magnitudes at different locations of the same bone[200][202]. Plenty of studies have confirmed this by finding that on the same bone where strains were high, bone formation occurred and where strains were lower, lower levels of formation or even resorption occurred[204][235-237].

Bone's osteogenic potential is not determined by just strain magnitude alone, but also the rate of change of strain magnitude or strain rate during when the load is engendered and then released. This was first observed by O'Connor and colleagues in the early 1980's where they used an invasive sheep loading model which found that strain rate had more accounted variation in new bone formation than did strain magnitude in response to the loading regime[212]. In addition to that finding, they found that the maximum strain rate was not affected during the loading or unloading portion of the experiment[212]. To support this study's finding, a later study using a rat ulnar axial loading model which was more controlled compared to the previous study, found a proportional increase in bone formation in response to loading when strain rate was increased with all other loading parameters kept constant[238]. To further support these studies findings, Turner et al. also found similar results as that the amount of new bone would form in proportional to the strain rate[239]. However, there is a limitation to these studies which is in order to increase strain rate, but keep all other parameters constant a rest period needs to be inserted between the loading regime's cycles, therefore causes difficulties interpreting these studies findings. Although at the time this criticism was not appreciated, now there is evidence to support that the insertion of rest periods can enhance bone's response to loading. Despite the limitation mentioned above, a number of other studies support strain rate as being an important determinant of bone's osteogenic potential. The findings from the previous studies are consistent with some human studies that found that exercise programs with high levels of impact loading such as squash,

tennis and triple jump were more osteogenic then the low level of impact loading programs such as swimming and cycling[240-243].

1.11.3 Rest-period insertion

It has been demonstrated in plenty of studies that inserting rest between loading cycles will increase bone formation[244-249]. In a study done by Robling et al., they found that by splitting up 360 loading cycles by 4 bouts of 90 cycles or 6 bouts of 60 cycles per experimental day enhanced bone's osteogenic response to these loading parameters[250]. In addition to this study, Robling also demonstrated that the rest periods inserted between loading cycles needed to be 14-s in order to optimize bone formation response[244]. This information was then supported by LaMothe and Zernicke who used the cantilever bending model with loading parameters as 11s rest period at 30 Hz for a total of 100 s and found these parameters resulted in 72% increase in bone formation despite a very large decrease in loading cycles[245]. In addition to the studies above, Gross and colleagues supported the notion of inserting rest periods between loading cycles by using a cantilever bending model with 10 or 15s rest periods between each cycle which resulted into an enhanced bone formation in both young and old mice[246-248]. To further support the findings above, Turner and colleagues found that if the length of loading study period was increased, there was a decrease in the percentage of new bone formation in the following weeks. Therefore, they found by placing rest periods several times between the weeks of the loading study period, this could partly restore the decrease in the percentage of new bone formation[249].

It was first reported by Hurt and colleagues that the type of load that is engendered in bone affects weather the bone will (re)model or not. The type of loads Hert and colleagues are referring to is dynamic and static loads[209]. It was found that bone was affected by dynamic rather than static loads[209]. The first study by Hert and colleagues inferred this idea by utilizing isolated avian ulna loading model for 8 weeks to observe any bone adaptation differences in using a continuous static load or a dynamic load with the same loading magnitude[209 214]. The results of the study showed that the static load regime caused 13% bone lose by the expansion of the endosteum compartment with an increase in cortical porosity while the dynamic load regime resulted in a 24% increase in bone mass by bone formation in the periosteum compartment. In addition to the static loading group resulting in bone loss, the control group in this study exhibited the same amount of bone lose which that group underwent osteotomy but did not go through loading experiments. Based on the findings from this study, the majority of the other studies use dynamic external loading experiments with either triangular, sinusoidal or trapezoidal waveform[200 205 224 231 251 252]. As of right now, no data has been published to state any comparisons of these waveforms to the relative effects they have on bone formation.

Strain duration means the number of loading cycles without interruption that are applied over a time period. Two important studies have looked at the number of loading cycles required to engender bone formation. Rubin and Lanyon were the first to show that with an isolated avian ulna model that increasing the number of loading cycles from 36 to as much as 1,800 made no greater adaptive response to loading[213]. In addition to that finding, they found that as little as 4 cycles of loading a day was enough to prevent bone loss associated with disuse. Another study also supported the previous study by using an exercise rat jumping model to train the rats into jumping 40 cm and found little additional effect on bone adaptation if the rats jumps 5 or 40 times per day[179].

Even though it was found that relatively few loading cycles are needed for bone to maximize formation, some studies using *in-vivo* loading models with thousands of loading cycles to observe fatigue and damage repair[253]. However, for the majority of studies this high number of loading cycles can cause unnecessary and detrimental effects on the bone.

1.12   Translation of animal models to clinical implications

As stated above, animal models have provided our understanding for what mechanical loading features are necessary to engender the optimal skeletal adaptations to prevent and treat osteoporosis. In addition to the gain in knowledge about mechanical loading features, animal studies have provided the knowledge to form and conduct

numerous clinical studies in an age range of infant to older adulthood[241 254-256]. These

clinical studies have formulated exercise programs that specifically target bones. Exercise

programs that target optimal health benefit to bone are quite different to the other

exercise regimes for other body systems. For prescribing exercise for optimal bone

health, there are training principles that need to be considered which are: specificity,

overload and reversibility.

1.12.1 Specificity

When bone is loaded that adaptation does not occur through-out the whole

skeleton, but at the specific site to where the loads were engendered [241 254-256]. Therefore,

exercise programs must target specific locations with enough load magnitude or provide

high enough rate to stimulate bone adaptations[238-243]. The specific skeletal sites that needs

to be targeted in exercise are the ones that are most prone to fracture which include hip,

spine and distal radius[257]. Data from numerous studies using athletes that expose their

extremities to greater than normal loads, consistently shown the loaded bone(s)

adapted[241 254-256 258 259]. An example where specificity is nicely shown is in individual

sports where one of the limbs are exposed to the mechanical overload, with that one

limb's bone adapts[112 241 255 256]. This site specificity to loading in long bones can be

further broken down to individual bone level. The curved structure of long bones causes

production of varying strain levels within the cross-section of that bone. The observation

of this site specificity in long bones has been documented in animal model studies using

the ulna and tibia axial loading models where specific regions of the bones cross-section

produced more bone where a higher strain magnitude occurred and vice a versa for a lower strain magnitude production[35 224 260-262]. A specific example of this site specificity is in the rat ulna loading model, new bone is formed along the medial and lateral regions where compressive and tensile forces are generated and no new bone formation in the neutral axis[35 260].

1.12.2 Overload

The magnitude of load that is engendered in the skeleton is an important component when considering prescribing exercise specifically for bone health benefit. In addition to the load magnitude component, an exercise program needs to be dynamic rather than a static because a static load is held at a constant rate and magnitude, which results in the mechanosensing cells ignoring the signal[214 238 263]. Therefore, the best combination for an osteogenic exercise program includes a sufficient load magnitude that provides an overload without damage to a specific bone site with rests inserted between the loads. Examples of specific exercises that engenders high loads and rates of loads, include jumping, plyometrics, basketball, soccer and gymnastics while the low load magnitude and long duration exercises such as walking, swimming and cycling do not provide an osteogenic stimulus[264 265].

The osteogenic stimulus to an exercise program is specific for each individual. The stimulus depends on certain characteristics of the individual which includes training level and initial bone density and structure[244 264]. An example of someone with high osteogenic potential, is a sedentary individual with initially low bone density and

structure compared to a professional athlete who has initially high bone density and structure to the same program. While both of these individuals are at different exercise levels and initial bone density and structure, they are similar in that there still needs to be continual challenge to bone by progressively increasing load magnitude as the training program goes on in order for further gains in either bone mass or structure.

1.12.3 Reversibility

The reversibility principle pertaining to an exercise program means the response to bone when exercise is removed. The skeletal response to removal of exercise is age dependent meaning bone adaptations during infant to adolescence years are less reversible than in adulthood years. The geometric adaptations that occur due to exercise in the childhood years may persist on to adulthood which may then be maintained even if there is a decrease in activity level[162]. This information depicts how important exercise is during the childhood years due to the heightened modeling rate in order to gain the most accumulation of bone mass and allow the appropriate orientation and distribution of the bone. An example of this is a clinical control trial study investigated by Fuchs et al. where prepubertal boys and girls in the experimental group participated in a 7 month jumping program and resulted in an significant more bone mass gains at the hip and spines than the control group[263]. The study then reassessed the participants 8 years later and found still a significant despite smaller differences in higher bone mass in the experimental group compared to the control[263]. Due to the smaller differences between the groups, questions remain as to did the control group gain more bone mass due to

growth or did the experimental group lose bone mass due to cease in exercise. Unfortunately these questions cannot be answered because true bone structure could not be assessed due to the use of a DXA and not a pQCT. Despite the equipment limitation, there still could have been structural adaptations maintained in the experimental group even though bone mass decreased.

In contrast to the childhood years, ceasing exercise in the adulthood years has been found to result in loss of bone health benefits specifically the bone mass component[266]. A study investigated by Winters et al. observed this loss of exercise benefits by having postmenopausal women participate in weight vest plus impact exercise program for 12 months and then detrain[266]. The results of the 12 month exercise program found a significant 2.5% increase in hip bone mass while a detraining period of 6 months resulted in a complete loss of training induced bone mass gains[266]. This study like the Fuchs et al.[263] could observe if bone mass was gained or loss due to equipment used, therefore, there was no way of knowing if geometric bone property changes where the same following exercise cessation[266]. However, with new studies being able to assess bone structure with the pQCT and MRI, new information has led to the idea that there may be a lasting benefit of bone structure after exercise has been ceased[162 165]. Nonetheless, the aging population still needs to continue exercise to maintain those bone health benefits to an exercise regime.

The magnitude of bone loss after ceasing exercise is dependent on a few factors which include the age to which the person starts exercising and the age to which the person ends exercise[267 268]. An example of this would be an athlete who participated in a sport in early childhood years and then commences that sport early as well will still

having more bone mass in adulthood, but will also have lost some after ceasing participation in that sport[134 267]. Unlike the childhood athlete example, an adult who started participating in an osteogenic activity as an adult will lose all of the bone gains if the activity is ceased[267]. Even though there is some loss of benefit in bone health for discontinuation of regular exercise, the other added benefits of regular exercise are the reduction in the risk of falls and ultimately fracture. The incidences of complete cessation of weight bearing on the bones, which include space flight and long-term bed rest do not follow the principle of reversibility due to such an extreme situation[267].

1.13   Exercise and bone health across the lifespan

As stated above, the exercise principles for optimal bone health have been formulated by animal studies and confirmed by many clinical studies[241 254-256]. Based on these clinical studies, these principles can be applied across the lifespan with some modifications for each life stage[162 269 270]. These modifications happen due to when the bone's more responsive to exercise in childhood to when it is prone to fracture due to risk of osteoporosis in the older adult. Based on bone's responsiveness and when it is prone to fracture, results into changes in the exercise prescription. Each life stage, which are infancy, childhood, adulthood and older adult, uses the same exercise principles, however the difference in the modifications is on types of exercise used for each life stage.

1.13.1 Infancy

Benefits of physical activity on the skeleton has been documented as early as in utero[271-273]. These studies have found that the lack of fetal movement in utero had negative effects on the skeleton by observing fetuses who were born with conditions and syndromes related to nervous and muscular systems that reduce, restrict or prevent movement[273-278]. The resulted restricted movement in utero, caused a weak development of the musculoskeletal system with under mineralized bones and weak muscle strength[273-278]. It has also been observed that pre-term babies can suffer from weak bones due to removal of loads against the uterine wall, therefore, not allowing optimal bone mineral to accrue during the third trimester[279].

Physical activity for optimal bone health in infants ages; birth to the first year, can be done by manual movement of the limbs and message. Studies have shown that 4 to 8 weeks of 5-10 minutes of manual movement of limbs and message per day have strengthen the skeleton of pre-term infants and infants that had limited movement in utero [278 279]. Therefore, providing the combination of daily physical activity and optimal nutrition for infants could result into optimal bone health benefits.

1.13.2 Childhood

Physical activity during this period of life is very important because the bone cells are more responsive to changes in mechanical loading than any other life stage[280]. Therefore, this is the most opportune time to enhance the skeletal properties, bone mass

and structure which occurs from accelerated modeling[280-282]. The enhancement of skeletal properties in childhood years, could provide benefit in the later years when there is an increased risk for osteoporosis and fracture. Since there is high rate of osteoporosis in society, researchers have looked at: specific osteogenic exercise programs, target age; and type of bone property and if those properties persist and prevent osteoporosis into adulthood[242 283-289].

Studies comparing children who engage in regular physical activity to children who did not, found that those who are highly active have about a 10% to 15% higher bone mass than those who are sedentary[285-287]. In addition to participating in regular physical activity, the children who specifically engaged in higher load activities such as gymnastics, tennis, ballet, dancing and baseball have been shown to have a higher bone mass and enhanced bone structure specifically at the loaded sites as compared to those who participated in low to none impact activities such as swimming, cycling and walking[242 285-289]. Additionally, these benefits of high load activities have been supported by longitudinal control trials observing site specific skeletal changes over time in bone mass and structure in children who participated in gymnastics, dancing and tennis[288 290 291].

Original research in the area supported the popular theory that exercising while young it would add additional mineral which would maximize peak bone mass and provide greater reserves later in life to protect it from the bone loss due to aging[285 292-294]. This thought to maximize peak bone mass in childhood has been supported by the ideas that: almost 95% of the human skeleton is developed by the end of adolescence[285 293]; about 25-30% of bone mineral is accrued around puberty[285 294] and the beginning of

osteoporosis is thought to be delayed around 13 years with 10% increase in the peak bone mass[282]. Studies suggest that exercise induced gains in bone mass can be maintained for the short-term after exercise has ceased[295-297]. However, in the long-term, studies suggest bone mass benefits are not maintained[296 298]. Studies supporting this have found that in those who exercised when younger and then stopped, the bone mass benefits from exercise were progressively lost[296 298].

Since it was suggested that bone mass benefits obtained by osteogenic exercise while young, will not persist into adulthood, studies now have looked at the effects of exercise while young on bone structure. The reason why majority of studies in the past were observing skeletal response to exercise on bone mass and not structure was the use of the bone assessment technique DXA, which as mentioned before, provides inadequate information on the bone structural properties[299]. Now with the development of the CT based bone assessment tools, it has made it possible to measure those bone structural properties more adequately. Studies utilizing this imaging tool, have found both bone mass and structure adapt to exercise and provide contribution to overall strength of the bone[286 300-307]. However, bone structure adaptations to exercise contributed disproportionately more to the overall bone strength compared to bone mass. This was demonstrated in two studies utilizing the rat ulna axial loading model, where bone adaptations by mechanical loading resulted into increase bone strength by the majority contribution from structural properties[260 284]. The resultant gains in strength were from site-specific new bone formation at the locations where the load caused the greatest demand[260 284].

This site-specific new bone formation is an enhancement to bone's structural properties due to the new bone tissue being placed at locations where it is better able to resist mechanical loads. This distribution of new bone is usually placed farther from the axis of bending or rotation, as observed by a few clinical studies where exercise before puberty, resulted into the formation of new bone at the periosteal surfaces of the mechanical loaded bone[159][289][306]. This adaptation to loading is very important as it places bone mass and strength where the bone needs it most while not allowing overall bone mass to disproportionately increase (Figure 1.6).

Unlike bone mass, it is thought that bone structural property adaptations from exercise while young have a potential to be long-term even after physical activity is ceased. This hypothesis is made based on the idea that when people age, bone loss occurs in the endocortical surfaces and bone deposition at the periosteal surfaces[308][309]. Even though new bone can be formed on the periosteal surfaces while aging, the rate of formation is lower compared to the rate of bone loss at the endosteal surfaces which can result into skeletal structural decay. Exercise while young provides enhanced bone formation on the periosteal surfaces, where aging does not result into loss at this surface, therefore, this structural adaptation may persist long-term to reduce risk of structural decay and ultimately age-related osteoporotic fracture[310]. Both animal and clinical studies suggest that structural benefits obtained while exercising in the growing years may persist even after the activity has been ceased for years[164][165][311][312].
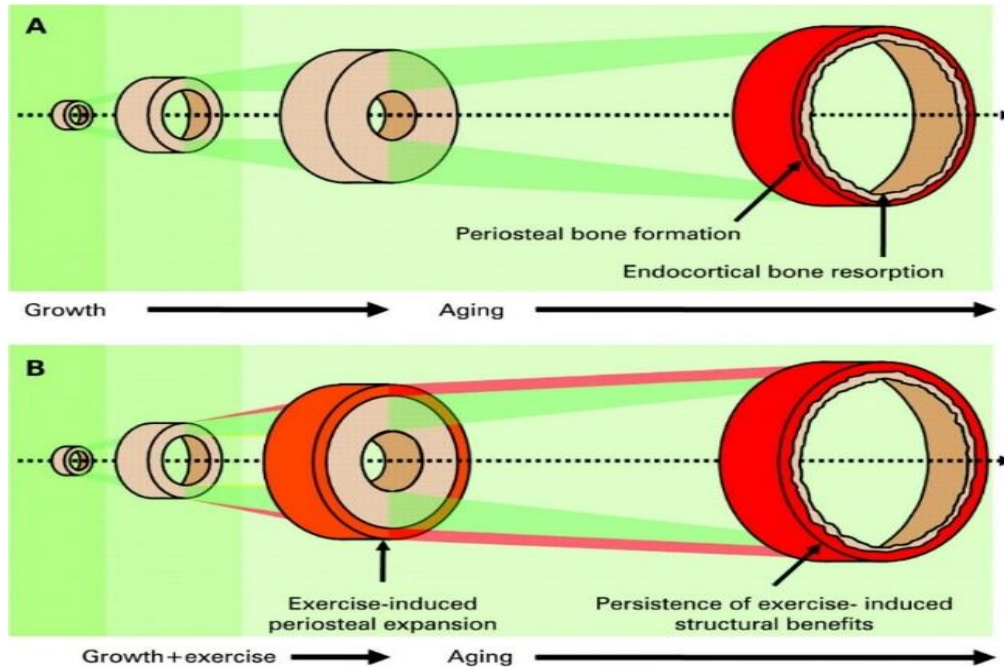
Figure 1.6. Bone geometric property changes due to A.) aging B.) exercise
(Reproduced from Warden et al.[283] with permission from BMJ Publishing Group Ltd.).

The specific age to which children should start exercising for the attainment of

optimum peak bone mass and structure and ultimately bone strength for reducing risk of

age-related osteoporotic fracture has been suggested to be at least 5 years prior to

puberty[157 288]. This time frame is important due to the ability of the child to reach or

exceed their genetic potential for optimum bone strength. The studies that support this

timeframe are one's that utilized racquet ball sports as exercise and found that children

who participated in the activity had the more gains in bone mass and structure compared

to the kids who started participating after puberty[157 288]. The specific structural gains in

studies aimed to determine the age that children should start exercising for optimum

benefits. These studies have found that if exercise was initiated prior to puberty, there

was enhanced bone formation on the periosteal surfaces with an increased diameter of the

endosteal surfaces[288 289]. While the opposite was found for the children who started to

exercise participate after puberty in which more bone was being formed on the endocortical surfaces[288 289]. The location where bone was formed plays a role in the overall strength by the younger children who started exercise have a stronger bone due to the mass being distributed further away from the bending axis compared to the older kids[159 289 306].

The specific reason why bone forms on different skeletal surfaces depending on when the child starts exercising is due to the introduction of hormones at puberty. Particularly in girls, the introduction of estrogen at the start of puberty results into blunting bone formation at the periosteal surfaces and stimulating endocortical bone formation in response to exercise[306]. This is why it is very important that girls start an osteogenic exercise program before puberty in order for optimum bone strength and significant reduction in risk of osteoporotic fracture. For boys, particularly it is important to start early as well to get the maximizing benefit of exercise from growth. However, boys have the introduction of the hormone testosterone without much estrogen at the early stages of puberty which allows them to have an enhanced response to bone formation at the periosteal surfaces compared to the girls[289].

The physical activity program for this life stage to enhance bone strength and potentially have lasting long-term benefits are weight-bearing exercises that provide high loads in different directions. Examples of the weight-bearing exercises are basketball, gymnastics, and simple jumping activities. The optimal length of time and frequency of the activity depends on how intense the activity is on the bone. Therefore, if the activity is low to moderately intense than it requires about 40-60 minutes at 3 times a week

compared to an high intensity exercise such as jumping where it only requires about 10 minutes at 3 times a week[263 313].

<u>1.13.3 Adulthood</u>

Physical activity during adulthood is still beneficial to the skeleton even though its osteogenic potential is reduced compared to the childhood years. The benefits to the skeleton from exercise are the preventing and slowing down age related bone loss. These benefits were demonstrated in a review that found that postmenopausal women who participated in a combination of weight-bearing exercises that included high impact activities with weight-training and low impact activities with jogging had the potential to prevent age related bone loss[163 314]. This review suggested that the adult skeleton still has the potential to adapt to physical activity. While there is little information on structural adaptations to exercise with aging because very few clinical studies have been done looking at this property. The studies that have been done, suggest that the mature skeleton responds to exercise by adding bone to the endocortical surfaces compared to the addition of new bone on the periosteal surfaces before puberty in kids which does not confer to optimizing the structural properties of bone[159 306].

The physical activity program for this life stage includes combining low-moderate impact exercises with resistance training. The combination of the two types of activities is important because it allows the preservation of bone mass and muscular strength as well as improved balance and flexibility. The improved balance and muscular strength with an exercise program is important because it reduces the chances of falling

and ultimately prevents fractures due to falling. The main guidelines at this life stage are to do activities that are low to moderate impact such as jumping, tennis, climbing stairs or walking with the combination of upper and lower body weight-training exercises.

1.13.4 Older adult

Physical activity in this life stage is still beneficial to the skeleton, but it is not just the skeleton that is the major objective for the exercise program. Based on some reviews, there are suggestions that exercise programs prescribed to the older adults should provide an overall functional benefit to allow for them to perform activities of daily living easily[163][314]. The reason for this type of exercise prescription, is that individuals in this life stage have higher risk for osteoporosis and with osteoporosis comes functional impairments[80][315]. Based on those same reviews and some additional studies, functional impairments lead to about 15% of falls in the older adult[80][163][314][315]. Reducing the incidence of falls in the elderly is important because the more frequent someone falls it increases the risk for fracture from that fall. By prescribing an exercise program specifically for overall functional benefits allows for fracture prevention. The exercise program prescribed for prevention of fracture includes activities for balance, weight-training and cardiovascular endurance.

By using this life stage approach to exercising across the lifespan, there might be a reduction in fracture occurrence due to aging. Whether this approach to exercise prescription specifically in the growing year's results into lasting long-term changes in

bone structure and estimated strength in the older years is still in need of more research due to limited number of studies.

1.14   Summary and aims

1.14.1 Summary

To summarize, osteoporosis is the most significant and common condition influencing bone strength and fracture risk within the skeleton. It is a metabolic bone disease characterized by reduced bone mass and structural deterioration of the skeleton resulting in an elevated low trauma fracture risk. Fractures occurring as a result of this disease increases mortality and morbidity. Although there is no cure for all osteoporotic fractures, there are ways to prevent the fractures such as prescribed drugs (i.e. Anabolic and Anti-catabolic) and lifestyle factors (i.e. nutrition and exercise) that both address aspects of the bone remodeling cycle to increase bone mass and enhance bone geometric properties for improved bone strength.

Although there is vast knowledge gained from animal and clinical studies on exercise essential for preventing osteoporosis and related fracture, there is still a void in the research. Most of the studies pertain to the benefits of exercise on bone mass independent of bone structure and strength. The reason why most of the studies in the past were observing skeletal response to exercise on bone mass and not structure was the use of the bone assessment technique DXA, which provides inadequate information on the bone structure. Now with the development of the CT based bone assessment tools, it

has made it possible to measure those bone properties more adequately. Studies utilizing this imaging tool, have found both bone mass and structure adapt to exercise and provide contribution to overall strength of the bone. However, bone structure adaptations to exercise contributes disproportionately more to the overall bone strength compared to bone mass. Since less is known on the adaptation of bone structure and estimated strength from exercise, there is a need for more research on this topic.

1.14.2 Dissertation overview

The purpose of this dissertation is to explore the response of the skeleton to exercise across the translational divide between animal- and human-based studies, with a particular emphasis on exercise-induced changes in bone structure and estimated strength. To explore the skeletal benefits of exercise, models were used wherein loading is introduced unilaterally to one extremity. Unilateral exercise enables the contralateral, non-exercised extremity to be used an internal control site for the influences of systemic factors, such as genetics and circulating hormones.

a) Study one

Study one of my dissertation research will be an animal-based study. Skeletal adaptation to mechanical loading will be observed using the mouse tibial axial compression loading model. The model has recently been described to allow simultaneous exploration of cortical and trabecular bone adaptation within the same loaded element. However, the model frequently induces cortical woven bone formation

and has produced inconsistent results with regards to trabecular bone adaptation. The aim of this study will be to investigate bone adaptation to incremental load magnitudes using the loading model, with the ultimate goal of revealing a load that simultaneously induced lamellar cortical and trabecular bone adaptation. Adult (16 week old) female C57BL/6 mice will be randomly divided into three load magnitude groups (5, 7 and 9 N), and have their right tibia axially loaded using a continuous 2-Hz haversine waveform for 360 cycles/d, 3 d/wk for 4 consecutive weeks. *In-vivo* pQCT will be used to longitudinally assess midshaft tibia cortical bone adaptation, while *ex-vivo* micro-computed tomography and histomorphometry will be used to assess both midshaft tibia cortical and proximal tibia trabecular bone adaptation.

b) *Study two*

Study two of my dissertation research is going to be done to explore the validity and intra- and inter-operator reproducibility of pQCT of the humerus. Since in the next two studies non-invasive pQCT measures will be used as estimates of bone strength, there is a need to explore the validity and reliability of taking these measurements. Validity will be assessed by imaging 20 human cadaver humerii before loading each humerus to failure using a materials testing device. Correlations will be performed between the pQCT-derived estimates of humeral strength and the actual strength of the bones obtained through mechanical testing. Reproducibility will be assessed by performing repeat imaging of the humerus in 30 healthy subjects. Subjects will undergo repeat pQCT imaging on two separate days a minimum of one week apart to enable both

intra- and inter-day reproducibility to be determined. Also, two operators will perform repeat assessments to enable determination of intra- and inter-operator reproducibility.

c) *Study three*

Study three of my dissertation research will be a cross-sectional human study using collegiate level athletes who compete in jumping activities (such as high and long jump) as a possible unilateral lower extremity model, as they repetitively put a lot of force through their jump leg. In the proposed study, we will compare lower extremity bone health in the jump and lead legs using a combination of DXA and pQCT outcome measures. A cohort of matched, non-jumping control subjects will also be tested to control for any side-to-side differences in lower extremity bone health due to side-to-side differences in habitual loading.

d) *Study four*

Study four of my dissertation research will be a human longitudinal study to investigate the humeral bone structural adaptation in growing overhand throwing athletes. Throwing athletes are used as a translational model to explore the benefit of exercise on the skeleton as the elevated unilateral loading associated with throwing enables the contralateral upper extremity to serve as an internal control site for the influence of systemic factors including growth. This will be a 12-month longitudinal study that will recruit 20 [8-11 year olds] male throwing athletes. Subjects will be assessed at 0 (baseline) and 12 months (follow-up) enrollment into the study. Participants must anticipate playing a minimum of 5 months in upcoming year to ensure adequate exposure

and adaptation to the mechanical forces associated with throwing. DXA will be performed to assess whole-body % fat and lean mass. Bone health within the upper extremities will be assessed using a pQCT machine. Scans will be performed on both the throwing and nonthrowing upper extremity at the distal humeral diaphysis to assess bone structure and estimated strength. Subjects will also complete five questionnaires—1) sexual maturation, 2) demographics and health information, 3) diet (calcium intake), 4) throwing history.

1.14.3 Aims

1.   Study one aims to establish a load magnitude that resulted into lamellar cortical and trabecular bone adaptation using a mouse tibial axial compressive loading model.

2.   Study two aims to explore the predictive ability and short-term precision of pQCT estimates of midshaft humerus mechanical properties.

3.   Study three aims to assess tibial cortical and trabecular bone side-to-side differences in jumping athletes and controls.

4.   Study four aims to prospectively assess gain in bone properties between the throwing (exercised) and nonthrowing (non-exercised) arms within prepubertal baseball players

This research expands upon previous research in several ways. Study one will use different load magnitudes with the animal model. Study two will use the pQCT to look at predictive ability and precision of human upper extremity bone's mechanical properties with pQCT's predictive ability and precision at proximal sites currently being unknown. Study three will be the first to use collegiate level high and long jumpers as a unilateral lower extremity bone model. Finally, the fourth study will be assessing bone properties of prepubescent children who will be participating in baseball for one season, with a longitudinal study of this unilateral model not previously being reported in the literature.

CHAPTER TWO: THE EFFECTS OF TIBIAL AXIAL COMPRESSION LOADING

MODEL ON TRABECULAR AND CORTICAL BONE IN MICE

2.1   Introduction

Animal models wherein controlled loads are introduced to the skeleton have been

instrumental in advancing understanding of the response of bone to mechanical stimuli.

As a result of studies utilizing animal models, we now know bone preferentially responds

to dynamic rather than static stimuli, only short durations of loading are required to

initiate an adaptive response and bone cells accommodate to unique mechanical loading

environments[316]. With the sequencing of the mouse genome and subsequent generation of

transgenic mice, attention has shifted to exploration of molecular pathways underlying

the skeletal response to loading. For instance, recent work utilizing transgenic animal

models has demonstrated important mechanotransductive roles for molecules within the

Wnt signaling pathway, including low-density lipoprotein receptor-related protein 5 and

sclerostin[226 317].

The rodent ulna axial compression loading model has evolved as a useful model

to investigate the response of bone to mechanical loading[199 223]. It allows controlled

mechanical loads to be introduced both non-invasively and unilaterally, enabling bone

responses to be explored in the absence of trauma and with the contralateral side serving

as an internal control site. These features represent an advance on alternative loading

models, such as jump training and treadmill running which load the skeleton bilaterally,

and the rodent 4-point loading model which causes traumatic periosteal woven bone

formation (see Robling et al.[318] for review). However, the ulna axial compression loading model does not readily allow investigation of trabecular bone responses to loading due to the principally cortical bone structure of the rodent ulna with virtual lack of trabeculae.

The mouse tibial axial compression loading model has recently been described to enable simultaneous exploration of cortical and trabecular bone adaptation to mechanical loading within a single bone[200 261]. The model involves axially loading the tibia through a flexed knee and dorsiflexed ankle. Because of the natural curvature of the tibia, the compressive load applied to the bone is converted into bending with peak compressive strain engendered at the posterolateral border and peak tensile strain at the anteromedial surface of the tibial diaphysis[203 231 319]. Studies utilizing the model have generally demonstrated a loading benefit on trabecular bone volume fraction (bone volume [BV]/total volume [TV]) within the proximal tibia[170 200 203 229 230 261 320-327]. However, BV/TV decreased in some studies depending on experimental conditions[200 231 328 329], and a dose response to load magnitude on BV/TV within the proximal tibia has yet to be clearly demonstrated[229-231 324]. In terms of cortical bone, previous work using the mouse tibial axial compression loading model has demonstrated a clear dose response to load magnitude at the tibial diaphysis[200 229-231]; however, woven bone formation on the periosteal surface is often evident[170 203 230 231 324-327 330]. As woven bone apposition is considered a pathological response to excessive load and subsequent damage accumulation[331], its frequent observation limits the ability of the mouse tibial axial compression loading model to allow simultaneous exploration of non-pathological (i.e. lamellar) cortical and trabecular bone adaptation to mechanical loading.

To further the understanding of the mouse tibial axial compression loading model, the current study aimed to investigate combined cortical and trabecular bone adaptation to incremental load magnitudes. The ultimate goal was to reveal a load magnitude that simultaneously induced lamellar cortical and trabecular bone adaptation.

2.2   Methods

2.2.1   Animals

Forty female C57BL/6 mice were purchased (Jackson Laboratories, Bar Harbor, ME) and acclimated until 16 weeks of age. Animals were housed under standardized conditions with *ad libitum* access to standard mouse chow and water. All procedures were performed with prior approval from the Institutional Animal Care and Use Committee of Indiana University.

2.2.2   Strain gauge

Four mice were randomly selected for a load-strain calibration study. The right hind limbs were harvested after euthanasia and stored at -20°C. Limbs were allowed to warm to room temperature over several hours on the day of strain gauge measurement and the medial surface of the mid-diaphysis was minimally exposed. A single element strain gauge (EA-06-015DJ-120; Measurements Group, Inc., Raleigh, NC) was bonded with cyanoacrylate (M-Bond 200; Measurements Group, Inc., Raleigh, NC) to the middle

of the medial surface of the midshaft tibia. The leg was axially loaded at a frequency of 2 Hz and peak loads of 3, 5, 7 and 9 N using the same loading system as used for experimentation (see *In-vivo axial tibial loading*). The strain gauge voltage signal was routed through a signal conditioning amplifier (Model 2210; Measurements Group, Inc., Raleigh, NC), and the peak-to-peak voltage measured on a digital oscilloscope. Voltage was converted to strain using a calibration factor derived from measured and calculated (using beam theory) strains collected using an aluminum cantilever.

2.2.3   Axial tibial loading

Thirty-six mice were randomly divided into three load magnitude groups—5, 7 and 9 N. The right leg was fixed between molded knee and foot cups on a computer-controlled electromagnetic mechanical actuator (Enduratec ELF 3200; Bose Corporation, Eden Prairie, MN), with the animal under isoflurane anesthesia (Abbott Laboratories, North Chicago, IL). The tibia was axially loaded across a near fully flexed knee and dorsiflexed ankle. Loading was applied with a continuous 2-Hz haversine waveform for 360 cycles/d, 3 d/wk for 4 consecutive weeks. Left legs were not loaded, with left tibiae serving as internal controls. A recent study using the tibial axial compression loading model found loading effects were isolated to loaded bones[170]. Normal cage activity was allowed between loading sessions.

<u>2.2.4</u>   *<u>In-vivo</u>* <u>pQCT</u>

Cortical bone adaptation to mechanical loading was assessed *in-vivo* using peripheral quantitative computed tomography (Stratec XCT Research SA+; Stratec Medizintechnik GmbH, Pforzheim, Germany). Animals were positioned on a custom scanning platform at baseline and following the 4 wk loading regime, with the animal under isoflurane anesthesia (Abbott Laboratories, North Chicago, IL). Each leg was centered in the machine gantry and a scout scan of the tibia performed for tomographic scan localization. A tomographic scan was performed at the midshaft tibia using a 0.46-mm collimation and 70 μm voxel size. This voxel size is relatively large compared to the cortical thickness of the mouse tibial midshaft increasing the potential for partial volume effects. However, good agreement has previously been shown between pQCT, micro-computerized tomography (μCT) and histological measures of cortical bone properties in mice[332]. Analyses were restricted to cortical bone using contour mode 1 with a threshold of 400 mg/cm^3 within the Stratec software (version 6.20C; Stratec Medizintechnik GmbH, Pforzheim, Germany). Total bone mineral content (Tt.BMC; mg/cm), total bone area (Tt.Ar; mm^2), and cortical area (Ct.Ar; mm^2) were recorded for each bone, and the minimum (I_{MIN}; mm^4) and maximum second moments of area (I_{MAX}; mm^4) derived according to Gere and Timoshenko[333]. Medullary area (Me.Ar; mm^2) was derived as Tt.Ar minus Ct.Ar.

2.2.5 _Ex-vivo_ μCT

Animals were euthanized following the 4 wk loading regime, and the right and left tibias dissected free and placed in 10% neutral buffered formalin for 48 hours before being stored in 70% alcohol. A desktop micro-computerized tomography machine (μCT-20; Scanco Medical AG, Auenring, Switzerland) scanning with an isotropic voxel size of 9 μm was used to assess cortical bone geometry at 1 mm increments along the entire tibial diaphysis. Tomographic images were imported into ImageJ (National Institutes of Health, MD) wherein the polar moment of inertia (I_P) was derived as the sum of the I_{MAX} and I_{MIN} measurements, with I_{MAX} and I_{MIN} being determined using standard and custom macros. The same desktop micro-computerized tomography machine was also used to assess trabecular bone properties within the proximal tibial metaphysis. 122 slices were acquired distal to the proximal tibial growth plate using a 13 μm voxel size. Images were reconstructed using a standard convolution-back projection procedure with a Shepp-Logan filter at a threshold of 275, and trabecular BV/TV (%), number (Tb.N; mm^{-1}), thickness (Tb.Th; mm) and separation (Tb.Sp; mm) acquired.

2.2.6 Histomorphometry

Alizarin (15 mg/kg; Sigma Chemical Co., St. Louis, MO) was given 27 days, and calcein (10 mg/kg; Sigma Chemical Co., St. Louis, MO) was given 10 days and 6 days before euthanasia by intraperitoneal injection to permit determination of bone formation rates. The tibiae were harvested and fixed in 10% neutral buffer formalin for 48 hours

before being stored in 70% ethanol. The bones were embedded in decalcified in 99%

methyl-methacrylate with 3% dibutyl phthalate (Sigma-Aldrich, St. Louis, MO).

Transverse thick (40-50 µm) sections were removed from the tibial midshaft using a

diamond-embedded wire saw (Histo-saw; Delaware Diamond Knives), and mounted

unstained to assess periosteal bone formation rate. Frontal plane thin (4 µm) sections of

the proximal tibia were taken using a microtome (Reichert-Jung 2050; Reichert-Jung,

Heidelberg, Germany), and mounted either unstained to enable determination of

trabecular bone formation rate or stained with tartrate-resistant acid phosphatase and

counterstained with hematoxylin (Sigma-Aldrich, Kit #387A-1KT, St. Louis, MO) to

allow identification of trabecular osteoclasts.

Sections were montaged using Image-Pro Plus (Version 7.0; Media Cybernetics,

Inc., Bethesda, MD) on a Leica DMI6000 inverted microscope (Leica Mikrosysteme

Vertrieb GmbH, Wetzlar, *Germany*) and stored digitally. Dynamic parameters were

measured from the unstained midshaft and proximal tibia sections, and included single-

label perimeter (sL.Pm), double-label area (dL.Ar) and perimeter (dL.Pm), and interlabel

width (Ir.L.Wi). Cortical bone dynamic parameters were measured using the alizarin and

calcein labels (21 day interlabel period), whereas trabecular bone dynamic parameters

were measured using the dual calcein labels (4 day interlabel period). The following were

derived from the primary data: mineralizing surface (MS/BS=[1/2sL.Pm+dL.Pm]/B.Pm;

%), mineral apposition rate (MAR=mean Ir.L.Wi/interlabel period; µm/d), and bone

formation rate (BFR/BS=MARxMS/BSx3.65; $\mu m^3/\mu m^2/yr$). The region of interest within

the proximal tibia consisted of a 1 mm^2 box positioned 1.0 mm distal from the growth

plate within the secondary spongiosa. Bone resorption was determined from stained

sections of the proximal tibia by counting the number of bone-adherent, multinucleate, tartrate-resistant acid phosphatase positive cells (osteoclasts) within 1 mm^2 of the secondary spongiosa and normalizing to bone surface (Oc.N/BS).

2.2.7 Statistical analysis

Statistical analyses were performed with the Statistical Package for Social Sciences for Windows (Version 19.0; SPSS Inc., Chicago, USA), with a level of significance set at 0.05 for all tests. The effect of loading (loaded vs. nonloaded) within each load magnitude group was assessed by paired t-tests. The effect of load magnitude (5 N vs. 7 N vs. 9 N) on the loaded side was assessed using one-way analyses of covariance (ANCOVA) followed by Bonferroni pairwise comparisons, with the nonloaded side serving as the covariate.

2.3 Results

One mouse in each of the 5 N and 7 N groups experienced a tibial fracture on the first day of loading due to malfunction with the loading machine. One mouse from the 9 N group experienced a tibial fracture during the first week of loading, presumably due to mechanical overload. Each of these mice were immediately euthanized and their data excluded from the study.

2.3.1 Strain gauge data

The results of the preliminary load-strain calibration are illustrated in Figure 2.1. Bone strain on the medial surface of the midshaft tibia demonstrated a linear increase in response to incremental externally applied loads ($R^2 = 0.99$; $P < 0.001$), with 9 N inducing a tensile strain of 1,833 $\mu\varepsilon$ (95% confidence interval [CI], 1,460 $\mu\varepsilon$ to 2,206 $\mu\varepsilon$).
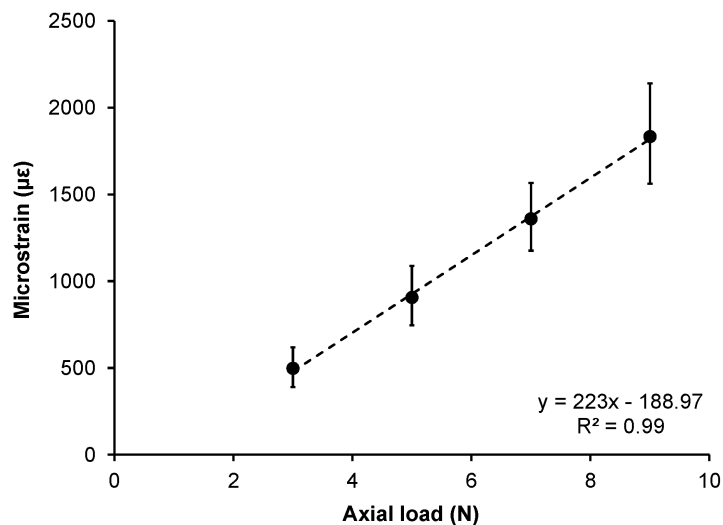
Figure 2.1. Strain engendered on the medial surface of the midshaft tibia in response to incremental external load magnitudes. Error bars represent 95% confidence intervals.

2.3.2 Cortical bone adaptation

The effects of loading and load magnitude on *in-vivo* adaptation of the cortical midshaft tibia are shown in Figure 2.2. The loaded hind limb in all load magnitude groups had greater gains in Tt.BMC, Ct.Ar and I_{MIN} than in the contralateral non-loaded hind limb (all $P < 0.05$), with loading at 9 N inducing relative gains of 23.1% (95% CI,

17.6% to 28.7%), 19.7% (95% CI, 11.8% to 27.6%) and 27.5% (95% CI, 14.7% to 40.4%) in Tt.BMC, Ct.Ar and I_{MIN}, respectively. The loaded hind limb in the 5 N and 9 N groups also had greater gains in Tt.Ar and I_{MAX} than in the non-loaded hind limb (all $P <$ 0.05), with loading at 9 N inducing relative gains of 13.9% (95% CI, 7.1% to 20.7%) and 42.2% (95% CI, 20.6% to 63.9%) in Tt.Ar and I_{MAX}, respectively. There was no effect of loading on Me.Ar in any load magnitude group (all $P > 0. 05$).

There was a dose-response to external loading magnitude at the midshaft tibia, with higher loads inducing greater adaptation. The 9 N group had greater gains in all properties of the loaded midshaft tibia compared to the 5 N group (all $P < 0.05$) (Figure 2.2). Loading at 9 N also induced greater gains in Tt.BMC, Tt.Ar and I_{MAX} of the loaded midshaft tibia compared to 7 N (all $P < 0.05$). There were no differences in midshaft tibia adaptation between loading at 5 N and 7 N (all $P > 0.05$).

Cortical bone adaptation (as indicated by I_P) was greatest at the midshaft tibia in all load magnitude groups; however, loading induced adaptation both proximal and distal to the midshaft (Figure 2.3). Adaptation in the 9 N group was significantly greater in the proximal two-thirds and half of the bone than the 5 N and 7 N groups, respectively. There were no differences in cortical bone adaptation along the bone length between the 5 N and 7 N groups (all $P > 0.05$).
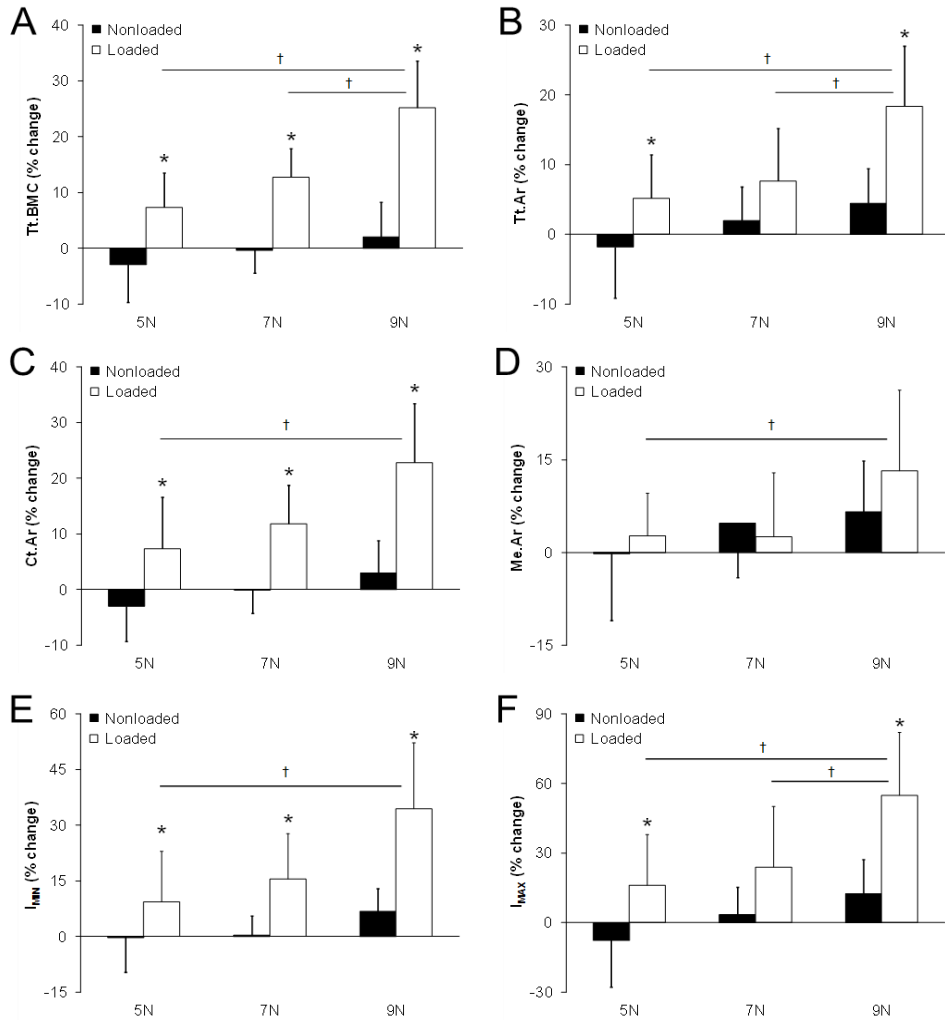
Figure 2.2. Effect of loading and load magnitude on percent change in tibial midshaft: A) Tt.BMC; B) Tt.Ar; C) Ct.Ar; D) Me.Ar; E) I$_{MIN}$, and; F) I$_{MAX}$. Bars represent mean ± SD. *indicates significant loading effect (nonloaded vs. loaded) within respective load magnitude group, as assessed by paired t-test. †indicates significant difference in loaded tibiae between respective load magnitude groups, as assessed by one-way analyses of covariance (with the nonloaded side serving as the covariate) followed by Bonferroni pairwise comparisons.

Figure 2.3. Effect of loading and load magnitude on percent difference in I_P between loaded and nonloaded tibiae at 1 mm increments along the bone length. Error bars indicate 95% confidence intervals, with bars not crossing zero (x-axis) indicating a significant loading (loaded vs. nonloaded) effect within the respective load magnitude group. Symbols indicate that the percent difference (loaded vs. nonloaded) in I_P in the 9 N differed significantly from in the 5 N (*) and 7 N (†) groups, as assessed by one-way analyses of covariance followed by Bonferroni pairwise comparisons.

Histomorphometrically, there was no evidence of woven bone formation in any loaded tibia (Figure 2.4). The loaded hind limb in all load magnitude groups had higher periosteal MS/BS at the midshaft tibia compared to the contralateral nonloaded hind limb (all $P < 0.05$) (Figure 2.5), with loading at 9 N inducing relative gains of 40.4% (95% CI, 31.1% to 49.7%). The loaded hind limb in the 5 N and 9 N groups also had greater gains in periosteal MAR and BFR/BS than in the nonloaded hind limb (all $P < 0.05$), with loading at 9 N increasing MAR and BFR/BS by 4- and 7-fold respectively. There was a load magnitude response at the midshaft tibia with the 9 N group having greater gains in periosteal MS/BS, MAR and BFR/BS compared to both the 5 N and 7 N groups (all $P <$

0.05) (Figure 2.4). There were no differences in midshaft tibia adaptation between the 5

N and 7 N groups (all *P* >0.05).
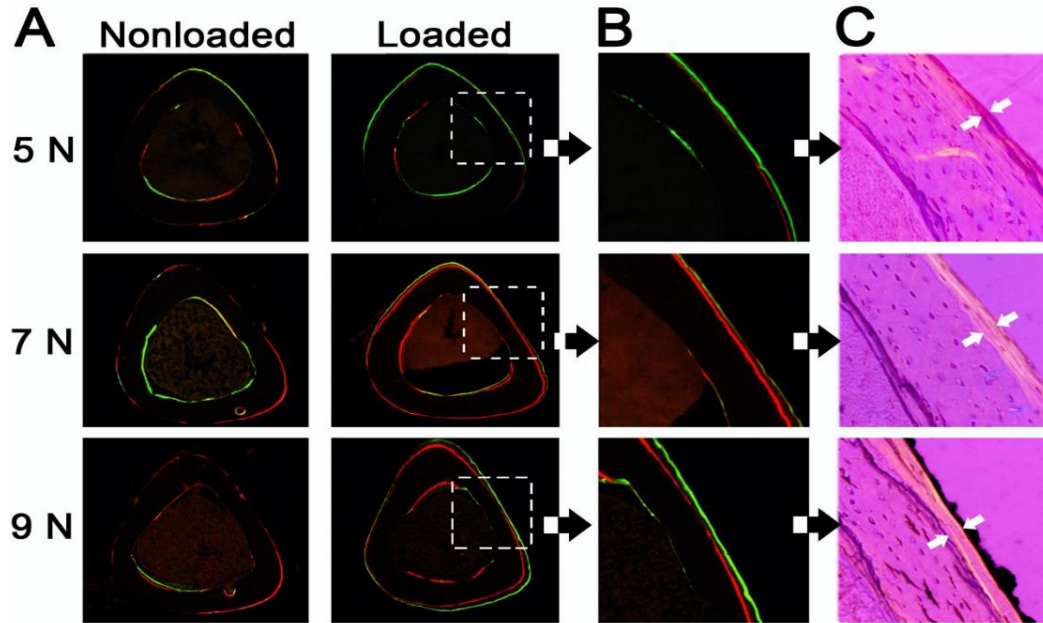
Figure 2.4. Representative histological images of the midshaft tibia from nonloaded and loaded tibiae in each load magnitude group under: A-B) fluorescent and C) polarized light. A) Note the greater labeling in the loaded tibia, with B) uniform double labeling [lamellar bone formation] and absence of diffuse labeling [woven bone formation]. C) Lamellar bone formation in the region of alizarin and calcein labeling (white arrows) was confirmed under polarized light.
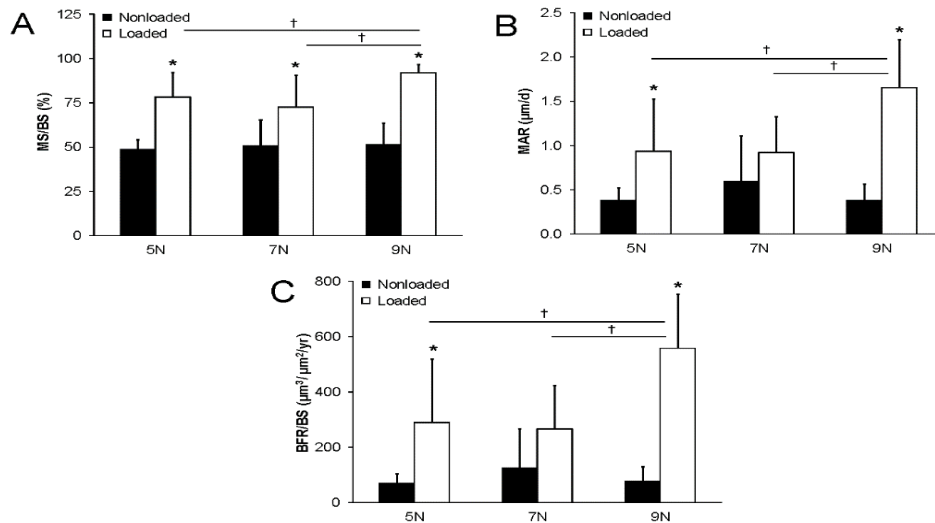
Figure 2.5. Effect of loading and load magnitude on tibial midshaft periosteal: A) MS/BS; B) MAR, and; C) BFR/BS. Bars represent mean ± SD. *indicates significant loading effect (nonloaded vs. loaded) within respective load magnitude group, as assessed by paired t-test. †indicates significant difference in loaded tibiae between respective load magnitudes, as assessed by one-way analyses of covariance (with the nonloaded side serving as the covariate) followed by Bonferroni pairwise comparisons.

2.3.3   Trabecular bone adaptation

The effects of loading and load magnitude on trabecular bone adaptation within the proximal tibia are shown in Figure 2.6. The loaded hind limb in the 9 N group had 30.8% (95% CI, 12.9% to 48.7%) and 23.8% (95% CI, 16.9% to 30.8%) higher BV/TV and Tb.Th compared to the contralateral nonloaded hind limb, respectively (all $P < 0.05$). There were no loading effects on any trabecular bone properties in the 5 N and 7 N groups, or on Tb.N or Tb.Sp in the 9 N group (all $P > 0.05$). Comparing across load magnitudes (and using the nonloaded hind limb as a covariate), the 9 N group had 21.9% (95% CI, 3.95% to 39.8%) higher BV/TV within the proximal tibia compared to the 5 N group, and 23.0% (95% CI, 3.95% to 39.8%) and 15.3% (95% CI, 7.69 % to 23.1%) higher Tb.Th than both the 5 N and 7 N groups, respectively (all $P < 0.05$) (Figure 2.6).

Histomorphometrically, there was no effect of load on trabecular bone formation (MS/BS, MAR, BFR/BS) or resorption (Oc.N/BS) indexes within the proximal tibia of the loaded hind limb when compared to the contralateral nonloaded hind limb (Figure 2.7). Comparing across load magnitudes (and using the nonloaded hind limb as a covariate), the loaded hind limb in the 9 N group had 19.3% (95% CI, .8795 % to 37.8%) higher trabecular MAR within the proximal tibia compared to the 5 N group ($P = 0.038$) (Figure 2.7). There was no effect of load magnitude on trabecular MS/BS, BFR/BS or Oc.N/BS (all $P > 0.05$).
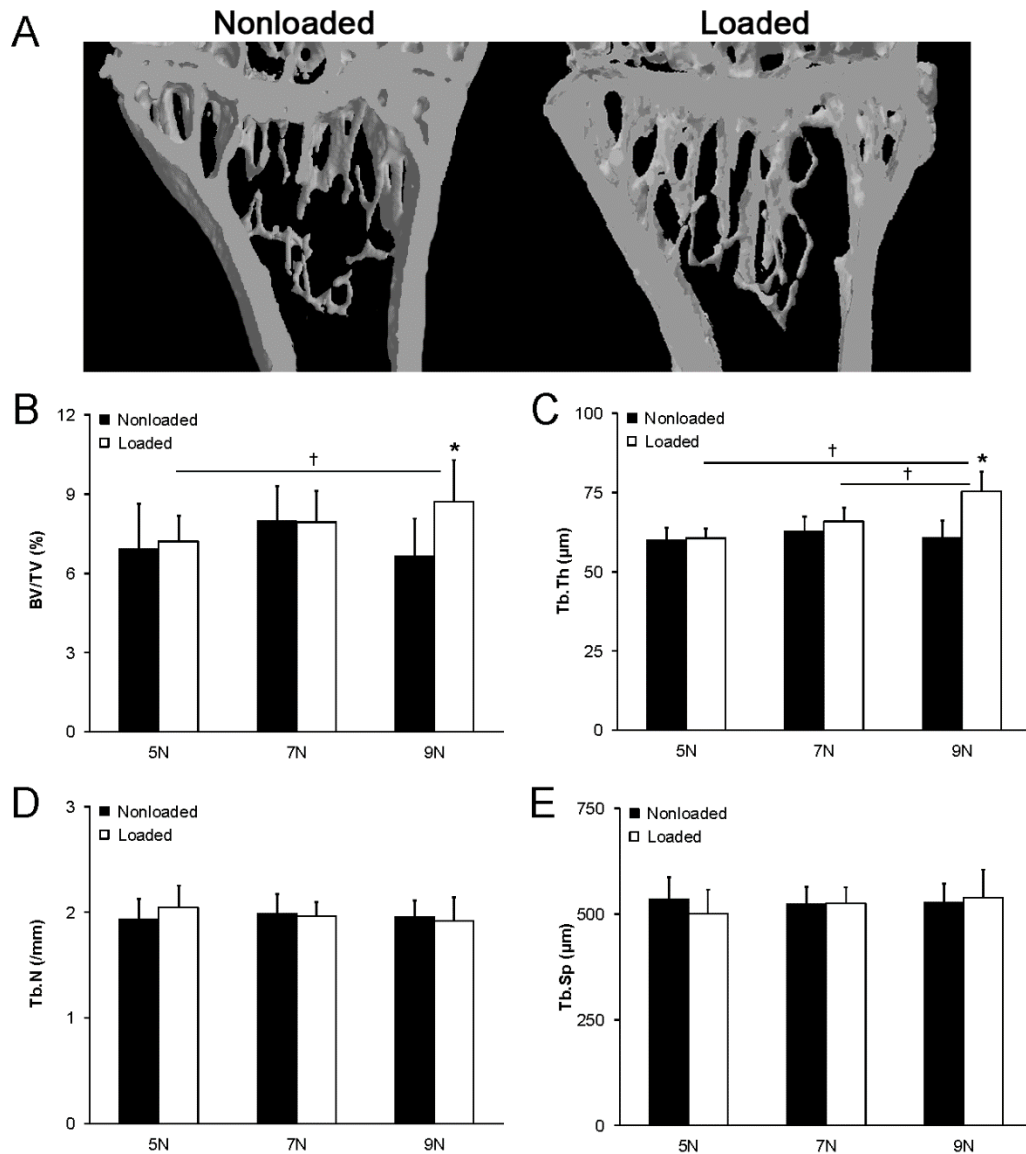
Figure 2.6. Effect of loading and load magnitude on: A) representative (150 μm thick) frontal plane three-dimensional reconstructions of trabecular architecture within the proximal tibia of the highest [9N] load group; B) BV/TV]; C) Tb.Th; D) Tb.N, and; E) Tb.Sp. In A), note the increased BV/TV and Tb.Th in the loaded proximal tibia. Bars in (B-E) represent mean ± SD. *indicates significant loading effect (nonloaded vs. loaded) within respective load magnitude group, as assessed by paired t-test. †indicates significant difference in loaded tibiae between respective load magnitudes, as assessed by one-way analyses of covariance (with the nonloaded side serving as the covariate) followed by Bonferroni pairwise comparisons.

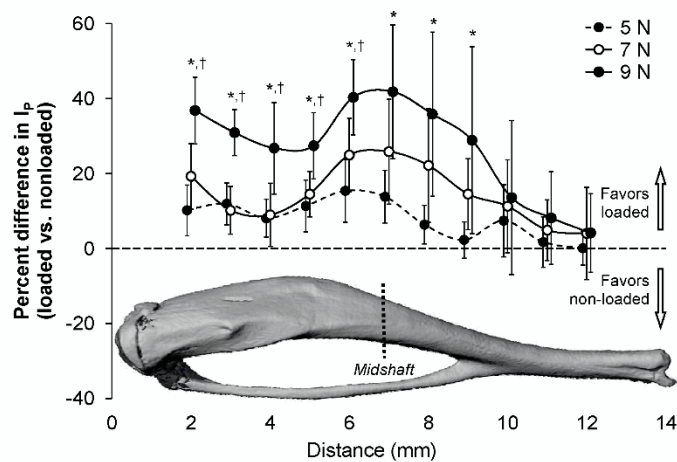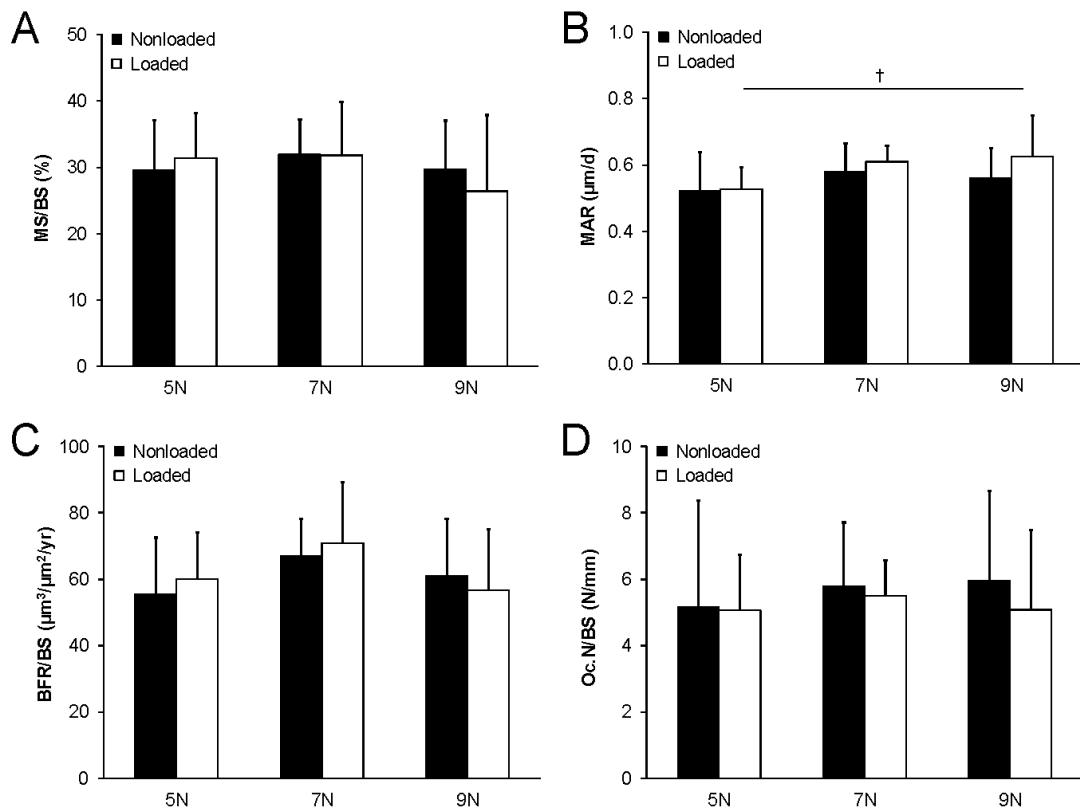**Figure 2.7. Effect of loading and load magnitude on proximal tibia trabecular: A) MS/BS; B) MAR; C) BFR/BS, and D) N.Oc/BS.** Bars represent mean ± SD. †indicates significant difference in loaded tibiae between respective load magnitudes, as assessed by one-way analyses of covariance (with the nonloaded side serving as the covariate) followed by Bonferroni pairwise comparisons.

2.4   Discussion

The current study investigated the influence of load magnitude on cortical and trabecular bone adaptation using the mouse tibial axial compression loading model. A dose response to loading magnitude within cortical bone was observed, with increasing load magnitude inducing increasing levels of cortical bone adaptation within the upper two thirds of the tibial diaphysis. The greatest cortical adaptation was observed at the midshaft tibia where there was a 42% increase in estimated mechanical properties (I_P)

over the 4 week loading period in the highest (9 N) load group. The increase in estimated mechanical properties resulted from an increase in periosteal lamellar bone apposition. A dose response to load magnitude was not clearly evident within trabecular bone, with only the highest load (9 N) being able to induce measureable adaptation (31% increase in BV/TV at the proximal tibia). The ultimate finding of the study was that a load of 9 N (engendering a tensile strain of 1,833 με on medial surface of the midshaft tibia) was able to simultaneously induce lamellar cortical and trabecular bone adaptation when using the mouse tibial axial compression loading model in 16 week old female C57BL/6 mice.

The observed dose response of cortical bone to loading magnitude is consistent with the vast body of evidence provided from alternative loading models, as well as previous studies using the mouse tibial axial compression loading model[200 229-231]. A maximum load of 9 N was chosen for the current investigation as preliminary work in our laboratory using the mouse tibial axial compression loading model demonstrated loads in excess of 10 N resulted in periosteal woven bone formation and fractures (*unpublished data*). Also, representative microCT and histology images in previously published studies using the mouse tibial axial compression loading model are suggestive of woven bone formation when higher load magnitudes (>10 N) are introduced[170 203 230 324-327 330].

When comparing skeletal responses to mechanical load across studies it is important to consider the tissue level strain engendered. Strain provides an indication of the tissue level mechanical stimulus, and varies for a given external load magnitude as a result of alterations in bone quality (which includes bone structure, geometry and composition). Cortical bone strains in the current study were on the high end of those previously reported using the mouse tibial axial compression loading model. For

instance, loading in the current study engendered a tensile strain of 223 µε/N on the

medial surface of the midshaft tibia, which compares to strains in the range of 77 µε/N to

250 µε/N[200 229 230 261 321 329 334 335] reported in previous studies. Possible explanations for

the relatively high strains per given external load in the current study are unknown, but

may include the age, sex and genotype of animals being investigated, strain gauge

measurements being performed *ex-vivo*, strain gauge position relative to the bending axis,

and position of the knee joint during loading (see discussion below), to name a few.

Irrespective of the reason for the difference in measured strain per unit load between

studies, the fact remains that woven bone was not induced in the current study at the

loads introduced and subsequent strains engendered.

Cortical bone adaptation in the current study occurred in the proximal two-thirds

of the diaphysis and principally at the midshaft tibia. This pattern of adaptation differs

from that reported by van der Meulen and colleagues[261 336]. The latter investigators

loaded 10 week old male C57BL/6 mice for up to 6 weeks using the mouse tibial axial

compression loading model to induce adaptation in the proximal half of the tibial

diaphysis (as indicated by *ex-vivo* micro-CT measures of I_{MAX} and I_{MIN}) with the greatest

adaptation proximally, as opposed to at the midshaft. A possible explanation for the

disparity between studies in the location of maximal adaptation is the position of the knee

joint during loading which may influence strain distribution within the tibia. The knee

was positioned in near full flexion during loading in the current study, as opposed to 90°

flexion in the studies by van der Meulen and colleagues. The greater knee flexion in the

current study potentially moved the femoral condyles more caudally on the tibial plateau

increasing the bending lever arm and promoting conversion of the axial compressive load into bending at the tibial midshaft.

Axial compressive loading of the tibia induced trabecular bone adaptation within the proximal tibia, with BV/TV increasing by 31% in the highest load (9 N) group over the 4 week loading period. This magnitude of change is comparable to published studies; however, a wide range has previously been reported. For instance, some studies have reported a loss of BV/TV when using the tibial axial compression loading model[200 230 231 328 329], whereas others loading for as little as 2 weeks have reported BV/TV increases of between 11% and 81%[170 229 230 261 321 324-327 330], and changes of 15% to 68% when loading for as long as 6 weeks[261 336]. Factors potentially contributing to these large ranges include the age, sex and genotype of animals being investigated, loading parameters (such as the loading waveform shape, load magnitude, inclusion of rest periods between cycles, duration of loading, number of loading cycles), and region analyzed within the proximal tibia.

BV/TV increased in the current study as a result of new bone being deposited on pre-existing trabeculae (as indicated by an increase in Tb.Th), as opposed to the construction of new trabeculae (as indicated by the absence of a load effect on Tb.N) or a decrease in bone resorption (as indicated by the absence of a load effect on Oc.N/BS). A concomitant increase in trabecular bone formation was not measured histomorphometrically; however, this may reflect a decline in mechanoresponsiveness with continued loading[249] and our measurement of trabecular bone formation indexes towards the end of the loading program. The absence of a significant histomorphometrical finding may also be due to the greater variance associated with

histomorphometric measures of trabecular bone and consequent reduction in statistical power.

There was a lack of a clear dose response of trabecular bone to load magnitude in the current study, with trabecular bone adaptation only being detected in the highest load (9 N) group. Other investigators using a variety of loading models including the mouse tibial axial loading model have demonstrated progressive trabecular bone adaptation to increasing loads[217 229 230 324 337]. The inability to demonstrate trabecular adaptation in the lower load groups (5 N and 7 N) in the current study may relate to the inability of these lower loads to surpass the osteogenic threshold at the site assessed or the induction of lameness with the mouse tibial axial loading model. In terms of the latter, there is a possibility that the model causes some degree of lameness-induced unloading which may have obscured any trabecular bone benefits in the lower load groups. We did not assess lameness following tibial axial loading through the quantification of ground reaction forces; however, lameness may explain why some studies using this model have observed a loss of BV/TV[200 231 328], and needs further exploration considering axial loading of the mouse leg through a near fully flexed knee has been associated with knee joint degeneration[338].

In summary, the current data indicate that tibial axial loading is a useful model to explore combined cortical and trabecular bone adaption in mice, and that a load of 9 N (engendering a tensile strain of 1,833 $\mu\varepsilon$ on medial surface of the midshaft tibia) is able to simultaneously induce lamellar cortical and trabecular bone adaptation in 16 week old female C57BL/6 mice.

CHAPTER THREE: PREDICTIVE ABILITY AND SHORT-TERM PRECISION OF

pQCT ESTIMATES OF MIDSHAFT HUMERUS MECHANICAL PROPERTIES

3.1 Introduction

Peripheral quantitative computed tomography (pQCT) uses a small purpose-built

scanner with a low radiation X-ray source to obtain tomographic images of the

extremities. While not comparable to dual-energy X-ray absorptiometry (DXA) in terms

of clinical availability and acceptance, pQCT has become a popular research tool for

assessing bone properties as it has the advantage of being able to image bone tissue in

three dimensions. The three dimensional nature of pQCT measures enables assessment of

volumetric density and cross-sectional structure, measures that may have advantages in

estimating bone size and strength. For instance, the addition of pQCT-derived indices of

estimated strength improved fracture prediction beyond that provided by DXA-derived

areal bone mineral density (aBMD) alone[339][340]. Also, pQCT may reveal novel

observations that may otherwise be missed with the sole use of DXA. For example,

pQCT was recently used to demonstrate that exercise completed when young had lasting

benefits on bone size and estimated strength, despite the loss of DXA-derived bone mass

benefits[164][165].

To facilitate the use and acceptance of pQCT, its needs to provide precise (i.e.

reproducible) measures that are good predictors of actual bone properties. Previous

studies have explored the predictive ability and short-term precision of pQCT measures

of estimated bone strength at the most popular imaging sites—tibial and radial diaphysis

and distal metaphysis[341-355]. At diaphyseal sites, pQCT provides estimates of bone strength via the calculation of cross-sectional moments of inertia and section moduli. Multiplying these structural-based measures by the quotient of pQCT measured cortical density and physiologic density (1200 mg/cm^3) is used to account for the influence of bone material properties, with the density-weighted section modulus provided by pQCT being generally referred to as the Strength Strain Index (SSI)[356 357]. SSI (and analogous pQCT-derived strength estimates) of the radial and tibial diaphysis have been shown to be relatively predictive and precise, predicting 66-98% of the variance in the ability to resist bending forces[346-348 355] and having root mean squared coefficients of variation (RMS-CV) typically <2.5%[342 343 345 351-354].

While pQCT provides predictive and precise estimates of bone mechanical properties at distal imaging sites, its predictive ability and precision at more proximal sites remains unknown. The upper arm is a proximal site gaining popularity for pQCT imaging as the humeral diaphysis is a frequent site for pQCT studies exploring the skeletal effects of exercise[159 165 358-366]. It is possible that precision of pQCT measures of the upper arm is less than at distal sites due to a combination of factors, including heightened difficulty repetitively positioning subjects further than usual within the machine gantry, greater potential for subtle movement artifacts due to difficulty stabilizing the proximal end of the bone against subtle trunk motions (including respiration), and a larger limb volume than present distally which heightens beam hardening and reduces pQCT accuracy and precision[352 353]. In support of possibly reduced pQCT precision when imaging the upper arm, preliminary work by Sievänen et al.[352] reported a RMS-CV of 5.6% for estimated strength measures of the midshaft humerus.

The aim of the current study was to explore the predictive ability and short-term precision of pQCT estimates of midshaft humerus mechanical properties. Predictive ability was determined *ex-vivo* by assessing the ability of pQCT-derived estimates of torsional mechanical properties in cadaver humeri to predict actual torsional properties. Short-term precision was assessed *in-vivo* by six repeat pQCT scans performed at the level of the midshaft humerus in 30 healthy individuals, with repeat scans performed by the same and different testers and on the same and different days to explore the influences of different testers and time between repeat scans on precision errors.

3.2   Methods

3.2.1   *Ex-vivo* predictive ability

a) Cellular elements specimens and imaging

Unilateral humeri were dissected from 20 fresh human cadavers following approval from the Institutional Review Board of Indiana University. The bones were cleaned of soft-tissues, wrapped in saline-soaked dressings, and stored at -20°C. Prior to imaging, humerii were thawed to room temperature and had their length measured to the nearest 1 mm using a sliding anthropometer. Length was measured as the distance between the superior aspect of the greater tubercle and inferior aspect of the capitulum, which is consistent with how humeral length is measured *in-vivo* prior to pQCT[165 358 366]. Each humerus was positioned on their posterior side in the gantry of a Stratec XCT 3000 machine equipped with Stratec software version 6.20C (Stratec Medizintechnik GmbH,

Pforzheim, Germany). A scout scan was performed and a reference line placed at the inferior aspect of the capitulum. A tomographic slice (thickness=2.3 mm; voxel size=300 μm; scan speed=20 mm/s) was taken at 50% of humeral length (midshaft) from the reference line. The specimens were kept moist during imaging via saline-soaked dressings.

Each tomographic slice was analyzed using the Stratec software to obtain bone mineral density, structure, and estimated strength. Cortical mode 1 (threshold, 710 mg/cm^3) was used to obtain cortical volumetric bone mineral density (Ct.vBMD, mg/cm^3), bone mineral content (Ct.BMC, mg/mm), and area (Ct.Ar, cm^2). Total area (Tt.Ar, cm^2), periosteal (Ps.Pm, mm) and endocortical (Ec.Pm, mm) perimeters, and average cortical thickness (Ct.Th, mm) were obtained by analyzing the slices using contour mode 1 (threshold, 710 mg/cm^3) to define the outer bone edge and peel mode 2 (threshold, 400 mg/cm^3) to separate the cortical and subcortical/medullary compartments. Thickness and perimeter measures used a circular ring model, and medullary area (mm^2) was derived as total area minus cortical area. Bone strength was estimated by the density-weighted polar moment of inertia (I$_P$, mm^4) and polar SSI (SSI$_P$, mm^3) obtained in a separate analysis using cortical mode 2 (threshold = 400 mg/cm^3). A lower threshold was used for the assessments of I$_P$ and SSI$_P$ as the use of density-weighting minimizes partial volume effects[367].

b) *Mechanical testing*

112

Mechanical testing was performed at room temperature with the specimens being kept moist with frequent saline solution irrigation. The proximal and distal ends of each humerus were potted in custom-designed aluminum potting boxes using high strength resin (Bondo Body Filler; 3M Collision Repair Solutions, St. Paul, MN USA). The boxes were subsequently rigidly coupled to a servohydraulic materials testing machine (Bionix; MTS Systems Corporation, Eden Prairie, MN) equipped with an axial/torsional load cell rated to ±25 kN (axial load) and ±250 N.m (torsional load) (Figure 3.1A). The longitudinal axis of the diaphysis was aligned with the load frame and an axial compressive preload of 20 N was applied to establish a consistent reference configuration. The proximal humerus was externally rotated in displacement control at 10˚/s until failure, which was defined as a sharp decrease in the monotonically increasing torque profile. Biomechanical parameters of interest included maximum torque at failure (N.m) and torsional rigidity (N.m/˚), with the latter being defined as the linear portion of the torque versus angular displacement curve (Figure 3.1B). Data were collected at 50 Hz, and mode and location of failure were documented with digital images.
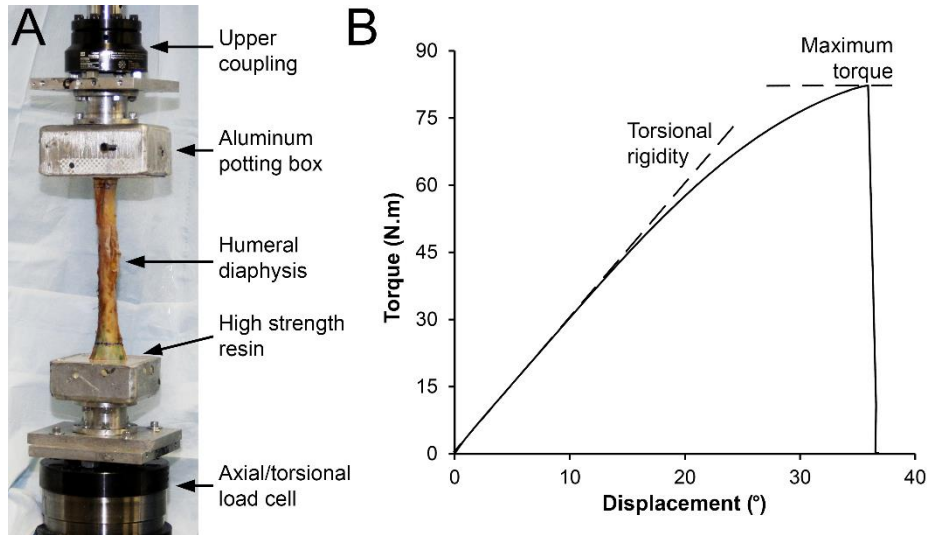
Figure 3.1. A) Experimental set-up for torsional mechanical testing of the humeral diaphysis. B) Representative torque-displacement curve generated from torsional testing of a cadaveric humerus. Properties derived from the curve were maximum torque at failure (peak of the curve on the y-axis) and torsional rigidity (slope of the linear portion of the curve).

3.2.2 *In-vivo* short-term precision

a) Subjects

A convenience sample of 30 healthy subjects was recruited. Subjects were included if they were ≥18 years of age, did not have implanted metal, and were not pregnant. Subjects presented for repeat testing on two separate days, a minimum of one week apart. Height, weight and humeral length were measured, and pQCT performed during the first study visit. During the second study visit, only humeral length was measured and pQCT performed. Assessments in each subject were performed on the non-dominant arm. The study was approved by the Institutional Review Board of Indiana University and all subjects provided informed consent prior to participation.

b) Anthropometric measures

Height (to nearest 0.1 cm) and weight (to nearest 0.1 kg) were measured using a wall mounted digital stadiometer and electronic balance scale, respectively. Body mass index (BMI, kg/m^2) was calculated as mass divided by height squared. Humeral length (to nearest 1 mm) was measured using a sliding anthropometer as the distance between the lateral border of the acromion (representing the superior aspect of the greater tubercle) and the radiohumeral joint line (representing the inferior aspect of the capitulum). Humeral length was measured during each study visit by two testers to determine within- and between-tester and within- and between-day reproducibility. The mean of the measures obtained during the first study visit was used as humeral length for localization of pQCT scans.

c) pQCT

Six scans of the humerus within the non-dominant upper extremity were performed using the same pQCT machine and scanning parameters as used to image the cadaver specimens. Four scans were performed during the first study visit, with each tester performing two scans with interim repositioning. During the second study visit, each subject was scanned twice with testers performing one scan each. A cone phantom was scanned at the beginning of each scan day to confirm machine calibration. For scanning, subjects were positioned supine with their non-dominant arm in 90˚ shoulder abduction and centered in the gantry of the pQCT machine. A concave, plastic, padded holder was placed under the arm for support and elastic restraints were positioned around the supracondylar region and surgical neck of the humerus to minimize movement. A

scout scan was performed to observe the radiohumeral joint, a reference line placed

through the joint at the distal edge of the humeral capitulum, and a tomographic slice

taken at 50% of humeral length (midshaft) from the reference line. Each tomographic

slice was analyzed as described for the cadaveric specimens to obtain bone mineral

density, structure, and estimated strength. In addition, each slice was analyzed to obtain

soft tissue composition at the level of midshaft humerus using contour mode 3 (threshold,

-100 mg/cm^3) to locate the skin surface and peel mode 2 (threshold, 40 mg/cm^3) to locate

the subcutaneous fat–muscle boundary. A 3×3 kernel filter to filter all voxels between

-500 and 500 mg/cm^3 followed by a 5×5 kernel filter to filter all voxels between -500

and 300 mg/cm^3 (F03F05 filter) was used to remove noise. Soft tissue variables of

interest included total tissue cross-sectional area (CSA, mm^2), absolute (cm^2) and relative

(%) muscle and fat CSA, and muscle density (mg/cm^3).

3.2.3   Statistical analysis

Statistical analyses were performed using IBM SPSS Statistics for Windows

(v22.0; IBM Corp., Armonk, NY) and were two-tailed with a level of significance (α) set

at 0.05. Linear regression analysis was performed to assess the ability of pQCT-derived

measures of bone mineral density, structure, and estimated strength to predict cadaver

humeri mechanical properties (maximum torque and torsional rigidity). The fit of each

univariate model was assessed using coefficients of determination (R^2). Within- and

between-tester and within- and between-day agreement for humeral length measures were

determined via calculation of intraclass correlation coefficients (ICC [2, 1]). The RMS

method was used to compute the overall standard deviation (RMS-SD, expressed in the respective unit of measure) and coefficient of variations (RMS-CV, %) of the precision error of pQCT measures for the six replicate scans in the 30 subjects (total degrees of freedom = 150). The RMS-SD and RMS-CV are referred to as absolute and relative precision, respectively. The absolute and relative LSC at the 95% confidence level were derived for each RMS-SD and RMS-CV precision error estimate by multiplying by 2.77, respectively[368]. To determine the influence of tester (within- vs. between-tester) and timing (within- vs. between-day) on pQCT precision, two-way factorial analyses of variance (ANOVAs) were performed on individual subject absolute precision error measurements (SD) for the following subgroups of duplicate scans: 1) within-tester and within-day; 2) between-tester and within-day; 3) within-tester and between-day and; 4) between-tester and within-day. Each subgroup possessed the minimum 30 degrees of freedom (i.e. duplicate scans performed in 30 individuals), as recommended by the International Society of Clinical Densitometry (ISCD) [369-372].

3.3   Results

3.3.1   *Ex-vivo* predictive ability

Cadavers had varying characteristics resulting in the acquirement of humeri with a range of pQCT and mechanical properties (Table 3.1). None of the humeri exhibited any visible signs of injury (such as fracture or orthopedic surgery) or pathology (such as malignancy). All of the humeri failed via a spiral-type fracture (Figure 3.2). Fractures

initiated at the mid-diaphysis in the majority of humeri (n=13), while fractures initiating

in the proximal and distal diaphysis occurred in 3 and 4 humeri, respectively. Ct.BMC,

Tt.Ar, Ct.Ar and Ps.Pm predicted 61%-85% of the variance in maximum torque and

torsional rigidity, while Ct.Th predicted 35%-50% (all $P<0.01$, Table 3.2). Ct.vBMD did

not predict humeri torsional mechanical properties (all $P=0.43-0.74$). I_P and SSI_P both

independently explained over 90% of the variance in maximum torque and torsional

rigidity (all $P<0.001$, Figure 3.3). For every unit increase in I_P, there was a 34.1 N.m and

1.2 N.m/° increase in maximum torque and torsional rigidity, respectively. There was a

51.6 N.m and 1.7 N.m/° increase in maximum torque and torsional rigidity for every unit

increase in SSI_P, respectively.

Table 3.1. Characteristics of the cadavers and subjects used in the *ex-vivo* predictive ability and *in-vivo* short-term precision studies, respectively.

	Cadavers		Subjects[a]	
	Mean ± SD	Range	Mean ± SD	Range
Cadaver characteristics				
Sex (M:F)	10:10	-	16:14	-
Age (yr)	72.1 ± 16.8	24 - 91	25.7 ± 6.5	21 - 29
Height (m)	1.69 ± 0.11	1.50 - 1.83	1.73 ± 0.10	1.50 - 1.92
Weight (kg)	70.4 ± 11.9	40.9 - 90.9	73.4 ± 13.7	48.7 - 108.7
BMI (kg/m^2)	24.8 ± 4.1	18.2 - 32.5	24.3 ± 3.3	18.5 - 34.9
Humeri pQCT properties				
Ct.vBMD (mg/cm^3)	1215 ± 52	1104 - 1296	1184 ± 33	1112 - 1241
Ct.BMC (mg/mm)	213.8 ± 65.1	98.0 - 343.6	261.6 ± 56.4	174.4 - 366.7
Tt.Ar (cm^2)	3.04 ± 0.64	2.12 - 4.38	3.25 ± 0.76	2.19 - 5.38
Ct.Ar (cm^2)	1.76 ± 0.51	0.84 - 2.77	2.21 ± 0.51	1.44 - 3.20
Ct.Th (mm)	3.49 ± 1.04	1.82 - 5.28	4.46 ± 0.74	2.86 - 6.04
Ps.Pm (mm)	61.3 ± 6.4	51.6 - 74.2	63.6 ± 7.3	52.5 - 82.1
Ec.Pm (mm)	39.1 ± 7.6	24.9 - 55.8	35.5 ± 6.4	27.5 - 56.6
I_P (cm^4)	1.37 ± 0.54	0.51 - 2.34	1.70 ± 0.72	0.74 - 3.60
SSI_P (cm^3)	1.16 ± 0.37	0.48 - 1.79	1.35 ± 0.43	0.76 - 2.35
Humeri mechanical properties				
Maximum Torque (N.m)	60.6 ± 19.5	24.1 - 94.2	-	-
Torsional Rigidity (N.m/°)	2.37 ± 0.66	1.26 - 3.31	-	-

[a] Data in each subject determined from average of six replicate scans
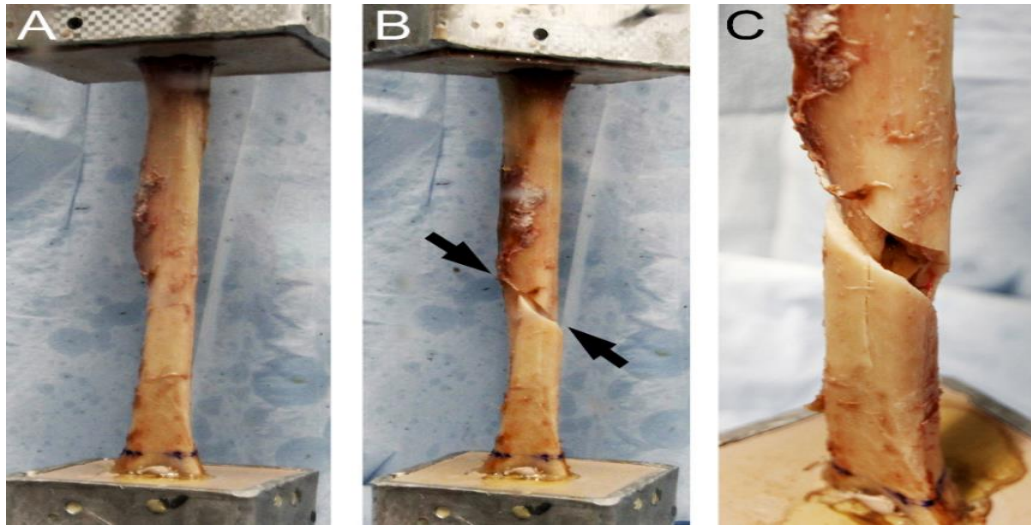
Figure 3.2. Spiral-type fracture of the humeral diaphysis during torsional mechanical testing. A) Humeral diaphysis prior to mechanical testing. B) Spiral-type fracture (arrows) of the humeral diaphysis following external rotation of the humeral head. C) Magnified view of the fracture shown in B.

Table 3.2. Coefficients of determination (R^2) between pQCT measures and torsional mechanical properties in cadaver humeri (n= 20).

pQCT measure	Maximum Torque		Torsional Rigidity	
	R^2	P-value	R^2	P-value
Ct.vBMD	0.01	NS	0.04	NS
Ct.BMC	0.76	<0.001	0.61	<0.001
Tt.Ar	0.71	<0.001	0.81	<0.001
Ct.Ar	0.85	<0.001	0.71	<0.001
Ps.Pm	0.72	<0.001	0.83	<0.001
Ec.Ps	0.01	NS	0.07	NS
Ct.Th	0.50	<0.001	0.35	<0.01
I_P	0.90	<0.001	0.90	<0.001
SSI_P	0.94	<0.001	0.92	<0.001
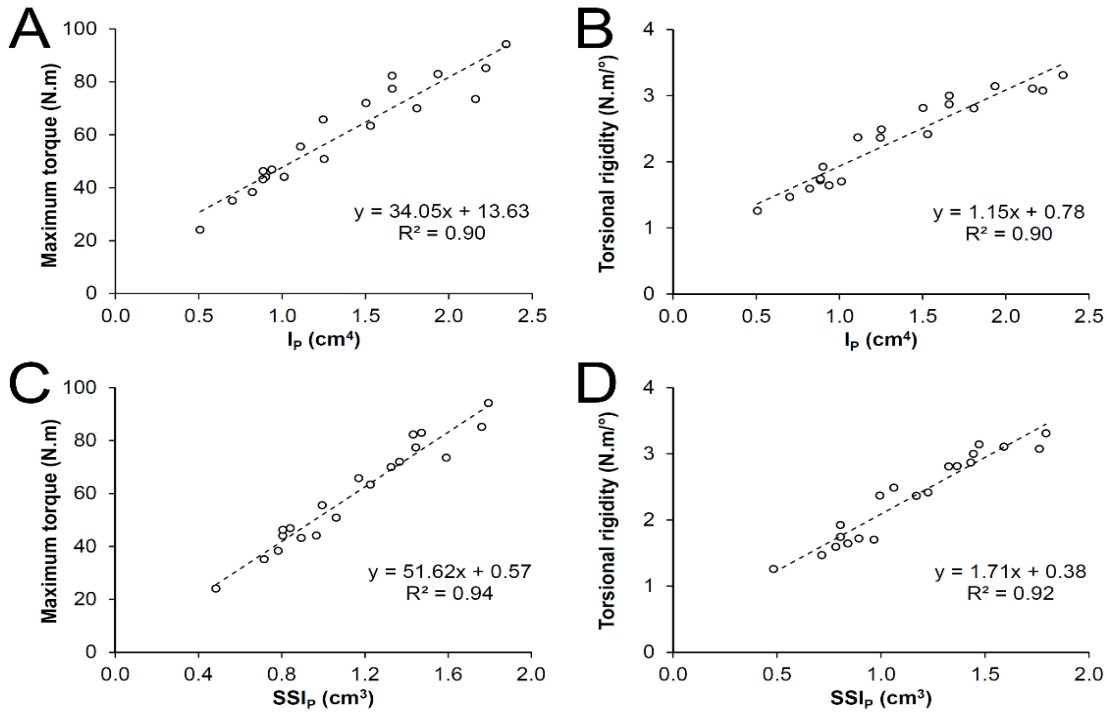
Figure 3.3. Scatterplots illustrating the relationship between pQCT-derived estimated strength (density-weighted polar moment of inertia [I_P; panels A,B] and polar Strength Strain Index [SSI_P; panels C,D]) and cadaver humeri mechanical properties (maximum torque [panels A,C] and (torsional rigidity [panels B,D]).

3.3.2   *In-vivo* short-term precision

Subject characteristics are shown in Table 3.1. There was high within- and between-tester, and within- and between-day agreement for humeral length measures (all ICC [2, 1] $r \geq 0.98$). The overall absolute and relative precision measurements and the respective absolute and relative LSC values at the 95% confidence level are given in Table 3.3. The relative RMS for all six replicate scans ranged from 0.47-1.44% for bone measures and 0.70-2.75% for soft-tissue measures. The subsequent relative LSC values ranged from 1.29-3.99% for bone measures and 1.95-7.63% for soft-tissue measures.

The influences of tester and timing on the precision of pQCT measures are provided in Table 3.4. There were no significant tester by timing interactions on precision for any measure meaning that the two variables had independent effects on precision error (all P=0.07-0.96). There was a significant main effect for tester on precision of Ct.vBMD (P<0.01); however, tester had no significant main effect on precision for any other measure (all P=0.25-0.94) indicating that the measures performed by the two different testers were equally precise. Timing had a significant effect on precision measures for total tissue CSA, absolute muscle CSA and absolute fat CSA (all P<0.05) with between day measures being less precise.

Table 3.3. Overall precision measurements calculated by RMS method and 95% confidence LSC values for 30 subjects scanned six times each (degrees of freedom = 150).

pQCT measure	RMS		LSC	
	Absolute (units)	Relative (%)	Absolute (units)	Relative (%)
Bone measures				
Ct.vBMD (mg/cm^3)	5.51	0.47	15.27	1.29
Ct.BMC (mg/mm)	2.55	1.00	7.05	2.76
Tt.Ar (mm^2)	3.78	1.02	10.48	2.82
Ct.Ar (mm^2)	2.06	0.91	5.71	2.51
Ps.Pm (mm)	0.34	0.50	0.93	1.39
Ec.Pm (mm)	0.45	1.17	1.24	3.23
Ct.Th (mm)	0.04	0.86	0.10	2.38
I_P (mm^4)	252.6	1.40	699.7	3.88
SSI_P (mm^3)	19.1	1.44	52.9	3.99
Soft tissue measures				
Total tissue CSA (cm^2)	1.36	1.86	3.76	5.16
Muscle				
Absolute CSA (cm^2)	0.61	1.91	1.69	5.30
Relative CSA (%)	0.46	1.11	1.26	3.06
Density (mg/cm^3)	0.58	0.70	1.60	1.95
Fat				
Absolute CSA (cm^2)	1.10	2.75	3.05	7.63
Relative CSA (%)	0.49	1.00	1.36	2.78

Table 3.4. Influence of tester and timing on pQCT precision error.[a]

pQCT measure	Within-day		Between-day		Two-way ANOVA results		
	Within-tester	Between-tester	Within-tester	Between-tester	Tester	Timing	Interaction
Bone measures							
Ct.vBMD (mg/cm^3)	3.36 ± 2.30	4.35 ± 3.28	2.60 ± 2.92	4.77 ± 3.26	<0.01	NS	NS
Ct.BMC (mg/mm)	1.74 ± 1.70	1.97 ± 1.69	1.53 ± 1.69	1.68 ± 1.12	NS	NS	NS
Tt.Ar (mm^2)	2.00 ± 2.00	2.02 ± 2.06	2.37 ± 2.68	2.62 ± 3.12	NS	NS	NS
Ct.Ar (mm^2)	1.42 ± 1.29	1.63 ± 1.38	1.51 ± 1.38	1.48 ± 1.13	NS	NS	NS
Ct.Th (mm)	0.024 ± 0.027	0.030 ± 0.025	0.029 ± 0.024	0.030 ± 0.026	NS	NS	NS
Ps.Pm (mm)	0.19 ± 0.19	0.18 ± 0.19	0.25 ± 0.25	0.27 ± 0.27	NS	NS	NS
Ec.Pm (mm)	0.26 ± 0.35	0.26 ± 0.36	0.37 ± 0.45	0.37 ± 0.37	NS	NS	NS
I_P (mm^4)	147 ± 149	156 ± 161	169 ± 195	168 ± 184	NS	NS	NS
SSI_P (mm^3)	11.6 ± 13.0	17.0 ± 16.0	14.9 ± 12.4	15.1 ± 11.1	NS	NS	NS
Soft tissue composition							
Total tissue CSA (cm^2)	0.66 ± 0.53	0.60 ± 0.48	1.28 ± 0.84	1.08 ± 1.05	NS	<0.001	NS
Muscle							
Absolute CSA (cm^2)	0.29 ± 0.23	0.36 ± 0.28	0.61 ± 0.38	0.51 ± 0.45	NS	<0.001	NS
Relative CSA (%)	0.31 ± 0.23	0.40 ± 0.33	0.43 ± 0.37	0.43 ± 0.36	NS	NS	NS
Density (mg/cm^3)	0.40 ± 0.33	0.43 ± 0.47	0.55 ± 0.57	0.55 ± 0.51	NS	NS	NS
Fat							
Absolute CSA (cm^2)	0.51 ± 0.38	0.48 ± 0.35	0.88 ± 0.82	0.87 ± 0.75	NS	0.001	NS
Relative CSA (%)	0.34 ± 0.26	0.39 ± 0.33	0.45 ± 0.42	0.39 ± 0.33	NS	NS	NS

[a] Data indicate individual absolute precision error measurements (SD)

3.4 Discussion

The current data indicate that pQCT provides very good prediction of midshaft humerus mechanical with good short-term precision. I_P and SSI_P predicted at least 90% of the variance in *ex-vivo* midshaft humerus mechanical properties in bones obtained from cadavers, while overall values for relative precision error (RMS-CV) for *in-vivo* measures of I_P and SSI_P at the midshaft humerus were less than 1.5%. Precision errors for skeletal measures were not influenced by pQCT assessments being performed by different testers or on different days, except for Ct.vBMD which was less precise when measured by different testers. Precision errors were slightly higher for measures of soft-tissue composition at the level of the midshaft humerus, with relative precision error for muscle and fat measures being <2.0% and <3.0%, respectively. Precision error increased for some soft tissue composition measures (total tissue CSA, and absolute muscle and fat CSA) when scans were repeated on different days. These cumulative data indicate that pQCT provides predictive and precise estimates of bone mechanical properties and relatively precise measures of soft tissue composition at the level of the midshaft humerus, with measures being generally robust against the influences of different testers and time between repeat scans.

pQCT measures in the current study predicted torsional mechanical properties of cadaver humeri. Previous studies exploring the ability of pQCT measures to predict cadaver bone mechanical properties exclusively exposed bones to bending and/or axial compressive forces[341 346-350 355 373]. Bending and axial compression are common directions of bone loading *in-vivo*, but the measurement of high shear strains when completing

functional tasks in *in-vivo* strain gauge experiments indicates the presence of significant torsional loads[374 375]. Torsional loading of the humerus is thought to be particularly prominent due to counteracting torques often being applied at the shoulder and elbow ends of the bone[165 366 376], and contributes to exaggerated humeral head retroversion and the occurrence of spiral-type humeral diaphysis fractures in the dominant arm of overhead athletes[377 378]. To our knowledge, only one previous study has explored the ability of pQCT to predict bone torsional mechanical properties. Lind et al.[379] observed SSI_P to predict 15% and 33% of maximal torque and torsional rigidity in rodent humeri, respectively. These values are much lower than observed in the current study; however, data collected from rodent humeri are not comparable to those obtained from cadaveric humeri due to the presence of a variable, yet large deltoid tuberosity in rodents and generally greater difficulty torsional testing rodent sized bones.

Bone mechanical properties are influenced by the amount, distribution and intrinsic properties of bone material present in the direction of loading. As SSI_P and density-weighted I_P take into account each of these contributors as they relate to resisting torques around a central torsional axis, it is not surprising that SSI_P and I_P were both better predictors of *ex-vivo* torsional mechanical properties than the independent measures of bone mass, structure or intrinsic properties. SSI_P and I_P both independently predicted ≥90% of *ex-vivo* mechanical properties and, thus, either can be used with confidence to predict mechanical properties of the midshaft humerus. However, SSI_P in the current study was a slightly better predictor of mechanical properties than I_P. This observation is consistent with Wilhelm et al.[355] who found SSI_P to predict slightly more of the variance in fracture load of cadaveric radii during three-point bending than I_P (98%

vs. 94%). SSI_P and I_P are related, with SSI_P being calculated as I_P divided by the maximum distance of the furthest voxel to the central torsional axis. As the greatest shear stresses during torsional loading are experienced in the material furthest from the loading axis, the incorporation of the distance of the most extreme voxels from the central torsional axis by SSI_P enables it provide a slightly better prediction of mechanical properties than I_P.

In addition to demonstrating the ability of pQCT measures to predict midshaft humerus mechanical properties, the current work also demonstrates that pQCT is able to provide *in-vivo* measures of the midshaft humerus with good short-term precision. Measures with small precision errors are desirable as they allow for the detection of small differences over time or between groups, ultimately reducing study sample sizes to detect a desirable difference. Precision errors for skeletal measures of the midshaft humerus were up to double those we previously reported for measures performed of the tibial diaphysis using the same study design (six repeat scans performed in 30 subjects, with repeat scans performed by the same and different testers and on the same and different days)[353]. Reasons for the higher short-term precision errors of pQCT measures of the humeral diaphysis relative to tibial diaphysis were not assessed in the current study; however, possible explanations include those described in the introduction with regards to imaging more proximal skeletal sites (i.e. heightened difficulty repetitively positioning subjects further than usual within the machine gantry and greater potential for subtle movement artifacts due to difficulty stabilizing the proximal end of the bone against subtle trunk motions). Altered repositioning can contribute to altered limb angle in the gantry leading to the acquisition of a tomographic slice in a slightly different horizontal

plane or at a slightly different longitudinal limb location. Small changes in the later have

been shown to contribute to position error in pQCT measures of the distal radius and

tibia[380]. A further possible explanation for lower precision of pQCT measures of the

midshaft humerus in the current study is the performance of scans by different assessors

than those in our previous work. However, one of the assessors in the current study

(A.L.H.) was very experienced performing pQCT scans of the midshaft humerus having

previously performed several hundred scans and both assessors (A.M.W. and A.L.H.)

were equally precise suggesting assessor experience was not a contributing factor.

Despite precision errors for pQCT scans of the midshaft humerus apparently

being higher than those previously shown for the tibial diaphysis, they were still low

(<1.5%) and within acceptable levels for bone densitometry[372]. In addition, they were

substantially lower than those reported by Sievänen et al.[352] who reported a RMS-CV of

5.6% for estimated strength measures of the midshaft humerus. Reasons for our better

short-term precision compared to Sievänen et al.[352] are not clear; however, there are

differences between our respective studies. Limb positioning and stabilization procedures

differed between the studies which can influence the potential for movement artifacts.

However, a greater occurrence of subtle movement artifacts in the study by Sievänen et

al.[352] is unlikely to explain their higher precision errors as movement artifacts impact on

Ct.vBMD measures and short-term precision of Ct.vBMD in our respective studies were

comparable (0.5% vs. 0.5%). Sievänen et al.[352] estimated midshaft humerus mechanical

properties via the calculation of a bone strength index which was calculated as I_P

multiplied by the pQCT measured Ct.vBMD. This method of density-weighting differs to

current methods which involve multiplying SSI_P or I_P by the quotient of pQCT measured

Ct.vBMD and physiologic density (1200 mg/cm^3). However, the use of physiologic density to normalize Ct.vBMD essentially introduces a constant factor that does not influence precision measures. Both studies followed the recommendations of the ISCD which state that short-term precision error for densitometry assessments should obtained using the root mean square (RMS) approach from an assessment with 30 degrees of freedom[369-372]. However, overall precision error in the current study was determined from a much higher number of degrees of freedom compared to Sievänen et al.[352] (150 vs. 31 degrees of freedom), with degrees of freedom potentially influencing precision estimates and degrees of freedom higher than recommended by the ISCD providing greater confidence in the precision estimate[381 382].

Overall, this study found pQCT provides very good prediction of midshaft humerus mechanical properties with good short-term precision. Density-weighted I$_P$ and SSI$_P$ both provided predicted actual midshaft humerus torsional mechanical properties, with SSI$_P$ providing slightly better prediction than I$_P$. Precision errors for skeletal measures were generally not influenced by scanning being performed by different testers or by repeat scans being performed on different days as opposed to the same day. Based on these data, investigators performing pQCT measures of the midshaft humerus can have confidence in the utility of pQCT in obtaining estimates of midshaft humerus mechanical properties.

CHAPTER FOUR: THE EFFECTS OF UNILATERAL JUMPING ON TIBIAL BONE
MASS, SIZE AND ESTIMATED STRENGTH

4.1 Introduction

Exercise is promoted as a means of improving bone health as the skeleton
responds and adapts to mechanical forces. Many studies have provided strong evidence
of improved bone health as a result of exercise at both the lower and upper extremities[256]
[263 288 289 295 296 306 383]. With the lower extremities, studies have observed that activities
such as gymnastics and jumping enhanced the tibia and femur bone properties[383-385].
While majority of these studies have provided positive evidence that there are skeletal
benefits of exercise at these sites, there were some studies in which study designs were
comparing bone health in individuals who exercise to sedentary controls[263 295 296].
Unfortunately, the study designs that use a between-subjects approach introduce a range
of variables beyond exercise (i.e. genetics, hormones, nutrition, and other systemic
factors) that may account for skeletal differences between groups. To control for the
influence of systemic factors, we seek models wherein individuals exercise one side of
the body, but not the other. Unilateral exercise models enable the skeletal benefits of
exercise to be explored within-rather than between-individuals so as to control for the
influence of systemic factors.

Two established upper-extremity unilateral exercise models, the tennis and
throwing models, have provided information on site and surface-specific bone structure
(i.e. size and geometry) and estimated strength adaptations to exercise[254 386-388]. While
these models have observed positive bone health benefits with the upper extremity, with

the lower extremity there has only been a few studies that used a within-subject study design[389] [390]. One study using a within-subject design within the lower extremities was investigated by Young et al.[390], where they found in ten pin bowlers side-to-side bone property differences at the femur. However, a major limitation existed in this study which was not comparing the bowlers' side-to-side bone property differences to a matched control group. Therefore, the effects of bowling could not be isolated from the influence of side-to-side differences in habitual loading associated with leg dominance. The second study investigated by Ireland et al.[389], found tibial cortical and trabecular bone property side-to-side differences in master jumping athletes (high and long jumpers). However, when comparing those bone property differences to a matched control group of sprinters, only one bone property measure was significantly different[389]. Whether similar findings from the Ireland et al.[389] study are present in collegiate-level high and long jumpers is currently unknown.

The primary aim of this cross-sectional cohort study was to investigate lower extremity bone health in collegiate-level jumping athletes. This was achieved by comparing the jump and lead (non-jump) legs bone mass, structure and estimated strength in male high and long jumpers to differences in matched controls. Athletes who compete in jumping activities (such as high and long jump) are a possible model, as they repetitively apply significant force through their jump leg[391-394]. The peak vertical ground reaction forces during long and high jumps are twice as greater than during maximal sprinting[391-394]. Dual-energy x-ray absorptiometry (DXA) and peripheral quantitative computed tomography (pQCT) assessed those outcome measures.

4.2   Methods

<u>4.2.1   Subjects</u>

Male collegiate-level jumping (jumpers; n = 12) and cross-country (controls; n = 11) athletes aged 18-30 years were recruited. Jumpers were included if they were currently competing or practicing in collegiate-level long and/or high jump and had been continuously participating in competitive jumping for at least 3 years. Participants in both groups were excluded if they had: 1) participated >2 times per month for >6 months within the previous 3 years in an athletic activity (including basketball, triple jump, volleyball) that may preferentially load one lower extremity (except high or long jump in jumpers), or; 2) been exposed to lower extremity surgery or lower extremity immobilization for >2 weeks within the past 2 years. The jump leg was defined as the take-off leg in jumpers. The dominant leg in controls was defined as the opposite side of their throwing arm. The contralateral leg was defined as lead and non-dominant leg in jumpers and controls, respectively. The study was approved by the Institutional Review Board of Indiana University and all participants provided written informed consent.

<u>4.2.2   Demographic and anthropometric characteristics</u>

Jumpers completed a questionnaire to document their participation and best performance in jumping endeavors. Height (to nearest 0.1 cm) and weight (to nearest 0.1 kg) were measured using a wall mounted digital stadiometer and electronic balance scale, respectively. Body mass index (BMI, kg/m^2) was calculated as mass divided by height squared. Tibial length (to nearest 1 mm) was measured using a sliding anthropometer as the distance between the medial tibial plateau and center of the medial malleolus. Whole-

body lean (kg) and fat mass (%) were assessed in all subjects via whole-body dual-energy X-ray absorptiometry (DXA) using the manufacturer's standard protocols on a Hologic Discovery-W machine equipped with Apex v4.0 software (Hologic, Inc., Waltham, MA, USA). Subregional analyses were performed to obtain whole jump and lead leg lean mass (kg), with the neck of femur being the landmark for the division of the lower extremities from the pelvis.

4.2.3   Jump performance

Jump height and force for both the jump and lead legs were assessed during single-leg counter-movement jumps with freely moving arms. Subjects took a single step and jumped as high as possible off of the leg being tested. Jump height was measured using a Vertec vertical jump meter with moveable vanes every one-half inch (1.27 cm) (Sports Imports, Columbus, OH). Single-hand vertical reach was measured from a flat-foot standing position before subjects performed a single-leg countermovement jump to displace the highest vane possible. Vertical jump height (cm) was measured as the distance difference between standing and jump reach. Subjects were permitted to perform 3 trials on each leg separated by ≥1 min, with the best jump on each leg recorded as jump height.

Jump force was measured as per jump height, but with subjects performing jump movements on an AMTI force platform (OR6-7-1000 with Gen5 digital amplifiers; Advanced Mechanical Technologies, Inc., Watertown, MA). Subjects stood quietly on the force platform to first measure the force exerted by body mass. Subjects subsequently

performed single-leg countermovement jumps on each leg during which force within the acceleration phase of the jump was collected at 100 Hz using Vicon Nexus software (version 1.8.5; Vicon, Oxford, UK). Subjects were permitted to perform 3 jumps on each leg separated by ≥1 min, with the highest force on each leg recorded as the jump force. Jump force data for each leg was subsequently converted into units of body weight (BW) by dividing by body mass force.

4.2.4   pQCT

pQCT was performed using a Stratec XCT 3000 machine equipped with software version 6.20C (Stratec Medizintechnik GmbH, Germany). Subjects were positioned supine with the test leg centered within the machine's gantry and anchored by stretchable straps to limit movement during testing. A scout scan was performed to localize the talocrural joint and a reference line was placed at the distal tibial plateau, bisecting the region of highest density at the lateral side of the distal tibia. Tomographic slices (thickness = 2.3 mm; voxel size = 400 μm; scan speed = 20 mm/s) were taken at 66% (tibial diaphysis) and 4% (distal tibia) of tibial length proximal from the reference line, with tibial length measured earlier using a sliding anthropometer. The procedure was repeated on both the jump and lead legs.

Analysis of the tibial diaphysis slice was restricted to cortical bone parameters as trabecular bone is not present at this site. Cortical mode 1 (threshold, 710 mg/cm^3) was used to obtain total area (Tt.Ar, cm^2), and cortical volumetric bone mineral density (Ct.vBMD, mg/cm^3), bone mineral content (Ct.BMC, mg/mm), and area (Ct.Ar, cm^2). Medullary area (Me.Ar, mm^2) was derived as Tt.Ar minus Ct.Ar. Average cortical

thickness (Ct.Th, mm) was obtained using a circular ring model by analyzing the slices using contour mode 1 (threshold, 710 mg/cm^3) to define the outer bone edge and peel mode 2 (threshold, 400 mg/cm^3) to separate the cortical and subcortical/medullary compartments.

Bone strength of the tibial diaphysis was estimated by the density-weighted minimum (I$_{MIN}$, cm^4) and maximum (I$_{MAX}$, cm^4) second moments of area, and polar moment of inertia (I$_P$, mm^4) obtained using cortical mode 2 (threshold = 400 mg/cm^3). I$_{MIN}$ and I$_{MAX}$ were estimated according to Gere and Timoshenko[333], and represent the distribution of bone material about the planes of least and most bending resistance, respectively. They estimate the ability of the bone structure to resist bending in orthogonal planes. I$_P$ was calculated by the Stratec software as the sum of I$_{MIN}$ and I$_{MAX}$. I$_P$ estimates the ability of a bone structure to resist torsion[128].

Each tomographic slice at the level of the tibial diaphysis was also analyzed to obtain lower leg lean cross-sectional area (CSA, mm^2). Contour mode 3 (threshold, −100 mg/cm^3) was used to locate the skin surface and peel mode 2 (threshold, 40 mg/cm^3) used to locate the subcutaneous fat–muscle boundary. A F03F05 filter was used to remove noise. Short-term precision for the pQCT scanning procedure on 30 healthy individuals scanned six times with interim repositioning showed root mean square coefficients of variation (RMS-CVs) of <1% for bone density, mass, structure, and estimated strength measures, and <1.5% for lean CSA[395].

To determine site-specificity of bone geometry adaptive responses associated with jumping, polar pericortical and endocortical radii at the tibial diaphysis were obtained for the jump and lead legs in jumpers. Stratec pQCT image files and data were opened in

ImageJ (v1.45s; National Institutes of Health) and analyzed using the BoneJ plugin[396], as previously described[397]. Images were rotated to align the bones according to the I_{MAX} and I_{MIN} axes, and right-sided images were flipped to superimpose left-side images. Using a threshold value of 350 mg/cm^3 to locate bone tissue, the distance of the endocortical and pericortical surfaces from the centroid of the medullary cavity were measured in 36 10° polar sectors.

Analyses of the distal tibia slice included both total and trabecular measures, and were achieved using contour mode 3 (threshold=400 mg/cm^3) and peel mode 1 (concentric peel=45%). Properties recorded included total vBMD (Tt.vBMD, mg/cm^3), area (Tt.Ar, cm^2) and BMC (Tt.BMC, mg/mm), and trabecular vBMD (Tb.vBMD, mg/cm^3), area (Tb.Ar, cm^2) and BMC (Tb.BMC, mg/mm). Cortical properties were not recorded at the distal tibia slice due to the thin cortical shell and consequent heightened risk for partial volume artifacts. Strength of the distal tibia to resist compressive forces was estimated by the Bone Strength Index (BSI, mg^2/mm^4). BSI was calculated as the product of Tt.Ar and squared Tt.vBMD, and is predictive of compressive failure load[111].

4.2.5   Statistical analysis

Two-tailed analyses with a level of significance set at 0.05 were performed with IBM SPSS Statistics (v21; SPSS Inc., Chicago, IL). Demographic and anthropometric characteristics were compared between jumpers and controls using independent sample t-tests. Jumping versus lead leg effects on tibial properties were assessed *within* jumpers and controls by calculating mean percent differences ([jump leg − lead leg] / lead leg × 100%) and their 95% confidence intervals (CIs). 95% CIs not crossing 0% were

134

considered statistically significant, as determined by single sample t-tests on the mean

percent differences with a population mean of 0%. Jumping effects *between* jumpers and

controls were determined by comparing the percent difference values between groups

using independent sample t-tests. Differences between the jumping and lead legs in

jumpers for pericortical and endocortical radii in each polar section were assessed using

paired t-tests.

4.3   Results

Participant characteristics are detailed in Table 4.1. Jumpers and controls were

matched for age and height; however, jumpers had greater total and lean mass than

controls (all $P < 0.001$). There were no jump-to-lead leg differences in lean measures in

either jumpers or controls, or jump-to-lead leg differences in jump performance in

controls (all $P = 0.675$ to 0.970; Table 4.2). In contrast, jumpers exerted 10.4% (95% CI

= 2.6% to 18.2%) more force when jumping off their jump leg compared to their lead leg

(all $P < 0.01$; Table 4.2).

Table 4.1. Demographic and anthropometric characteristics of jumpers and controls[a].

	Controls	Jumpers
Demographics		
Age (yr)	22.3 ± 3.0	21.8 ± 2.1
Preferred jump leg (L:R)	11:0	9:3
Age starting competitive jumping (yr)	—	14.2 ± 1.8
Year competing (yr)	—	6.2 ± 2.9
Jumping sport (long:high jump)	—	12:6[b]
Jump training per week (min)	—	193 ± 107
Jumps per week (n)	—	71 ± 58
Personal best: long jump (m)	—	7.11 ± 0.49
Personal best: high jump (m)	—	1.97 ± 0.18
Whole-body anthropometry		
Height (m)	1.79 ± 0.07	1.82 ± 0.07
Mass (kg)	67.7 ± 8.7	78.5 ± 5.9*
BMI (kg/m^2)	21.1 ± 1.9	23.7 ± 1.8*
aBMD (g/cm^2)[c,d]	1.23 ± 0.10	1.35 ± 0.10
Lean mass (kg)[c]	49.0 ± 5.7	58.6 ± 4.5*
Fat mass (%)[c]	16.3 ± 4.4	14.0 ± 1.3

[a] Data indicate mean ± SD (except for frequencies)

[b] 6 jumpers participated in both long and high jump

[c] Obtained via dual-energy x-ray absorptiometry

[d] Corrected for whole-body lean mass

[†] $p < 0.001$ (χ^2 test: controls vs. jumpers)

[*] $p < 0.001$ (independent sample t-test: controls vs. jumpers)

There were no jump-to-lead leg differences in controls at either the tibial diaphysis or distal tibia (all $P = 0.070$ to 0.969; Table 4.3). The jump leg in jumpers had greater Ct.BMC, Ct.Ar, Ct.Th, I$_{MAX}$ and I$_P$ at the tibial diaphysis and greater Tt.vBMD, Tt.BMC and BSI at the distal tibia than in the lead leg (all $P < 0.05$; Table 4.3). There were no jump-to-lead leg differences in jumpers for Ct.vBMD, Tt.Ar, Me.Ar or I$_{MIN}$ at the tibial diaphysis or Tt.Ar, Tb.vBMD, Tb.Ar or Tb.BMC at the distal tibia (all $P = 0.387$ to 0.874; Table 4.3).

Table 4.2. Bilateral lean, jumping performance and bone mass measures in the legs of jumpers and controls.

Measure	Controls			Jumpers		
	Nondominant[a]	Dominant[a]	% difference (95% CI)[b]	Lead[a]	Jump[a]	% difference (95% CI)[b]
Lean measures						
Whole leg lean mass (kg)[c]	9.0 ± 1.1	9.0± 1.2	-0.2% (-2.1, 1.6%)	10.8 ± 0.92	10.8 ± 0.94	-0.1%(-2.2, 2.1%)
Lower leg lean CSA (cm^2)[d]	59.5 ± 4.7	59.6 ± 4.8	-0.3% (-1.4, 2.1%)	65.1 ± 5.9	65.1 ± 6.0	-0.0% (-1.7, 1.7%)
Jump performance						
Height (cm)	44.9 ± 10.9	46.3 ± 10.1	4.2% (-2.8, 11.3%)	67.5 ± 25.8	67.1 ± 20.7	3.9% (-9.5, 17.3%)
Force (BW)	2.80 ± 0.44	2.74 ± 0.28	-1.2% (-7.0, 4.7%)	3.04 ± 0.36	3.35 ± 0.46	10.4% (2.6, 18.2%)**
Bone mass						
Whole leg BMC (g)[c]	566.2 ± 90.1	574.4 ± 83.1	-1.7% (-1.1, 4.7%)	703.8 ± 80.6	715.4 ± 75.4	1.8% (-0.5, 4.2%)

[a] Data are mean ± SD

[b] Mean percent differences between jump and lead leg (controls:dominant and nondominant) were assessed using single sample t-tests with a population mean of 0. Significance is indicated by: *$p<0.05$, **$p<0.01$.

[c] Assessed using DXA

[d] Assessed using pQCT

Table 4.3. Bilateral bone density, mass, structure and estimated strength at the tibial diaphysis and distal tibia in the legs of jumpers and controls.

	Controls			Jumpers		
	Nondominant[a]	Dominant[a]	% diff. (95% CI)[b]	Lead[a]	Jump[a]	% diff. (95% CI)[b]
Tibial diaphysis						
Ct.vBMD (mg/cm^3)	1142 ± 12	1147 ± 16	0.5% (-0.1, 1.1%)	1153 ± 18	1152 ± 20	-0.1% (-0.6, 0.4%)
Ct.BMC (mg/mm)	449 ± 50	451 ± 51	0.5% (-1.2, 2.3%)	513 ± 58	531 ± 67	3.6% (0.6, 6.5%)*
Tt.Ar (cm^2)	6.81 ± 0.82	6.81 ± 0.72	0.2% (-1.5, 1.8%)	7.76 ± 0.88	7.87 ± 0.84	1.5% (-0.5, 3.5%)
Ct.Ar (cm^2)	3.94 ± 0.45	3.94 ± 0.46	0.1% (-1.8,1.9%)	4.45 ± 0.48	4.61 ± 0.56	3.7% (1.0, 6.3%)**
Me.Ar (cm^2)	2.87 ± 0.66	2.87 ± 0.62	0.3% (-3.1, 3.8%)	3.32 ± 0.81	3.26 ± 0.75	-1.2% (-4.2, 1.8%)
Ct.Th (mm)	5.19 ± 0.58	5.19 ±0.63	-0.1% (-2.2, 2.1%)	5.49 ± 0.72	5.68 ± 0.78	3.5% (0.9, 6.0%)**
I$_{MIN}$ (cm^4)	1.87 ± 0.43	1.87 ± 0.41	0.3% (-2.5, 3.1%)	2.62 ± 0.60	2.64 ± 0.60	1.1% (-4.3, 6.4%)
I$_{MAX}$ (cm^4)	5.51 ± 1.29	5.48 ± 1.11	0.3% (-3.6, 4.2%)	6.41 ± 1.04	6.88 ± 1.19	7.5% (2.5, 12.5%)**
I$_P$ (cm^4)	7.38 ± 1.62	7.36 ± 1.42	0.2%(-2.9, 3.4%)	9.02 ± 1.59	9.52 ± 1.70	5.7% (1.0, 10.3%)*
Distal tibia						
Tt.vBMD (mg/cm^3)	388 ± 46	393 ± 50	1.4% (-2.1, 4.9%)	406 ± 44	417 ± 40	2.8% (1.1, 4.6%)**
Tt.BMC (mg/mm)	427 ± 45	430 ± 47	0.9% (-3.6, 5.3%)	501 ± 47	517 ± 53	3.0% (1.5, 4.4%)***
Tt.Ar (cm^2)	11.1 ± 1.5	11.1 ± 1.9	-0.2% (-6.4, 6.0%)	12.4 ± 1.5	12.4 ± 1.3	0.2% (-2.2, 2.5%)
BSI (mg^2/cm^4)	166 ± 31	169 ± 28	2.2% (-2.7, 7.1%)	204 ± 38	217 ± 41	5.9% (3.6, 8.2%)***

[a] Data are mean ± SD.

[b] Mean percent differences between jump and lead leg (controls:dominant and nondominant) were assessed using single sample t-tests with a population mean of 0. Significance is indicated by: *p<0.05, **p<0.01, ***p<0.001.

At the tibial diaphysis, jumpers had greater jump-to-lead leg differences in structure and estimated strength than controls (Figure 4.1). However, there was no jump-to-lead leg differences in bone mass measures, Ct.vBMD and Ct.BMC between jumpers and controls; although, the difference for Ct.BMC approached significance ($P = 0.07$). In bone structural measures, jump-to-lead leg differences were found in Ct.Ar and Ct.Th with the jumping group having 3.6% (95% Cl =0.5% to 6.8%) and 3.5% (95% Cl = 0.4% to 6.6%) greater than controls, respectively (all $P< 0.05$; Figure 4.1). The enhanced structural measures in the jumping group resulted in greater jump-to-lead leg differences in estimated strength, with the jumping group having 7.2 % (95%Cl, 1.2- 13.2%) and 5.7% (95%Cl, 1.7-9.8%) greater I_{Max} and I_P respectively, compared to the controls (all $P<0.05$; Figure 4.1). The enhanced structure of the jump leg in jumpers provided the tibial diaphysis with greater plane-specific estimated strength gains at the medial and posterior pericortical and lateral endocortical surfaces with losses at the lateral pericortical surface (all $P<0.05$; Figure 4.2). In contrast to the tibial diaphysis, at the distal tibia there was no jumping effect observed in any measure (all $P= 0.13$ to 0.90).
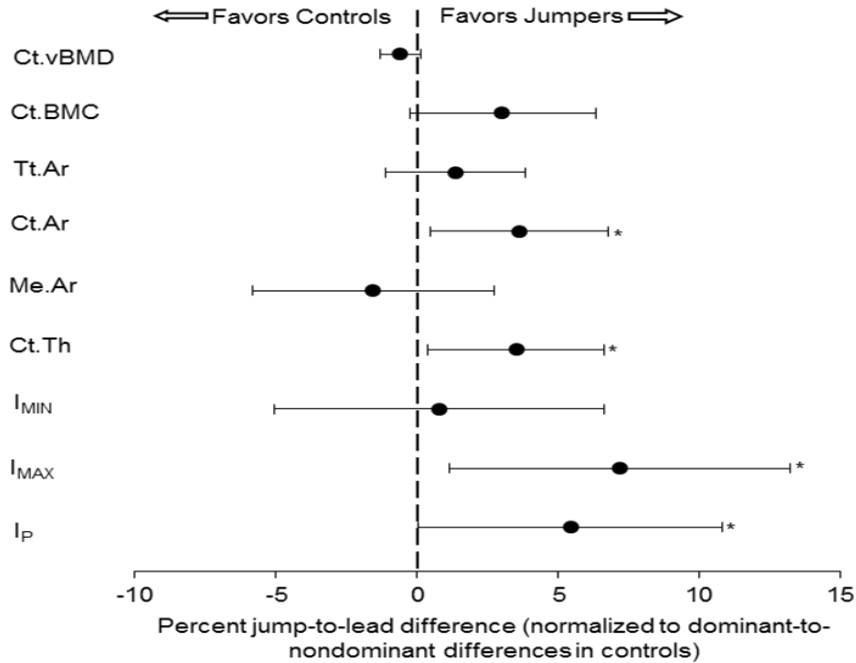
Figure 4.1. Effect of jumping on pQCT measures of the tibial diaphysis. Data indicate the mean percent difference and 95%Cl between the jump and lead legs in jumpers normalized to dominant-to-nondominant differences in controls. Significant jump to lead leg differences indicated by *P<0.05.
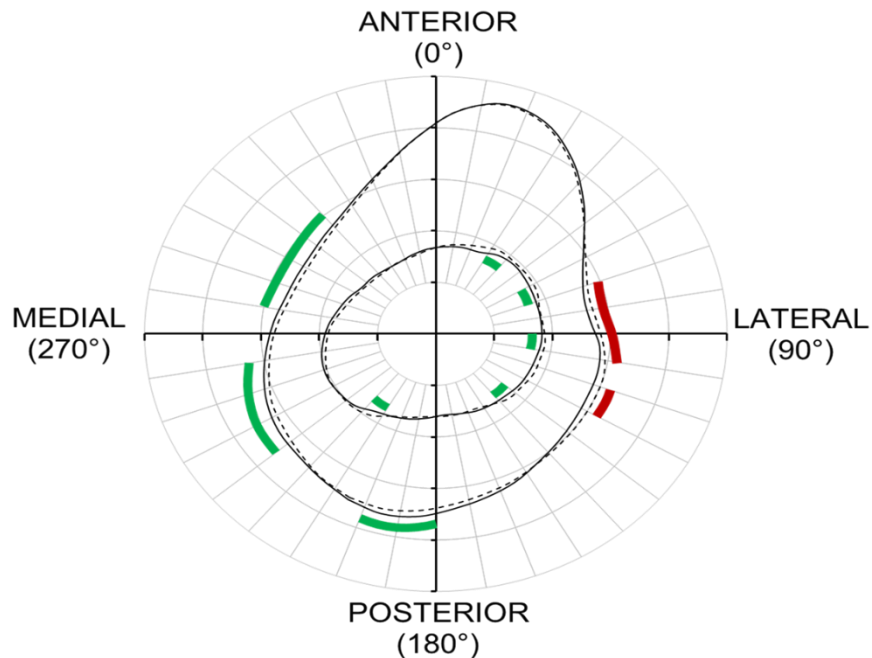
Figure 4.2. Map of tibial diaphysis surface-specific bone structural differences between the jump (solid line) and lead (dashed line) legs in jumpers. Green and red lines indicate polar radii wherein takeoff legs had significant bone structural gains and losses, respectively (P<0.05).

4.4 Discussion

In this cross-sectional study, we observed significant bone health differences between the jumping and control group. Specifically, the jumpers had greater side-to-side differences in cortical bone structure and estimated strength compared to the controls. The largest effect of jumping was for cortical bone estimated strength where the jumping group had about 6% greater estimated bone strength than controls. The bone structural contributions to enhanced estimated bone strength in jumpers were a result of greater surface-specific cortical bone differences in the jumping leg at the medial and posterior periosteal and lateral endosteal surfaces. These cortical bone surface-specific adaptations in jumpers resulted into a 7.2% greater I_{MAX} than controls. In contrast to cortical bone, trabecular bone had side-to-side differences in bone properties within jumpers, but not when expressed relative to controls. Collectively, these data indicate that jumping in the form of long and high jump induces cortical bone adaptation at the tibia.

Previous animal- and human-based studies have revealed that mechanical loading when young has lifelong benefits on bone structure and strength, independent of any lasting effect on bone mass[312 386 398]. This finding indicates exercise performed during growth may have lifelong benefits on osteoporotic fracture risk, and means that studies investigating the skeletal effects of exercise should focus on skeletal structure as opposed to simply mass. In particular, studies should focus on bone cross-sectional size as bone mechanical properties are proportional to the fourth power of the bone radius.

At the tibial diaphysis where cortical bone is located, jumpers had greater cortical bone side-to-side differences in bone structure and estimated strength properties compared to controls. Specifically, the structural bone property adaptations that were

141

significant are due to a thicker cortical bone cortex with a larger cortical bone area in jumpers, with a subsequent 7.2% greater jump-to-lead-leg differences in I_{MAX} than controls. At this site, material density or mass did not appear to contribute to estimate bone strength. Bone mass and material density were not contributors to estimated bone strength in the jumping leg of the jumpers, because bone geometric properties were enhanced by more cortical bone formed along the I_{MAX} and less along the I_{MIN} plane. This suggests that jumper's tibial diaphysis is subjected to large bending forces due to more bone along the I_{MAX} plane[112 389].

At the distal tibia where trabecular bone is located, jumpers had side-to-side differences in bone mass and estimated strength, but not relative to controls. A potential reason for this is the strain threshold above limb dominance for bone adaptation at this site might not have occurred; therefore, no significant trabecular bone adaptation was observed in this study[35]. Based on our current method to measure bone properties, we were unable to observe if there were differences in trabecular bone microarchitecture[399].

There is only one study that has used a within-subject study design in jumping athletes to assess tibia bone properties[389]. This study was investigated by Ireland et al.[389] who found side-to-side cortical and trabecular bone property differences in master jumping athletes. However, when the comparing to a control group, only one measure was found differently. Reasons for these differences between our studies could be they did not control for other single-leg activities, and they grouped males and females together.

Cross-country runners used as controls did not exhibit side-to-side differences between their dominant and nondominant legs. Bone's ability to adapt is based on strain

rate which is the product of strain magnitude and frequency[239]. Activities that have been shown to specifically adapt bone's properties are dynamic, very intense, short burst, direction changing such as jumping, hopping or sprints[400 401] compared to repetitive low-intensity activities such as walking or running[402]. Running is low-intensity and very repetitive bilateral activity. Studies have suggested that bone cells do not respond after long periods of continuous loading because they become desensitized to that strain environment[179 260 403].

In summary, the current data suggests that jumping athletes who subjected one of their tibias to elevated loads resulted into enhanced cortical bone structure and estimated strength. Using a within-subject controlled study design to protect against the influence of selection bias, the tibial diaphysis in the jump leg of male collegiate-level jumping athletes had about 6% greater estimated strength compared to the contralateral lead (non-jump) leg, respectively. The side-to-side cortical bone property differences in jumpers were greater than observed athletic controls, suggesting that these bone adaptations are not simply results of limb dominance. In contrast to cortical bone properties, jumpers had side-to-side differences in trabecular bone properties, but not relative to controls. Ultimately, unilateral jumping athletes may represent a useful and efficient model for further exploring and elucidating the adaptation of the tibia to mechanical loads.

CHAPTER FIVE: THE EFFECTS OF ONE YEAR OF BASEBALL ON HUMERAL BONE MASS, SIZE AND ESTIMATED STRENGTH

5.1   Introduction

The ability of the skeleton to respond and adapt to exercise has been shown to diminish with age[157 404]. Previous studies looking at when the skeleton is most responsive to exercise have suggested that exercise prior to puberty, as opposed to after puberty, is more beneficial[263 288 290 295 306]. Specifically, the studies have shown that children who were exposed to elevated exercise loads in the form of playing racket sports, gymnastics or jumping before puberty had site-specific enhanced bone properties compared to the children who started after puberty[263 288 290 295 306]. Additionally, jump training intervention studies with pubertal and post-pubertal children showed that training for more than 6 months resulted in detectable enhancement of bone properties[405 406].

While the majority of these studies have provided positive evidence that prepubertal children have an enhanced bone response to exercise, some of those study designs had limitations[263 295 405 406]. The study design limitations included requiring participants to perform some form of forced exercise (i.e. jumping exercise) to show an exercise effect and/or comparing bone health to individuals who exercise to sedentary controls[263 295 405 406]. The latter limitation unfortunately introduces a range of variables beyond exercise (i.e. genetics, hormones, nutrition and other systemic factors) that may account for skeletal differences between groups. To control for the influence of systemic factors, we seek models wherein individuals exercise one side of the body, but not the other. Unilateral exercise models enable the skeletal benefits of exercise to be explored

within rather than between individuals so as to control for the influence of systemic factors.

Throwing (baseball) athletes have been used as models to explore the benefit of exercise on the skeleton as the elevated unilateral loading associated with throwing enables the contralateral upper extremity to serve as an internal control site for the influence of systemic factors. Previous cross-sectional studies using the throwing model have demonstrated mid-shaft humeral bone property side-to-side differences with the throwing arm of Major/Minor League Baseball players having nearly double the estimated strength of the humerus in their nonthrowing arm[386 407]. Additionally, a cross-sectional study using the throwing model with prepubertal baseball players suggested that exercise during growth induced an increase in estimated bone strength of approximately 2% per year[407]. However, there is currently no prospective study using this model.

The proposed study will further the cross-sectional data by prospectively following male prepubertal throwing athletes over 12 months (spanning one competitive season) and comparing gain in throwing-to-nonthrowing arm difference in bone mass, size and estimated strength. Peripheral quantitative computed tomography (pQCT) will assess those outcome measures.

5.2   Methods

5.2.1   Subjects

This was a 12-month longitudinal study that recruited 12 male throwing athletes (i.e. baseball) aged 8-11 years with a sexual maturation rating of 1 or 2 for genital development (see below questionnaires) at baseline. Subjects were assessed at 0 (baseline) and 12 months following enrollment into the study. Participants were included if they anticipated playing a minimum of 5 months in the upcoming year to ensure adequate exposure and adaptation to the mechanical forces associated with throwing. The participants were excluded if they had: 1) any disorder or condition that compromises the ability of the subject to comply with study procedures; 2) any known metabolic bone disease (i.e. osteomalacia or osteogenesis imperfecta) or developmental disease (i.e. cerebral palsy) which may interfere with bone mass or size measures; 3) administration of any pharmacological agents known to influence skeletal metabolism; 4) participation more than twice per month for no longer than 6 months in an athletic activity that primarily involves unilateral upper limb use (except baseball), including racquet sports, volleyball, football (quarterback position), discus throw, javelin, shot-put and bowling; 5) shoulder pain in the previous 12 months that required professional advice; 6) previous history of an upper arm bone (humerus) fracture or stress fracture, as these artificially impact upper arm bone mass and size; 7) fracture or stress fracture of any other upper extremity bone within the past 2 years, as the immobilization required for healing of these injuries may artificially impact upper arm bone mass and size or; previous history of a shoulder (glenohumeral) joint dislocation. The study was approved by the

Institutional Review Board of Indiana University and all participants provided written informed consent.

5.2.2   Anthropometrics

Height (to nearest 0.1 cm) and weight (to nearest 0.1 kg) were measured using a wall mounted digital stadiometer and electronic balance scale, respectively. Body mass index (BMI, kg/m^2) was calculated as mass divided by height squared. Humeral length (to nearest 1 mm) was measured using a sliding anthropometer as the distance between the lateral border of the acromion and the radiohumeral joint line.

5.2.3   Questionnaires

Self-reported sexual maturation was reported with parental/guardian guidance by using the 5 stage Tanner scale[408]. Subjects looked at 5 photographs and/or drawings of genital areas, and circled the image most closely resembling the subject. Subjects that were included in this study were in the early stages of puberty where they rated themselves a 1 or 2 for genital development.

The subjects with guidance of their parents/guardian completed health, estimated calcium and throwing questionnaires. These questionnaires were used for subject inclusion, demographics, and bone predictor measures in upper extremity throwing-to-nonthrowing differences. Estimation of the calcium intake per day (mg/day) and hour per week of training were obtained from the calcium and throwing questionnaires. The subjects were given these questionnaires at both baseline and follow-up.

5.2.4   DXA

Dual-energy X-ray absorptiometry was performed to assess whole-body composition. A Hologic Discovery-W machine (Hologic, Inc., Waltham, MA) equipped with Apex v4.0 software was used for scanning. The scans were performed with the subject lying on supine on the padded table of the scanner. Analysis of scans included whole body lean (kg) and fat mass (%).

5.2.5   pQCT

Bone health within the upper extremities was assessed using a Stratec XCT 3000 pQCT machine (Stratec Medizintechnik GmbH, Germany). Scans were performed on both the throwing and nonthrowing upper extremity at the distal humeral diaphysis. Subjects were positioned supine on a padded plinth/table with one upper extremity positioned in 90° shoulder abduction. The upper extremity was centered within the gantry of the pQCT machine and strapped down using stretchable Velcro straps in order to limit movement during the scans. A scout scan was performed to enable tomographic scan localization, and tomographic slices (thickness = 2.3 mm; voxel size = 600 μm) were taken at 75% (distal humeral diaphysis) of humeral length from its distal end. The procedure was repeated on the contralateral side. Each participant had a total of two tomographic scans (throwing and nonthrowing distal humeral diaphysis diaphysis).

Analyses were restricted to cortical bone due to the absence of trabecular bone at the distal humeral diaphysis. Cortical mode 1 (threshold, 710 mg/cm^3) was used to obtain total area (Tt.Ar, cm^2), and cortical volumetric bone mineral density (Ct.vBMD,

mg/cm^3), bone mineral content (Ct.BMC, mg/mm), and area (Ct.Ar, cm^2). Medullary area (Me.Ar, cm^2) was derived as Tt.Ar minus Ct.Ar. Average cortical thickness (Ct.Th, mm) was obtained using a circular ring model by analyzing the slices using contour mode 1 (threshold, 710 mg/cm^3) to define the outer bone edge and peel mode 2 (threshold, 400 mg/cm^3) to separate the cortical and subcortical/medullary compartments.

Bone strength of the distal humeral diaphysis was estimated by the density-weighted minimum (I$_{MIN}$, cm^4) and maximum (I$_{MAX}$, cm^4) second moments of area, and polar Strength Strain Index (SSI$_P$, mm^3) obtained using cortical mode 2 (threshold = 400 mg/cm^3). I$_{MIN}$ and I$_{MAX}$ were estimated according to Gere and Timoshenko[333], and represent the distribution of bone material about the planes of least and most bending resistance, respectively. They estimate the ability of the bone structure to resist bending in orthogonal planes. SSI$_P$ was calculated by the Stratec software as the polar moment of inertia divided by the maximum distance of the furthest voxel to the torsional axis. SSI$_P$ estimates the ability of a bone structure to resist torsion.

To determine site-specificity of bone geometry adaptive responses associated with throwing, polar pericortical and endocortical radii at the distal humeral diaphysis were obtained for the throwing and nonthrowing arms. Stratec pQCT image files and data were opened in ImageJ (v1.45s; National Institutes of Health) and analyzed using the BoneJ plugin[396], as previously described[397]. Images were rotated to align the bones according to the I$_{MAX}$ and I$_{MIN}$ axes, and right-sided images were flipped to superimpose left-side images. Using a threshold value of 350 mg/cm^3 to locate bone tissue, the distance of the endocortical and pericortical surfaces from the centroid of the medullary cavity were measured in 36 10° polar sectors.

Two-tailed analyses with a level of significance set at 0.05 were performed with IBM SPSS Statistics (v21; SPSS Inc., Chicago, IL). Demographic and anthropometric characteristics were compared between baseline and follow-up using paired sample t-tests. Throwing versus nonthrowing effects on humeral properties were assessed by calculating mean percent differences ([throwing arm – nonthrowing arm] / nonthrowing arm $\times$ 100%) and their 95% confidence intervals (CIs). 95% CIs not crossing 0% were considered statistically significant, as determined by single sample t-tests on the mean percent differences with a population mean of 0%. Throwing effects between baseline and follow-up were determined by comparing the percent difference values between the time periods using paired sample t-tests. This will provide a single value for each subject indicating the amount of bone gain in the throwing upper extremity solely due to exercise and not influenced of growth. Change in pericortical and endocortical radii in each polar section over the 12 months in both the throwing and nonthrowing arms were assessed using paired t-tests. To establish the effect of throwing independent of growth, change in pericortical and endocortical radii in the throwing arm in each polar section were corrected for the percent change in the nonthrowing arm.

5.3   Results

Participant characteristics are detailed in Table 1. At baseline, the sexual maturation of the throwers were prepubertal and did not significantly change at follow-up (x^2=3.08; P=0.21; Table 1). Over the course of 12 months, throwers gained 5.4% (95%CI=2.7% to 8.1%) in height, 17.8% (95%CI=10.9% to 24.7%) in mass and 14.8% (95%CI=10.2% to 19.4%) in whole body lean mass (all. P<0.001; Table 5.1).

Table 5.1. Demographic and anthropometric characteristics of throwers[a].

	Baseline	Follow-up
Demographics		
Age (yr)	10.3 ± 0.6	11.3 ± 0.6**
Tanner Stage (1/2/3)	6/6/0	3/7/2
Playing position (P/C/F)[c]	2/2/8	1/2/9
Preferred throwing arm (L:R)	1:11	—
Age starting competitive baseball (yr)	4.8 ± 1.1	—
Years competing (yr)	5.4 ± 1.8	6.8 ± 1.7*
Training volume (hr/wk)	8.9 ± 4.7	12.3 ± 3.6
Calcium intake (mg/day)	1581 ± 739	1299 ± 593
Whole-body anthropometry		
Height (m)	1.43 ± 0.05	1.51 ± 0.06**
Mass (kg)	38.3 ± 5.3	44.9 ± 6.1**
BMI (kg/m^2)	18.6 ± 2.4	19.8 ± 2.9
Lean mass (kg)[b]	23.9 ± 2.3	27.4 ± 2.9**
Fat mass (%)[b]	26.8 ± 6.4	27.9 ± 8.7

[a] Data indicate mean ± SD (except for frequencies)

[b] Obtained via dual-energy x-ray absorptiometry

[c] Individuals were designated as a P, pitcher; C, catcher; F, fielder if they reported playing these positions as the most percentage of their playing time

*$p < 0.01$, ** $p < 0.001$ (paired sample t-test: baseline vs. follow-up)

†$p < 0.05$ (χ^2 test: baseline vs. follow-up)

There was no throwing-to-nonthrowing arm differences at baseline or follow-up in Ct.vBMD (all $P = 0.189$-0.571; Table 5.2). At baseline and follow-up the throwing arm had greater Ct.BMC than the nonthrowing arm (all $P < 0.001$; Table 5.2). The extra mass was distributed on the periosteal and endosteal surfaces as the throwing arm had greater Tt.Ar and smaller Me.Ar compared to the nonthrowing arm (all $P < 0.001$; Table 5.2). The larger periosteal area and smaller endosteal area at baseline and follow-up resulted in the throwing arm having greater Ct.Th than the nonthrowing arm (all $P < 0.001$; Table 5.2). Overall, the mass and geometric property changes at baseline and follow-up resulted into the throwing arm having greater I$_{MIN}$, I$_{MAX}$ and SSI$_P$ than in the nonthrowing arm (all $P < 0.001$; Table 5.2).

Table 5.2. Percent difference in throwing-to-nonthrowing upper extremity bone quality, structure and estimated strength at the distal humeral diaphysis

	Baseline			Follow-up		
	Nonthrowing[a]	Throwing[a]	% diff. (95% CI)[b]	Nonthrowing[a]	Throwing[a]	% diff. (95% CI)[b]
Ct.vBMD (mg/cm^3)	1138 ± 31.2	1132 ± 36.0	-0.5% (-1.3, 0.3%)	1148 ± 35.6	1147 ± 38.3	-0.1% (-0.6, 0.4%)
Ct.BMC (mg/mm)	137.1 ± 21.1	162.8 ± 20.4	19.6% (12.6, 26.5%)***	150.8 ± 20.7	185.9 ± 23.5	23.9% (16.9, 30.9%)***
Tt.Ar (cm^2)	195.0 ± 22.6	208.8 ± 23.5	7.2% (4.2, 10.1%)***	210.8 ± 26.5	231.6 ± 27.9	10.0% (6.7, 13.4%)***
Ct.Ar (cm^2)	120.5 ± 18.2	144.0 ± 19.6	20.2% (13.0, 27.5%)***	131.4 ± 18.3	162.3 ± 21.6	24.1% (17.0, 31.2%)***
Me.Ar (cm^2)	74.5 ± 14.0	64.8 ± 15.5	-13.3% (-20.7, -5.9%)***	79.4 ± 16.5	69.3 ± 15.0	-12.7% (-17.2, -8.2%)***
Ct.Th (mm)	3.0 ± 0.4	3.6 ± 0.5	21.0% (13.1, 29.0%)***	3.2 ± 0.4	3.9 ± 0.4	23.4% (16.7, 30.2%)***
I_{MIN} (cm^4)	0.23 ± 0.1	0.28 ± 0.1	21.7% (13.5, 29.9%)***	0.27 ± 0.1	0.34 ± 0.1	25.3% (17.4, 33.2%)***
I_{MAX} (cm^4)	0.33 ± 0.1	0.38 ± 0.1	15.7% (9.1, 22.4%)***	0.39 ± 0.1	0.49 ± 0.1	27.2% (17.0, 37.4%)***
SSI_P (mm^3)	554.2 ± 91.6	651.3 ± 93.9	18.3% (11.4, 25.2%)***	637.9 ± 100.8	766.6 ± 113.4	22.7% (16.1, 29.2%)***

[a] Data are mean ± SD.
[b] Mean percent differences between throwing and nonthrowing were assessed using single sample t-tests with a population mean of 0. Significance is indicated by: *p<0.05, **p<0.01, ***p<0.001.

Over the course of 12 months, the throwing arm had greater gains in mass, structure and estimated strength than nonthrowing arm (Figure 5.1). However, there was no significant throwing effect in Ct.vBMD, Ct.Th, and Me.Ar (all $P= 0.176$-0.818). In bone mass, throwing-to-nonthrowing arm differences were found in Ct.BMC with the throwing arm gaining 4.3% (95% Cl $=1.1\%$ to 7.5%) greater mass than nonthrowing arm over the course of 12 months ($P< 0.05$; Figure 1). The greater mass gains over the course of 12 months resulted in 3.9% (95% Cl$= 0.7\%$ to 7.0%) and 2.9% (95% Cl$= 0.3\%$ to 5.4%) greater gains in Ct.Ar and Tt.Ar, respectively (all $P< 0.05$; Figure 5.1). The site specific bone structural changes over 12 months in the nonthrowing arm were gains in the anterior, lateral and posterior pericortical surfaces and a loss in the posterior endocortical surface (all $P< 0.05$; Figure 5.2). In the throwing arm, there were gains in the anterior, medial, posterior and lateral pericortical surfaces and losses in the posterior, medial and anterior endocortical surfaces (all $P< 0.05$; Figure 5.2). Then in the throwing arm with corrections for the nonthrowing arm changes, were gains in the lateral and posterior and a loss in the anterior pericortical surfaces (all $P< 0.05$; Figure 5.2). However, there was no significant changes in the endocortical surface ($P=0.056$-$.965$; Figure 5.2). The overall mass and structural property gains in 12 months, resulted into the throwing arm gains in estimated bone strength, specifically 3.6% (95% Cl$= 0.1\%$ to 7.1%), 11.4% (95% Cl$= 0.8\%$ to 22.1%) and 4.4% (95% Cl$= 2.0\%$ to 6.8%) increase in I_{MIN}, I_{MAX} and SSI_P, respectively (all $P< 0.05$; Figure 5.1).
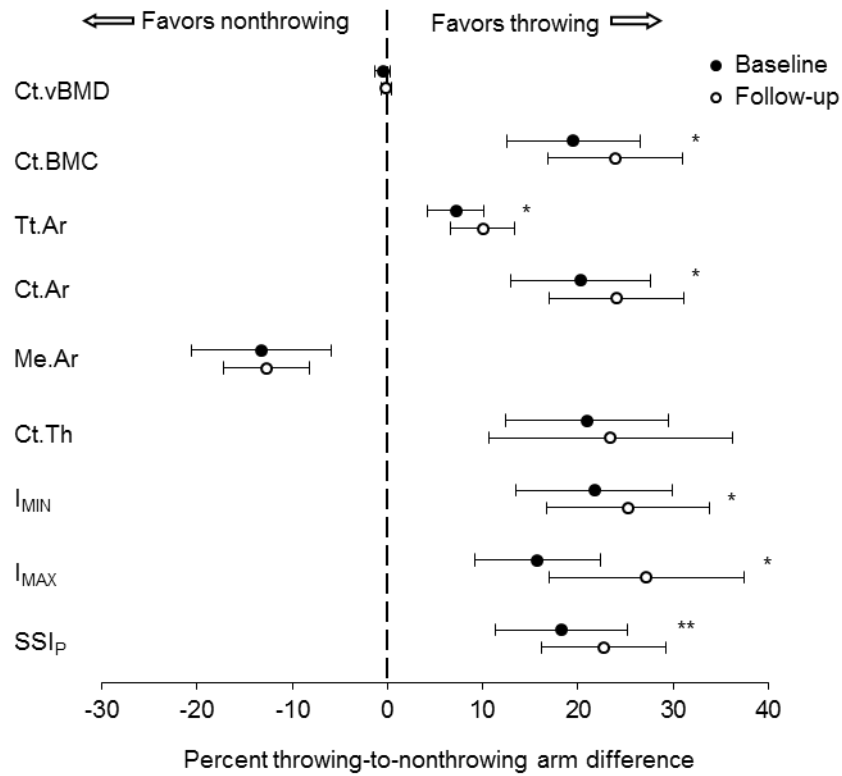
Figure 5.1. Effect of throwing for 12 months on pQCT measures of distal humeral diaphysis. Data indicate the baseline and 12 month mean percent difference and 95%Cl between the throwing and nonthrowing arms. Significant throwing-to-nonthrowing arm differences between baseline and 12 months are indicated by: *$p<0.05$ ** $p<0.01$.
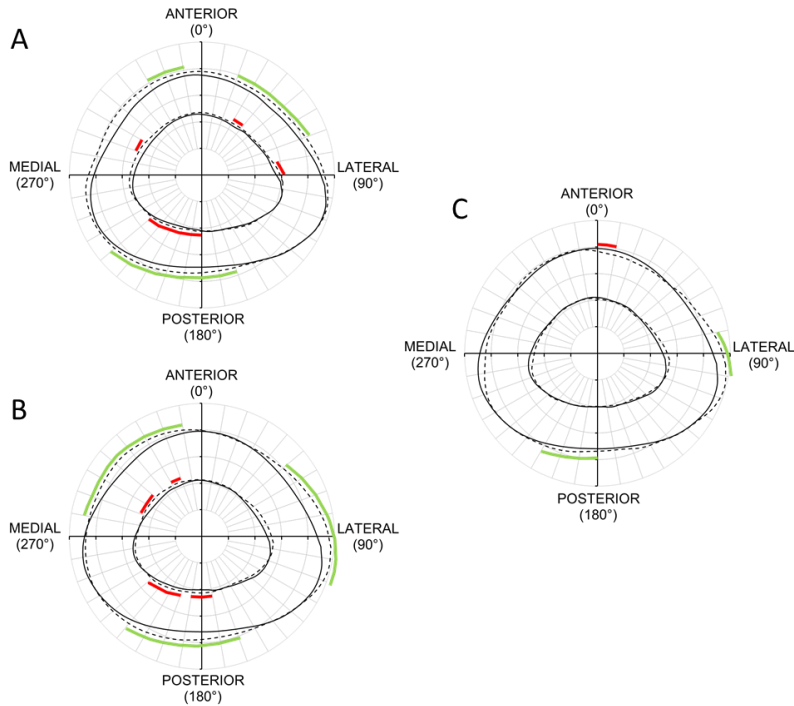
Figure 5.2. Map of distal humeral diaphysis surface-specific bone structural differences between baseline (solid line) and follow-up (dashed line). A. baseline and follow-up nonthrowing arm; B. baseline and follow-up throwing arm; C. baseline and follow-up throwing arms corrected for growth. Green and red lines indicate polar radii wherein the follow-up had significant bone structural gains and losses, respectively (p<0.05).

5.4   Discussion

The results of this prospective study in prepubertal baseball players show that throwing for a period of up to 12 months results in greater gains in distal humeral diaphysis bone properties. There were side-to-side differences in bone mass, size and estimated strength properties at both baseline and follow-up. The side-to-side differences at follow-up were greater than at baseline indicating a within-subject exercise effect. Specifically, there was an exercise effect at the distal humeral diaphysis that resulted in the throwing arm having greater total and cortical bone area with more cortical bone being distributed along the lateral and posterior periosteal surface. The cortical bone

155

surface and site-specific changes resulted in the throwing arm gaining about 4.5% in estimated strength in one year over-and-above growth changes. Collectively, these data suggest that prepubertal baseball players have throwing-related bone property adaptations at the distal humeral diaphysis in as little as 12 months.

The adaptive changes observed within the distal humeral diaphysis of prepubertal baseball players are consistent with the vast body of evidence from unilateral exercise models in animals[260 311 409] and human studies[256 288 410]. Specifically, the cortical bone adaptations observed in the throwing arms of the male prepubertal baseball players are similar to the other cross-sectional and longitudinal studies using prepubertal tennis and baseball players[288 289 306 407]. The cortical bone adaptations that were consistent with those studies included the loaded side being larger with more bone added to the periosteal as opposed to endosteal bone surface. In contrast, a study by Ducher et al.[289] reported that male prepubertal tennis players showed a significant endosteal contraction in the playing arm compared to nonplaying arm. The bone surface-specific adaptation inconsistencies between the current study and the study by Ducher et al.[289] could be explained by the cross-sectional study design used by Ducher et al.[289] and the different loading conditions between studies. Cross-sectional studies do not show a true bone adaptive change due to exercise and growth over time. While baseball and tennis players have been shown to load the humerus similarly[51 411], the strain magnitudes between studies might have resulted into different endosteal surface adaptations.

Estimated bone strength increases in this current study were a function of bone structure as a result of alterations in bone surfaces and area, rather than density because there were no changes in bone density. Other clinical studies have found bone structural

adaptations to exercise contributes more to the overall bone strength compared to bone density[286 300-307]. This has also been shown in animal studies that used an unilateral rat ulna axial loading model, where bone adaptations by mechanical loading resulted in increases in bone strength from structural property contributions rather than bone density[260 284]. The resultant gains in estimated strength in the current study and other studies suggest that it is site-specific new bone formation at the locations where the load caused the greatest demand[260 284]. The site-specific new bone formation at the distal humeral diaphysis in this current study was from new bone tissue laid down on the periosteal surfaces rather than endosteal surfaces. New bone laid on the outside surface as opposed to the inside provides the bone with better resistance to mechanical loads[159 289 306].

In summary, prepubertal baseball players followed for 12 months were shown to gain more bone mass, structure and estimated strength in their throwing arm relative to their nonthrowing arm. Specifically, throwing caused site- and surface-specific cortical bone adaptations at the distal humeral diaphysis that contributed to a gain of 4.5% in estimated strength. In conclusion, these longitudinal data support the cross-sectional studies and provide more definitive evidence that exercise during growth induces gains in bone structure and estimated strength.

CHAPTER SIX: SUMMARY AND FUTURE DIRECTIONS

6.1   Dissertation Summary

Studies in this dissertation explored the response of the skeleton to exercise across the translational divide between animal- and human-based studies, with a particular emphasis on exercise-induced changes in bone structure and estimated strength. Previous studies have explored exercise benefits on bone mass independent of bone structure and estimated strength. However, it has been known bone structure adaptations to exercise contributes disproportionately more to the overall bone strength compared to bone mass. To further the number of studies related to changes in bone structure and estimated strength, unilateral animal and human loading models were used as controlled evidence without having to perform large randomized control trials. Unilateral exercise models enables the contralateral, non-exercised extremity to be used an internal control site for the influences of systemic factors, such as genetics and circulating hormones. In study 1, a dose response between load magnitude and tibial midshaft cortical bone adaptation was observed in mice that had their right tibia loaded in axial compression at one of three load magnitudes for 3 d/wk over 4 weeks. In study 2, the ability of peripheral quantitative computed tomography to provide very good prediction of midshaft humerus mechanical properties with good short-term precision in human subjects was demonstrated. In study 3, collegiate-level jumping (long and/or high jump) athletes were shown to have larger side-to-side differences in tibial midshaft structure and estimated strength between their jump and lead legs than observed in non-jumping athletes. In study 4, prepubertal baseball players followed for 12 months were

shown to gain more bone mass, structure and estimated strength in their throwing arm relative to their nonthrowing arm over the course of 12 months. These cumulative data using a combination of experimental models ranging from animal to cross-sectional and longitudinal human models demonstrate the ability of the skeleton to adapt its structure and estimated strength to the mechanical loading associated with exercise.

6.2   Strengths, limitations and future direction

These studies found that using a combination of experimental models ranging from animal to cross-sectional and longitudinal human models demonstrate the ability of the skeleton to adapt its structure and estimated strength to the mechanical loading associated with exercise. The studies had some strengths and limitations that need to be addressed with future research focusing on addressing the limitations.

In the study one, the data were limited to the loading parameters and animals investigated. Different levels of adaptation may be induced in mice of a different age, sex or genotype, or when loading with a different loading waveform, duration or frequency. There was also a lack of quantification of the loading induced within the proximal tibia because it was assumed that increasing load magnitudes resulted in incremental loading within the proximal tibia; however, this was not quantified through direct measurement or finite element modeling. Future studies need to quantify this when comparing trabecular bone responsiveness to mechanical loading between mice with differing baseline skeletal phenotypes. Finally, there is a possibility that the model causes some degree of lameness-induced unloading which may have obscured any trabecular bone

benefits in the lower load groups. This study did not assess lameness following tibial axial loading through the quantification of ground reaction forces; however, lameness may explain why some studies using this model have observed a loss of BV/TV[200 231 328], and needs further exploration considering axial loading of the mouse leg through a near fully flexed knee has been associated with knee joint degeneration[338].

In study two, there were a number of strengths, including the testing of cadaveric humeri in a novel, yet functional direction, determination of overall precision errors using a large number of degrees of freedom, and investigation of the influences of different testers and time between repeat scans on precision errors. There are also several limitations associated with the work that warrant acknowledgement. During torsional testing of the cadaveric humeri, not all bones failed at the midshaft where pQCT imaging was performed. However, the ability of pQCT measures to predict mechanical properties were very good despite the discrepancies between the imaging and cadaveric bone failure locations possibly negatively impacting predictive relationships. Precision values reported are for the testing protocol utilized and may not be representative of different protocols. Future studies need to look at different scanning parameters (including voxel size and scan speed) and analysis techniques (including scan filtering and thresholding) which are known to influence tissue measures obtained via pQCT[412]. Finally, the precision values in the current study are limited to the subject population and anatomical site assessed. Future studies need to measure at alternate sites or to populations with differing characteristics, including age, size and musculoskeletal health status.

In study three, there were a number of strengths including the comparison of tibial bone properties within-subject to control for selection bias and the inclusion of an athletic

comparative group that did not unilaterally exposed one leg to elevated loads. However, our study also possessed a number of limitations. A relatively small sample size was recruited which may have reduced our power to detect subtle group differences in some measures such as, Ct.BMC and Tt.Ar at the tibial diaphysis. However, the other tibial measures were elevated in the jump leg in the jumpers and comparable to the other study by Ireland et al.[389] suggesting a true effect of jumping-associated forces on the bone. It was also difficult to recruit purely jumping athletes, since some of the athletes also competed in other track and field events as well as other sports that may influence side-to-side differences in bone's properties[413]. Finally, our data are limited to males, with adaptive responses and their magnitude potentially differing in females[414]. Future studies need to address these limitations and also use this athlete or a different athletic model to look at a clinically relevant site such as the proximal femur to observe any trabecular structural and estimated bone strength differences between legs.

In study four, there was a number of strengths, including the comparison of distal humeral diaphysis bone properties within-subject to control for selection bias and normal growth and the longitudinal study design to track the rate of bone adaptive changes due to exercise. However, our study also possessed a number of limitations which included not having a matched control group so the effects of throwing could not be isolated from the influence of side-to-side differences in habitual loading associated with arm dominance. However, the use of within subject longitudinal study design allowed for control of the influence of the systemic factors on the rate of skeletal adaptations due to throwing and other studies have found about 0-4% significant side-to-side differences in bone measures of prepubertal children who do not engage in upper extremity unilateral loading[157 407 415].

An additional limitation was not including information in our throwing questionnaire on the average number of throws so there was not insight on the throwing arm's amount of exposure to loading. A further limitation was the relatively small sample size was recruited which may have reduced our power to detect subtle changes over time in some measures such as, Ct.Th and Me.Ar at the distal humeral diaphysis. However, the other bone measures were elevated in the throwing arm of the prepubertal baseball players and comparable to the other studies by suggesting a true effect of throwing-associated forces on the bone[288 289]. Finally, the data are limited to prepubertal males, with adaptive responses and their magnitude potentially differing in females and other maturation stages[414]. Future studies need to address these limitations and also use this exercise model to explore the interaction between the skeletal benefits of exercise and other factors (such as calcium and vitamin D supplementation).

APPENDIX: PERMISSIONS

Licensee: Alyssa Weatherholt

License Date: May 15, 2015

License Number: 3630380488936

Publication: Journal of Hand Therapy

Title: Specialized Connective Tissue: Bone, the Structural Framework of the Upper
Extremity

Type Of Use: reuse in a thesis/dissertation

Licensee: Alyssa Weatherholt

License Date: May 18, 2015

License Number: 3631921406881

Publication: Clinical Orthopaedics and Related Research

Title: Whole Bone Mechanics and Bone Quality

Type Of Use: Thesis/Dissertation

Licensee: Alyssa Weatherholt

License Date: May 18, 2015

License Number: 3632041337574

Publication: Bone

Title: Bone mineralization density distribution in health and disease

Type Of Use: reuse in a thesis/dissertation

Licensee: Alyssa Weatherholt

License Date: May 19, 2015

License Number: 3632560591258

Publication: British Journal of Sports Medicine

Title: Exercise and bone health: optimising bone structure during growth is key, but all is not in vain during ageing

Type Of Use: Dissertation/Thesis

Licensee: Alyssa Weatherholt

License Date: May 18, 2015

Publication: Massachusetts Medical Society, Publisher of the New England Journal of Medicine.

Title: Mechanisms of anabolic therapies for osteoporosis

Type Of Use: Dissertation/Thesis

REFERENCES

1. Weatherholt AM, Fuchs RK, Warden SJ. Specialized connective tissue: bone, the structural framework of the upper extremity. Journal of Hand Therapy 2012;**25**(2):123-32.

2. O'Loughlin V, McKinley M. Human Anatomy: New York, NY: McGraw-Hill, 2006.

3. Roschger P, Paschalis E, Fratzl P, et al. Bone mineralization density distribution in health and disease. Bone 2008;**42**(3):456-66.

4. Melton LJ, 3rd, Christen D, Riggs BL, et al. Assessing forearm fracture risk in postmenopausal women. Osteoporos Int 2010;**21**(7):1161-9.

5. Mow VC, Ratcliffe A, Woo SL-Y. *Biomechanics of Diarthrodial Joints*. New York: Springer, 1990.

6. Riggs BL, Melton LJ, Robb RA, et al. A population-based assessment of rates of bone loss at multiple skeletal sites: evidence for substantial trabecular bone loss in young adult women and men. J Bone Miner Res 2008;**23**(2):205-14.

7. Taichman RS. Blood and bone: two tissues whose fates are intertwined to create the hematopoietic stem-cell niche. Blood 2005;**105**(7):2631-9.

8. Yin T, Li L. The stem cell niches in bone. J Clin Invest 2006;**116**(5):1195-201.

9. Currey JD. The many adaptations of bone. J Biomech 2003;**36**(10):1487-95.

10. Silva MJ, Touhey DC. Bone formation after damaging in vivo fatigue loading results in recovery of whole-bone monotonic strength and increased fatigue life. J Orthop Res 2007;**25**(2):252-61.

11. Buckwalter JA, Glimcher MJ, Cooper RR, et al. Bone biology. I: Structure, blood supply, cells, matrix, and mineralization. Instr Course Lect 1996;**45**:371-86.

12. Landis WJ, Hodgens KJ, Arena J, et al. Structural relations between collagen and mineral in bone as determined by high voltage electron microscopic tomography. Microsc Res Tech 1996;**33**(2):192-202.

13. Landis WJ, Hodgens KJ, Song MJ, et al. Mineralization of collagen may occur on fibril surfaces: evidence from conventional and high-voltage electron microscopy and three-dimensional imaging. J Struct Biol 1996;**117**(1):24-35.

14. McHugh KP, Hodivala-Dilke K, Zheng MH, et al. Mice lacking beta3 integrins are osteosclerotic because of dysfunctional osteoclasts. J Clin Invest 2000;**105**(4):433-40.

15. Teitelbaum SL. Bone resorption by osteoclasts. Science 2000;**289**(5484):1504-8.

16. Hirose S, Li M, Kojima T, et al. A histological assessment on the distribution of the osteocytic lacunar canalicular system using silver staining. J Bone Miner Metab 2007;**25**(6):374-82.

17. Bonewald LF. Mechanosensation and transduction in osteocytes. Bonekey Osteovision 2006;**3**(10):7-15.

18. Wang L, Wang Y, Han Y, et al. In situ measurement of solute transport in the bone lacunar-canalicular system. Proc Natl Acad Sci U S A 2005;**102**(33):11911-6.

19. Robling AG, Niziolek PJ, Baldridge LA, et al. Mechanical stimulation of bone in vivo reduces osteocyte expression of Sost/sclerostin. J Biol Chem 2007.

20. Tatsumi S, Ishii K, Amizuka N, et al. Targeted ablation of osteocytes induces osteoporosis with defective mechanotransduction. Cell Metab 2007;**5**(6):464-75.

21. Lane NE, Yao W, Balooch M, et al. Glucocorticoid-treated mice have localized changes in trabecular bone material properties and osteocyte lacunar size that are not observed in placebo-treated or estrogen-deficient mice. J Bone Miner Res 2006;**21**(3):466-76.

22. Feng JQ, Ward LM, Liu S, et al. Loss of DMP1 causes rickets and osteomalacia and identifies a role for osteocytes in mineral metabolism. Nat Genet 2006;**38**(11):1310-5.

23. Ahlborg HG, Johnell O, Turner CH, et al. Bone loss and bone size after menopause. N Engl J Med 2003;**349**(4):327-34.

24. Frost HM. Skeletal structural adaptations to mechanical usage (SATMU): 1. Redefining Wolff's law: the bone modeling problem. Anatomical Record 1990;**226**:403-13.

25. Dempster D. Bone modeling and remodeling. In: Dempster D, Felsenberg D, van Der Geest S, eds. The Bone Quality Book: A Guide to Factors Influencing Bone Strength. Amsterdam, Netherlands: Excerpta Medica, 2006:64-73.

26. Parfitt AM. The mechanism of coupling: a role for the vasculature. Bone 2000;**26**(4):319-23.

27. Hodsman AB, Bauer DC, Dempster DW, et al. Parathyroid hormone and teriparatide for the treatment of osteoporosis: a review of the evidence and suggested guidelines for its use. Endocr Rev 2005;**26**(5):688-703.

28. Canalis E, Giustina A, Bilezikian JP. Mechanisms of anabolic therapies for osteoporosis. New England Journal of Medicine 2007;**357**(9):905-16.

166

29. Shapiro F. Bone development and its relation to fracture repair: the role of mesenchymal osteoblasts and surface osteoblasts. Eur Cell Mater 2008;**15**:53-76.

30. Turner CH, Burr DB. Basic biomechanical measurements of bone: a tutorial. Bone 1993;**14**(4):595-608.

31. Burr D, Milgrom C, Fyhrie D, et al. In vivo measurement of human tibial strains during vigorous activity. Bone 1996;**18**(5):405-10.

32. Ekenman I, Halvorsen K, Westblad P, et al. Local bone deformation at two predominant sites for stress fractures of the tibia: an in vivo study. Foot & ankle international 1998;**19**(7):479-84.

33. Vashishth D, Tanner K, Bonfield W. Fatigue of cortical bone under combined axial-torsional loading. Journal of Orthopaedic Research 2001;**19**(3):414-20.

34. Cole JH, van der Meulen MC. Whole bone mechanics and bone quality. Clinical Orthopaedics and Related Research® 2011;**469**(8):2139-49.

35. Hsieh YF, Robling AG, Ambrosius WT, et al. Mechanical loading of diaphyseal bone in vivo: the strain threshold for an osteogenic response varies with location. Journal of Bone and Mineral Research 2001;**16**(12):2291-97.

36. Burr DB, Allen MR. *Basic and Applied Bone Biology*: Academic Press, 2013.

37. Gross T, McLeod KJ, Rubin CT. Characterizing bone strain distributions< i> in vivo</i> using three triple rosette strain gages. Journal of biomechanics 1992;**25**(9):1081-87.

38. Forwood MR, Parker AW. Effects of exercise on bone growth mechanical and physical properties studied in the rat. Clinical Biomechanics 1987;**2**(4):185-90.

39. Beaupied H, Lespessailles E, Benhamou C-L. Evaluation of macrostructural bone biomechanics. Joint Bone Spine 2007;**74**(3):233-39.

40. Levenston ME, Beaupré GS, van der Meulen MC. Improved method for analysis of whole bone torsion tests. Journal of Bone and Mineral Research 1994;**9**(9):1459-65.

41. Jämsä T, Jalovaara P, Peng Z, et al. Comparison of three-point bending test and peripheral quantitative computed tomography analysis in the evaluation of the strength of mouse femur and tibia. Bone 1998;**23**(2):155-61.

42. Bonadio J, Jepsen K, Mansoura M, et al. A murine skeletal adaptation that significantly increases cortical bone mechanical properties. Implications for human skeletal fragility. Journal of Clinical Investigation 1993;**92**(4):1697.

43. Jepsen KJ, Goldstein SA, Kuhn JL, et al. Type-I collagen mutation compromises the post-yield behavior of Mov13 long bone. Journal of orthopaedic research 1996;**14**(3):493-99.

44. Kazakia GJ, Majumdar S. New imaging technologies in the diagnosis of osteoporosis. Reviews in Endocrine and Metabolic Disorders 2006;**7**(1-2):67-74.

45. Goldstein SA, Wilson DL, Sonstegard DA, et al. The mechanical properties of human tibial trabecular bone as a function of metaphyseal location. Journal of biomechanics 1983;**16**(12):965-69.

46. Van der Meulen M, Jepsen K, Mikić B. Understanding bone strength: size isn't everything. Bone 2001;**29**(2):101-04.

47. Galante J, Rostoker W, Ray R. Physical properties of trabecular bone. Calcified tissue research 1970;**5**(1):236-46.

48. Ulrich D, Hildebrand T, Van Rietbergen B, et al. The quality of trabecular bone evaluated with micro-computed tomography, FEA and mechanical testing. Studies in health technology and informatics 1997:97-112.

49. Fields AJ, Lee GL, Liu XS, et al. Influence of vertical trabeculae on the compressive strength of the human vertebra. Journal of Bone and Mineral Research 2011;**26**(2):263-69.

50. Mosekilde L, Viidik A, Mosekilde L. Correlation between the compressive strength of iliac and vertebral trabecular bone in normal individuals. Bone 1985;**6**(5):291-95.

51. Battaglia TC, Tsou A-C, Taylor EA, et al. Ash content modulation of torsionally derived effective material properties in cortical mouse bone. Journal of biomechanical engineering 2003;**125**(5):615-19.

52. Burstein AH, Zika J, Heiple K, et al. Contribution of collagen and mineral to the elastic-plastic properties of bone. The Journal of Bone & Joint Surgery 1975;**57**(7):956-61.

53. Currey JD. The effect of porosity and mineral content on the Young's modulus of elasticity of compact bone. Journal of biomechanics 1988;**21**(2):131-39.

54. Akkus O, Adar F, Schaffler MB. Age-related changes in physicochemical properties of mineral crystals are related to impaired mechanical function of cortical bone. Bone 2004;**34**(3):443-53.

55. Donnelly E, Chen DX, Boskey AL, et al. Contribution of mineral to bone structural behavior and tissue mechanical properties. Calcified tissue international 2010;**87**(5):450-60.

56. Boskey A, Wright T, Blank R. Collagen and bone strength. Journal of Bone and Mineral Research 1999;**14**(3):330-35.

57. Burr D. The contribution of the organic matrix to bone's material properties. Bone 2002;**31**(1):8-11.

58. Burr DB, Martin RB, Schaffler MB, et al. Bone remodeling in response to< i> in vivo</i> fatigue microdamage. Journal of biomechanics 1985;**18**(3):189-200.

59. Ruppel ME, Burr DB, Miller LM. Chemical makeup of microdamaged bone differs from undamaged bone. Bone 2006;**39**(2):318-24.

60. Timlin JA, Carden A, Morris MD, et al. Raman spectroscopic imaging markers for fatigue-related microdamage in bovine bone. Analytical chemistry 2000;**72**(10):2229-36.

61. Nyman JS, Roy A, Shen X, et al. The influence of water removal on the strength and toughness of cortical bone. Journal of biomechanics 2006;**39**(5):931-38.

62. Vetter U, Pontz B, Zauner E, et al. Osteogenesis imperfecta: a clinical study of the first ten years of life. Calcified tissue international 1992;**50**(1):36-41.

63. Del Fattore A, Cappariello A, Teti A. Genetics, pathogenesis and complications of osteopetrosis. Bone 2008;**42**(1):19-29.

64. Wagner CL, Greer FR. Prevention of rickets and vitamin D deficiency in infants, children, and adolescents. Pediatrics 2008;**122**(5):1142-52.

65. Yakar S, Rosen CJ, Beamer WG, et al. Circulating levels of IGF-1 directly regulate bone growth and density. The Journal of clinical investigation 2002;**110**(110 (6)):771-81.

66. Warriner AH, Saag KG. Prevention and Treatment of Bone Changes Associated with Exposure to Glucocorticoids. Current osteoporosis reports 2013;**11**(4):341-47.

67. Farhat G, Yamout B, Mikati M, et al. Effect of antiepileptic drugs on bone density in ambulatory patients. Neurology 2002;**58**(9):1348-53.

68. Khan FA, Fisher JG, Bairdain S, et al. Metabolic bone disease in pediatric intestinal failure patients: Prevalence and risk factors. Journal of pediatric surgery 2015;**50**(1):136-39.

69. Shah M, Shahid F, Chakravarty K. Paget's disease: a clinical review. British journal of hospital medicine (London, England: 2005) 2015;**76**(1):25-30.

70. Fleet JC. Molecular regulation of calcium metabolism. Calcium in human health: Springer, 2006:163-89.

71. Weaver CM, Heaney RP. Food sources, supplements, and bioavailability. Calcium in human health: Springer, 2006:129-42.

72. Gutierrez K. Bone and joint infections in children. Pediatric clinics of North America 2005;**52**(3):779-94.

73. Houlihan CM, Stevenson RD. Bone density in cerebral palsy. Phys Med Rehabil Clin N Am 2009;**20**(3):493-508.

74. Demir SO, Oktay F, Uysal H, et al. Upper extremity shortness in children with hemiplegic cerebral palsy. J Pediatr Orthop 2006;**26**(6):764-8.

75. Golomb MR, McDonald BC, Warden SJ, et al. In-home virtual reality videogame telerehabilitation in adolescents with hemiplegic cerebral palsy. Arch Phys Med Rehabil 2010;**91**(1):1-8 e1.

76. Stevenson RD, Conaway M, Barrington JW, et al. Fracture rate in children with cerebral palsy. Pediatr Rehabil 2006;**9**(4):396-403.

77. Jorgensen L, Jacobsen BK, Wilsgaard T, et al. Walking after stroke: does it matter? Changes in bone mineral density within the first 12 months after stroke. A longitudinal study. Osteoporos Int 2000;**11**(5):381-7.

78. Burge R, Dawson-Hughes B, Solomon DH, et al. Incidence and economic burden of osteoporosis-related fractures in the United States, 2005–2025. Journal of bone and mineral research 2007;**22**(3):465-75.

79. Kanis JA, Johnell O, Oden A, et al. Long-term risk of osteoporotic fracture in Malmo. Osteoporos Int 2000;**11**(8):669-74.

80. Jarvinen TL, Sievanen H, Khan KM, et al. Shifting the focus in fracture prevention from osteoporosis to falls. BMJ 2008;**336**(7636):124-6.

81. Seeman E, Delmas PD. Bone quality--the material and structural basis of bone strength and fragility. N Engl J Med 2006;**354**(21):2250-61.

82. Manolagas SC. Birth and death of bone cells: basic regulatory mechanisms and implications for the pathogenesis and treatment of osteoporosis. Endocr Rev 2000;**21**(2):115-37.

83. Riggs BL, Khosla S, Melton III LJ. Sex steroids and the construction and conservation of the adult skeleton. Endocrine reviews 2002;**23**(3):279-302.

84. van der Linden JC, Homminga J, Verhaar JA, et al. Mechanical consequences of bone loss in cancellous bone. J Bone Miner Res 2001;**16**(3):457-65.

85. Zebaze RM, Ghasem-Zadeh A, Bohte A, et al. Intracortical remodelling and porosity in the distal radius and post-mortem femurs of women: a cross-sectional study. Lancet 2010;**375**:1729-36.

86. Mazess R, Chesnut III CH, McClung M, et al. Enhanced precision with dual-energy X-ray absorptiometry. Calcified tissue international 1992;**51**(1):14-17.

87. Kelly T, Slovik D, Schoenfeld D, et al. Quantitative Digital Radiography Versus Dual Photon Absorptiometry of the Lumbar Spine*. The Journal of Clinical Endocrinology & Metabolism 1988;**67**(4):839-44.

88. MacIntyre NJ, Lorbergs AL. Imaging-based methods for non-invasive assessment of bone properties influenced by mechanical loading. Physiotherapy Canada 2012;**64**(2):202-15.

89. BECK TJ, RUFF CB, WARDEN KE, et al. Predicting femoral neck strength from bone mineral data: a structural approach. Investigative radiology 1990;**25**(1):6-18.

90. Faulkner KG, Cummings SR, Black D, et al. Simple measurement of femoral geometry predicts hip fracture: the study of osteoporotic fractures. Journal of bone and mineral research 1993;**8**(10):1211-17.

91. Khoo BC, Wilson SG, Worth GK, et al. A comparative study between corresponding structural geometric variables using 2 commonly implemented hip structural analysis algorithms applied to dual-energy X-ray absorptiometry images. Journal of Clinical Densitometry 2009;**12**(4):461-67.

92. Prevrhal S, Shepherd JA, Faulkner KG, et al. Comparison of DXA hip structural analysis with volumetric QCT. Journal of Clinical Densitometry 2008;**11**(2):232-36.

93. Beck TJ, Oreskovic TL, Stone KL, et al. Structural adaptation to changing skeletal load in the progression toward hip fragility: the study of osteoporotic fractures. Journal of Bone and Mineral Research 2001;**16**(6):1108-19.

94. El-Kaissi S, Pasco J, Henry M, et al. Femoral neck geometry and hip fracture risk: the Geelong osteoporosis study. Osteoporosis international 2005;**16**(10):1299-303.

95. Lou Bonnick S. Hsa: Beyond bmd with dxa. Bone 2007;**41**(1):S9-S12.

96. Beck TJ. Extending DXA beyond bone mineral density: understanding hip structure analysis. Current osteoporosis reports 2007;**5**(2):49-55.

97. Webber CE, Papaioannou A, Winegard KJ, et al. A 6-mo home-based exercise program may slow vertebral height loss. Journal of Clinical Densitometry 2004;**6**(4):391-400.

98. Rosen CJ, Compston JE, Lian JB. *Primer on the metabolic bone diseases and disorders of mineral metabolism*: John Wiley & Sons, 2009.

99. Marshall D, Johnell O, Wedel H. Meta-analysis of how well measures of bone mineral density predict occurrence of osteoporotic fractures. Bmj 1996;**312**(7041):1254-59.

100. NIH Consensus Development Panel on Osteoporosis Prevention D, Therapy. Osteoporosis prevention, diagnosis, and therapy. Jama 2001;**285**(6).

101. Robling AG, Castillo AB, Turner CH. Biomechanical and molecular regulation of bone remodeling. Annu Rev Biomed Eng 2006;**8**:455-98.

102. Heaney RP. BMD: the problem. Osteoporosis International 2005;**16**(9):1013-15.

103. Schreiber JJ, Anderson PA, Rosas HG, et al. Hounsfield units for assessing bone mineral density and strength: a tool for osteoporosis management. The Journal of Bone & Joint Surgery 2011;**93**(11):1057-63.

104. Gittoes N. Osteoporosis: Pathophysiology and Clinical Management. Clinical endocrinology 2003;**59**(6):826-27.

105. Lang TF, Li J, Harris ST, et al. Assessment of vertebral bone mineral density using volumetric quantitative CT. Journal of computer assisted tomography 1999;**23**(1):130-37.

106. Mastmeyer A, Engelke K, Fuchs C, et al. A hierarchical 3D segmentation method and the definition of vertebral body coordinate systems for QCT of the lumbar spine. Medical Image Analysis 2006;**10**(4):560-77.

107. Habashy AH, Yan X, Brown JK, et al. Estimation of bone mineral density in children from diagnostic CT images: a comparison of methods with and without an internal calibration standard. Bone 2011;**48**(5):1087-94.

108. Stratec Medizintchnik X. 3000 manual, software version 6.20: Germany, 2009.

109. Cointry G, Capozza R, Negri A, et al. Biomechanical background for a noninvasive assessment of bone strength and muscle-bone interactions. Journal of Musculoskeletal and Neuronal Interactions 2004;**4**(1):1.

110. Wilhelm G, Felsenberg D, Bogusch G, et al. Biomechanical examinations for validation of the bone strength strain index SSI, calculated by peripheral quantitative computed tomography. Musculoskeletal interactions 1999;**2**:105-10.

111. Kontulainen S, Johnston J, Liu D, et al. Strength indices from pQCT imaging predict up to 85% of variance in bone failure properties at tibial epiphysis and diaphysis. J Musculoskelet Neuronal Interact 2008;**8**(4):401-9.

112. Haapasalo H, Kontulainen S, Sievänen H, et al. Exercise-induced bone gain is due to enlargement in bone size without a change in volumetric bone density: a peripheral quantitative computed tomography study of the upper arms of male tennis players. Bone 2000;**27**(3):351-57.

113. Cheng S, Sipilä S, Taaffe D, et al. Change in bone mass distribution induced by hormone replacement therapy and high-impact physical exercise in post-menopausal women. Bone 2002;**31**(1):126-35.

114. Ashe M, Fehling P, Eng J, et al. Bone geometric response to chronic disuse following stroke: a pQCT study. Journal of Musculoskeletal and Neuronal Interactions 2006;**6**(3):226.

115. Pang MY, Ashe MC, Eng JJ. Muscle weakness, spasticity and disuse contribute to demineralization and geometric changes in the radius following chronic stroke. Osteoporosis international 2007;**18**(9):1243-52.

116. Pang MY, Ashe MC, Eng JJ, et al. A 19-week exercise program for people with chronic stroke enhances bone geometry at the tibia: a peripheral quantitative computed tomography study. Osteoporosis international 2006;**17**(11):1615-25.

117. Crabtree N, Loveridge N, Parker M, et al. Intracapsular Hip Fracture and the Region-Specific Loss of Cortical Bone: Analysis by Peripheral Quantitative Computed Tomography. Journal of Bone and Mineral Research 2001;**16**(7):1318-28.

118. Martin RB, Burr DB, Sharkey NA. Analysis of bone remodeling. Skeletal tissue mechanics: Springer, 1998:79-125.

119. Huiskes R, Van Rietbergen B. Biomechanics of bone. Basic Orthopaedic Biomechanics and Mechano-Biology, 3rd ed, VC Mow and R Huiskes, eds, Lippincott Williams and Wilkins, Philadelphia, PA 2005:123-79.

120. MacIntyre NJ, Adachi JD, Webber CE. In vivo measurement of apparent trabecular bone structure of the radius in women with low bone density discriminates patients with recent wrist fracture from those without fracture. Journal of Clinical Densitometry 2003;**6**(1):35-43.

121. MacIntyre NJ, Adachi JD, Webber CE. In vivo detection of structural differences between dominant and nondominant radii using peripheral quantitative computed tomography. Journal of Clinical Densitometry 2000;**2**(4):413-22.

122. Khosla S, Riggs BL, Atkinson EJ, et al. Effects of sex and age on bone microstructure at the ultradistal radius: a population-based noninvasive in vivo assessment. Journal of Bone and Mineral Research 2006;**21**(1):124-31.

123. Nilsson M, Sundh D, Ohlsson C, et al. Exercise during growth and young adulthood is independently associated with cortical bone size and strength in old Swedish men. Journal of Bone and Mineral Research 2014.

124. Zhu TY, Griffith JF, Qin L, et al. Alterations of Bone Density, Microstructure and Strength of the Distal Radius in Male Patients with Rheumatoid Arthritis: A Case-Control Study with HR-pQCT. Journal of Bone and Mineral Research 2014.

125. Sornay-Rendu E, Cabrera-Bravo JL, Boutroy S, et al. Severity of vertebral fractures is associated with alterations of cortical architecture in postmenopausal women. Journal of Bone and Mineral Research 2009;**24**(4):737-43.

126. Nickolas TL, Stein E, Cohen A, et al. Bone mass and microarchitecture in CKD patients with fracture. Journal of the American Society of Nephrology 2010;**21**(8):1371-80.

127. Laib A, Rüegsegger P. Comparison of structure extraction methods for in vivo trabecular bone measurements. Computerized medical imaging and graphics 1999;**23**(2):69-74.

128. Weatherholt AM, Avin KG, Hurd AL, et al. Peripheral Quantitative Computed Tomography Predicts Humeral Diaphysis Torsional Mechanical Properties With Good Short-Term Precision. Journal of Clinical Densitometry 2014.

129. Majumdar S. Magnetic resonance imaging of trabecular bone structure. Topics in Magnetic Resonance Imaging 2002;**13**(5):323-34.

130. Krug R, Burghardt AJ, Majumdar S, et al. High-resolution imaging techniques for the assessment of osteoporosis. Radiologic Clinics of North America 2010;**48**(3):601.

131. Majumdar S, Genant H, Grampp S, et al. Correlation of trabecular bone structure with age, bone mineral density, and osteoporotic status: in vivo studies in the distal radius using high resolution magnetic resonance imaging. Journal of Bone and Mineral Research 1997;**12**(1):111-18.

132. Majumdar S, Link T, Augat P, et al. Trabecular bone architecture in the distal radius using magnetic resonance imaging in subjects with fractures of the proximal femur. Osteoporosis international 1999;**10**(3):231-39.

133. Majumdar S, Newitt D, Mathur A, et al. Magnetic resonance imaging of trabecular bone structure in the distal radius: relationship with X-ray tomographic microscopy and biomechanics. Osteoporosis international 1996;**6**(5):376-85.

134. Nikander R, Kannus P, Dastidar P, et al. Targeted exercises against hip fragility. Osteoporosis international 2009;**20**(8):1321-28.

135. Nikander R, Sievänen H, Heinonen A, et al. Load-specific differences in the structure of femoral neck and tibia between world-class moguls skiers and slalom skiers. Scandinavian journal of medicine & science in sports 2008;**18**(2):145-53.

136. Vieth V, Link TM, Lotter A, et al. Does the trabecular bone structure depicted by high-resolution MRI of the calcaneus reflect the true bone structure? Investigative radiology 2001;**36**(4):210-17.

137. Brock GR, Chen JT, Ingraffea AR, et al. The effect of osteoporosis treatments on fatigue properties of cortical bone tissue. Bone Reports 2015;**2**:8-13.

138. Allen MR, Burr DB. Mineralization, microdamage, and matrix: how bisphosphonates influence material properties of bone. BoneKEy-Osteovision 2007;**4**(2):49-60.

139. Yamagami Y, Mashiba T, Iwata K, et al. Effects of minodronic acid and alendronate on bone remodeling, microdamage accumulation, degree of mineralization and bone mechanical properties in ovariectomized cynomolgus monkeys. Bone 2013;**54**(1):1-7.

140. Allen MR, Burr DB. Bisphosphonate effects on bone turnover, microdamage, and mechanical properties: what we think we know and what we know that we don't know. Bone 2011;**49**(1):56-65.

141. Isaacs JD, Shidiak L, Harris IA, et al. Femoral insufficiency fractures associated with prolonged bisphosphonate therapy. Clinical Orthopaedics and Related Research® 2010;**468**(12):3384-92.

142. Investigators WGftWsHI. Risks and benefits of estrogen plus progestin in healthy postmenopausal women: principal results from the Women's Health Initiative randomized controlled trial. Jama 2002;**288**(3):321-33.

143. Ettinger B, Black DM, Mitlak BH, et al. Reduction of vertebral fracture risk in postmenopausal women with osteoporosis treated with raloxifene: results from a 3-year randomized clinical trial. Jama 1999;**282**(7):637-45.

144. Cardona J, Pastor E. Calcitonin versus etidronate for the treatment of postmenopausal osteoporosis: a meta-analysis of published clinical trials. Osteoporosis international 1997;**7**(3):165-74.

145. Papapoulos S, Chapurlat R, Libanati C, et al. Five years of denosumab exposure in women with postmenopausal osteoporosis: results from the first two years of the FREEDOM extension. Journal of Bone and Mineral Research 2012;**27**(3):694-701.

146. Ma YL, Zeng Q, Donley DW, et al. Teriparatide increases bone formation in modeling and remodeling osteons and enhances IGF-II immunoreactivity in

postmenopausal women with osteoporosis. Journal of Bone and Mineral Research 2006;**21**(6):855-64.

147. Miyauchi A, Matsumoto T, Sugimoto T, et al. Effects of teriparatide on bone mineral density and bone turnover markers in Japanese subjects with osteoporosis at high risk of fracture in a 24-month clinical study: 12-month, randomized, placebo-controlled, double-blind and 12-month open-label phases. Bone 2010;**47**(3):493-502.

148. Neer RM, Arnaud CD, Zanchetta JR, et al. Effect of parathyroid hormone (1-34) on fractures and bone mineral density in postmenopausal women with osteoporosis. New England Journal of Medicine 2001;**344**(19):1434-41.

149. Vahle JL, Sato M, Long GG, et al. Skeletal changes in rats given daily subcutaneous injections of recombinant human parathyroid hormone (1-34) for 2 years and relevance to human safety. Toxicologic pathology 2002;**30**(3):312-21.

150. Weaver CM, Janle E, Martin B, et al. Dairy versus calcium carbonate in promoting peak bone mass and bone maintenance during subsequent calcium deficiency. Journal of Bone and Mineral Research 2009;**24**(8):1411-19.

151. Bischoff-Ferrari HA, Dawson-Hughes B, Baron JA, et al. Calcium intake and hip fracture risk in men and women: a meta-analysis of prospective cohort studies and randomized controlled trials. The American journal of clinical nutrition 2007;**86**(6):1780-90.

152. Jackson RD, LaCroix AZ, Gass M, et al. Calcium plus vitamin D supplementation and the risk of fractures. New England Journal of Medicine 2006;**354**(7):669-83.

153. Rejnmark L, Avenell A, Masud T, et al. Vitamin D with calcium reduces mortality: patient level pooled analysis of 70,528 patients from eight major vitamin D trials. The Journal of Clinical Endocrinology & Metabolism 2012;**97**(8):2670-81.

154. Bischoff-Ferrari HA, Dawson-Hughes B, Staehelin HB, et al. Fall prevention with supplemental and active forms of vitamin D: a meta-analysis of randomised controlled trials. Bmj 2009;**339**:b3692.

155. Bischoff HA, Stähelin HB, Dick W, et al. Effects of vitamin D and calcium supplementation on falls: a randomized controlled trial. Journal of bone and mineral research 2003;**18**(2):343-51.

156. Ross AC, Manson JE, Abrams SA, et al. The 2011 report on dietary reference intakes for calcium and vitamin D from the Institute of Medicine: what clinicians need to know. The Journal of Clinical Endocrinology & Metabolism 2011;**96**(1):53-58.

157. Kannus P, Haapasalo H, Sankelo M, et al. Effect of starting age of physical activity on bone mass in the dominant arm of tennis and squash players. Annals of Internal Medicine 1995;**123**(1):27-31.

158. Hui SL, Slemenda CW, Johnston Jr CC. Age and bone mass as predictors of fracture in a prospective study. Journal of clinical investigation 1988;**81**(6):1804.

159. Kontulainen S, Sievanen H, Kannus P, et al. Effect of long-term impact-loading on mass, size, and estimated strength of humerus and radius of female racquet-sports players: a peripheral quantitative computed tomography study between young and old starters and controls. J Bone Miner Res 2003;**18**(2):352-9.

160. Prince RL, Smith M, Dick IM, et al. Prevention of postmenopausal osteoporosis: a comparative study of exercise, calcium supplementation, and hormone-replacement therapy. New England journal of medicine 1991;**325**(17):1189-95.

161. Henderson NK, White CP, Eisman JA. The roles of exercise and fall risk reduction in the prevention of osteoporosis. Endocrinology and metabolism clinics of North America 1998;**27**(2):369-87.

162. Kato T, Yamashita T, Mizutani S, et al. Adolescent exercise associated with long-term superior measures of bone geometry: a cross-sectional DXA and MRI study. British journal of sports medicine 2009;**43**(12):932-35.

163. Martyn-St James M, Carroll S. A meta-analysis of impact exercise on postmenopausal bone loss: the case for mixed loading exercise programmes. British Journal of Sports Medicine 2008.

164. Warden SJ, Mantila Roosa SM. Physical activity completed when young has residual bone benefits at 94 years of age: a within-subject controlled case study. J Musculoskelet Neuronal Interact 2014;**14**(2):239-43.

165. Warden SJ, Mantila Roosa SM, Kersh ME, et al. Physical activity when young provides lifelong benefits to cortical bone size and strength in men. Proc Natl Acad Sci U S A 2014;**111**:5337-42.

166. Wolff J. The law of bone transformation. Berlin: Hirschwald 1892.

167. Cowin S. Wolff's law of trabecular architecture at remodeling equilibrium. Journal of biomechanical engineering 1986;**108**(1):83-88.

168. Roesler H. The history of some fundamental concepts in bone biomechanics. Journal of biomechanics 1987;**20**(11):1025-34.

169. Frost HM. A 2003 update of bone physiology and Wolff's Law for clinicians. The Angle orthodontist 2004;**74**(1):3-15.

170. Sugiyama T, Price JS, Lanyon LE. Functional adaptation to mechanical loading in both cortical and cancellous bone is controlled locally and is confined to the loaded bones. Bone 2010;**46**(2):314-21.

171. Lanyon LE, Sugiyama T, Price JS. Regulation of bone mass: Local control or systemic influence or both? IBMS BoneKEy 2009;**6**(6):218-26.

172. Woo S, Kuei SC, Amiel D, et al. The effect of prolonged physical training on the properties of long bone: a study of Wolff's Law. The Journal of Bone & Joint Surgery 1981;**63**(5):780-87.

173. Loitz BJ, Zernicke RF. Strenuous exercise-induced remodelling of mature bone: relationships between in vivo strains and bone mechanics. Journal of experimental biology 1992;**170**(1):1-18.

174. Yeh JK, Aloia JF, Chen MM, et al. Influence of exercise on cancellous bone of the aged female rat. Journal of Bone and Mineral Research 1993;**8**(9):1117-25.

175. Bourrin S, Ghaemmaghami F, Vico L, et al. Effect of a five-week swimming program on rat bone: a histomorphometric study. Calcified tissue international 1992;**51**(2):137-42.

176. Snyder A, Zierath J, Hawley J, et al. The effects of exercise mode, swimming vs. running, upon bone growth in the rapidly growing female rat. Mechanisms of ageing and development 1992;**66**(1):59-69.

177. Martínez-Mota L, Ulloa R-E, Herrera-Pérez J, et al. Sex and age differences in the impact of the forced swimming test on the levels of steroid hormones. Physiology & behavior 2011;**104**(5):900-05.

178. Ju Y-I, Sone T, Ohnaru K, et al. Differential effects of jump versus running exercise on trabecular architecture during remobilization after suspension-induced osteopenia in growing rats. Journal of Applied Physiology 2012;**112**(5):766-72.

179. Umemura Y, Ishiko T, Yamauchi T, et al. Five jumps per day increase bone mass and breaking force in rats. Journal of Bone and Mineral Research 1997;**12**(9):1480-85.

180. Buhl KM, Jacobs CR, Turner RT, et al. Aged bone displays an increased responsiveness to low-intensity resistance exercise. Journal of applied physiology 2001;**90**(4):1359-64.

181. Meakin LB, Price JS, Lanyon LE. The contribution of experimental in vivo models to understanding the mechanisms of adaptation to mechanical loading in bone. Frontiers in endocrinology 2014;**5**.

182. Schefer V, Talan MI. Oxygen consumption in adult and aged C57BL/6J mice during acute treadmill exercise of different intensity. Experimental gerontology 1996;**31**(3):387-92.

183. Albouaini K, Egred M, Alahmar A, et al. Cardiopulmonary exercise testing and its application. Heart 2007;**93**(10):1285-92.

184. Price JS, Sugiyama T, Galea GL, et al. Role of endocrine and paracrine factors in the adaptation of bone to mechanical loading. Current osteoporosis reports 2011;**9**(2):76-82.

185. Bonewald LF, Kiel DP, Clemens TL, et al. Forum on bone and skeletal muscle interactions: summary of the proceedings of an ASBMR workshop. Journal of Bone and Mineral Research 2013;**28**(9):1857-65.

186. Lanyon L, Smith R. Measurements of bone strain in the walking animal. Research in veterinary science 1969;**10**(1):93-94.

187. Evans FG, Lissner HR, Pedersen HE. Deformation studies of the femur under dynamic vertical loading. The Anatomical Record 1948;**101**(2):225-41.

188. Lanyon L, Hampson W, Goodship A, et al. Bone deformation recorded in vivo from strain gauges attached to the human tibial shaft. Acta Orthopaedica 1975;**46**(2):256-68.

189. Lanyon L. Analysis of surface bone strain in the calcaneus of sheep during normal locomotion: Strain analysis of the calcaneus. Journal of biomechanics 1973;**6**(1):41-49.

190. Lanyon L. < i> In vivo</i> bone strain recorded from thoracic vertebrae of sheep. Journal of biomechanics 1972;**5**(3):277-81.

191. Lanyon L. Strain in sheep lumbar vertebrae recorded during life. Acta Orthopaedica 1971;**42**(1):102-12.

192. Lanyon L. The measurement of bone strain" in vivo". Acta orthopaedica belgica 1976;**42**:98.

193. Lanyon L, Hartman W. Strain related electrical potentials recorded in vitro and in vivo. Calcified tissue research 1977;**22**(1):315-27.

194. Lanyon L, Smith R. Bone strain in the tibia during normal quadrupedal locomotion. Acta Orthopaedica 1970;**41**(3):238-48.

195. Clark E, Goodship A, Lanyon L. Locomotor bone strain as the stimulus for bone's mechanical adaptability. J Physiol 1975;**245**(2):57P-?

196. Rubin CT, Lanyon LE. Limb mechanics as a function of speed and gait: a study of functional strains in the radius and tibia of horse and dog. Journal of experimental biology 1982;**101**(1):187-211.

197. Skerry T. One mechanostat or many? Modifications of the site-specific response of bone to mechanical loading by nature and nurture. Journal of Musculoskeletal and Neuronal Interactions 2006;**6**(2):122.

198. Lauder G, Lanyon L. Functional anatomy of feeding in the bluegill sunfish, Lepomis macrochirus: in vivo measurement of bone strain. The Journal of Experimental Biology 1980;**84**(1):33-55.

199. Lee KC, Maxwell A, Lanyon LE. Validation of a technique for studying functional adaptation of the mouse ulna in response to mechanical loading. Bone 2002;**31**(3):407-12.

200. De Souza RL, Matsuura M, Eckstein F, et al. Non-invasive axial loading of mouse tibiae increases cortical bone formation and modifies trabecular organization: a new model to study cortical and cancellous compartments in a single loaded element. Bone 2005;**37**(6):810-8.

201. Biewener AA. Musculoskeletal design in relation to body size. Journal of Biomechanics 1991;**24**:19-29.

202. Sztefek P, Vanleene M, Olsson R, et al. Using digital image correlation to determine bone surface strains during loading and after adaptation of the mouse tibia. Journal of biomechanics 2010;**43**(4):599-605.

203. Moustafa A, Sugiyama T, Prasad J, et al. Mechanical loading-related changes in osteocyte sclerostin expression in mice are more closely associated with the subsequent osteogenic response than the peak strains engendered. Osteoporos Int 2012;**23**(4):1225-34.

204. Gross TS, Edwards JL, Mcleod KJ, et al. Strain gradients correlate with sites of periosteal bone formation. Journal of Bone and Mineral Research 1997;**12**(6):982-88.

205. Willie BM, Birkhold AI, Razi H, et al. Diminished response to in vivo mechanical loading in trabecular and not cortical bone in adulthood of female C57Bl/6 mice coincides with a reduction in deformation to load. Bone 2013;**55**(2):335-46.

206. Lambers F, Stuker F, Weigt C, et al. Longitudinal< i> in vivo</i> imaging of bone formation and resorption using fluorescence molecular tomography. Bone 2013;**52**(2):587-95.

207. Lambers FM, Kuhn G, Schulte FA, et al. Longitudinal assessment of in vivo bone dynamics in a mouse tail model of postmenopausal osteoporosis. Calcified tissue international 2012;**90**(2):108-19.

208. Goodship A, Lanyon L, McFie H. Functional adaptation of bone to increased stress. J Bone Joint Surg A 1979;**61**:539-46.

209. Hert J, Liskova M, Landa J. Reaction of bone to mechanical stimuli. 1. Continuous and intermittent loading of tibia in rabbit. Folia morphologica 1971;**19**(3):290-300.

210. Liskova M, Hert J. Reaction of bone to mechanical stimuli. 2. Periosteal and endosteal reaction of tibial diaphysis in rabbit to intermittent loading. Folia morphologica 1971;**19**(3):301.

211. Hert J, Sklenska A, Liskova M. Reaction of bone to mechanical stimuli. 5. Effect of intermittent stress on the rabbit tibia after resection of the peripheral nerves. Folia morphologica 1970;**19**(4):378-87.

212. O'connor J, Lanyon L, MacFie H. The influence of strain rate on adaptive bone remodelling. Journal of biomechanics 1982;**15**(10):767-81.

213. Rubin CT, Lanyon L. Regulation of bone formation by applied dynamic loads. J Bone Joint Surg Am 1984;**66**(3):397-402.

214. Lanyon LE, Rubin C. Static vs dynamic loads as an influence on bone remodelling. Journal of biomechanics 1984;**17**(12):897-905.

215. Lanyon L. Functional strain as a determinant for bone remodeling. Calcified Tissue International 1984;**36**(1):S56-S61.

216. Chambers TJ, Evans M, Gardner TN, et al. Induction of bone formation in rat tail vertebrae by mechanical loading. Bone and mineral 1993;**20**(2):167-78.

217. Webster D, Wasserman E, Ehrbar M, et al. Mechanical loading of mouse caudal vertebrae increases trabecular and cortical bone mass-dependence on dose and genotype. Biomech Model Mechanobiol 2010;**9**(6):737-47.

218. Webster DJ, Morley PL, van Lenthe GH, et al. A novel in vivo mouse model for mechanically stimulated bone adaptation–a combined experimental and computational validation study. Computer methods in biomechanics and biomedical engineering 2008;**11**(5):435-41.

219. Lambers FM, Koch K, Kuhn G, et al. Trabecular bone adapts to long-term cyclic loading by increasing stiffness and normalization of dynamic morphometric rates. Bone 2013;**55**(2):325-34.

220. Turner C, Akhter M, Raab D, et al. A noninvasive, in vivo model for studying strain adaptive bone modeling. Bone 1991;**12**(2):73-79.

221. Turner CH, Forwood M, Rho JY, et al. Mechanical loading thresholds for lamellar and woven bone formation. Journal of bone and mineral research 1994;**9**(1):87-97.

222. Gross TS, Srinivasan S, Liu CC, et al. Noninvasive loading of the murine tibia: an in vivo model for the study of mechanotransduction. Journal of Bone and Mineral Research 2002;**17**(3):493-501.

223. Torrance AG, Mosley JR, Suswillo RF, et al. Noninvasive loading of the rat ulna in vivo induces a strain-related modeling response uncomplicated by trauma or periostal pressure. Calcif Tissue Int 1994;**54**(3):241-7.

224. Sugiyama T, Price JS, Lanyon LE. Functional adaptation to mechanical loading in both cortical and cancellous bone is controlled locally and is confined to the loaded bones. Bone 2010;**46**(2):314-21.

225. Moustafa A, Sugiyama T, Saxon LK, et al. The mouse fibula as a suitable bone for the study of functional adaptation to mechanical loading. Bone 2009;**44**(5):930-35.

226. Tu X, Rhee Y, Condon KW, et al. Sost downregulation and local Wnt signaling are required for the osteogenic response to mechanical loading. Bone 2012;**50**(1):209-17.

227. Mosley J, Lanyon L. Growth rate rather than gender determines the size of the adaptive response of the growing skeleton to mechanical strain. Bone 2002;**30**(1):314-19.

228. Ohashi N, Robling AG, Burr DB, et al. The effects of dynamic axial loading on the rat growth plate. Journal of Bone and Mineral Research 2002;**17**(2):284-92.

229. Saxon LK, Jackson BF, Sugiyama T, et al. Analysis of multiple bone responses to graded strains above functional levels, and to disuse, in mice in vivo show that the human Lrp5 G171V High Bone Mass mutation increases the osteogenic response to loading but that lack of Lrp5 activity reduces it. Bone 2011;**49**(2):184-93.

230. Sugiyama T, Meakin LB, Browne WJ, et al. Bones' adaptive response to mechanical loading is essentially linear between the low strains associated with disuse and the high strains associated with the lamellar/woven bone transition. J Bone Miner Res 2012.

231. Brodt MD, Silva MJ. Aged mice have enhanced endocortical response and normal periosteal response compared with young-adult mice following 1 week of axial tibial compression. J Bone Miner Res 2010;**25**(9):2006-15.

232. Rubin CT, Lanyon LE. Regulation of bone mass by mechanical strain magnitude. Calcified tissue international 1985;**37**(4):411-17.

233. Ellman R, Spatz J, Cloutier A, et al. Partial reductions in mechanical loading yield proportional changes in bone density, bone architecture, and muscle mass. Journal of Bone and Mineral Research 2013;**28**(4):875-85.

234. McKenzie JA, Silva MJ. Comparing histological, vascular and molecular responses associated with woven and lamellar bone formation induced by mechanical loading in the rat ulna. Bone 2011;**48**(2):250-58.

235. Lambers FM, Schulte FA, Kuhn G, et al. Mouse tail vertebrae adapt to cyclic mechanical loading by increasing bone formation rate and decreasing bone resorption rate as shown by time-lapsed< i> in vivo</i> imaging of dynamic bone morphometry. Bone 2011;**49**(6):1340-50.

236. Judex S, Gross TS, Zernicke RF. Strain gradients correlate with sites of exercise-induced bone-forming surfaces in the adult skeleton. Journal of Bone and Mineral Research 1997;**12**(10):1737-45.

237. Kotha S, Hsieh Y-F, Strigel R, et al. Experimental and finite element analysis of the rat ulnar loading model—correlations between strain and bone formation following fatigue loading. Journal of biomechanics 2004;**37**(4):541-48.

238. Mosley J, Lanyon L. Strain rate as a controlling influence on adaptive modeling in response to dynamic loading of the ulna in growing male rats. Bone 1998;**23**(4):313-18.

239. Turner CH, Owan I, Takano Y. Mechanotransduction in bone: role of strain rate. American Journal of Physiology-Endocrinology And Metabolism 1995;**32**(3):E438.

240. Taaffe DR, Robinson TL, Snow CM, et al. High-Impact Exercise Promotes Bone Gain in Well-Trained Female Athletes. Journal of bone and mineral research 1997;**12**(2):255-60.

241. Jones HH, Priest JD, Hayes WC, et al. Humeral hypertrophy in response to exercise. J Bone Joint Surg Am 1977;**59**(2):204-8.

242. Deere K, Sayers A, Rittweger J, et al. Habitual levels of high, but not moderate or low, impact activity are positively related to hip BMD and geometry: Results from a population-based study of adolescents. Journal of Bone and Mineral Research 2012;**27**(9):1887-95.

243. Bennell K, Malcolm S, Khan K, et al. Bone mass and bone turnover in power athletes, endurance athletes, and controls: a 12-month longitudinal study. Bone 1997;**20**(5):477-84.

244. Robling AG, Burr DB, Turner CH. Recovery periods restore mechanosensitivity to dynamically loaded bone. Journal of Experimental Biology 2001;**204**(19):3389-99.

245. LaMothe JM, Zernicke RF. Rest insertion combined with high-frequency loading enhances osteogenesis. Journal of Applied Physiology 2004;**96**(5):1788-93.

246. Srinivasan S, Agans SC, King KA, et al. Enabling bone formation in the aged skeleton via rest-inserted mechanical loading. Bone 2003;**33**(6):946-55.

247. Srinivasan S, Ausk BJ, Poliachik SL, et al. Rest-inserted loading rapidly amplifies the response of bone to small increases in strain and load cycles. Journal of applied physiology 2007;**102**(5):1945-52.

248. Srinivasan S, Weimer DA, Agans SC, et al. Low-Magnitude Mechanical Loading Becomes Osteogenic When Rest Is Inserted Between Each Load Cycle. Journal of Bone and Mineral Research 2002;**17**(9):1613-20.

249. Saxon LK, Robling AG, Alam I, et al. Mechanosensitivity of the rat skeleton decreases after a long period of loading, but is improved with time off. Bone 2005;**36**(3):454-64.

250. Robling AG, Burr DB, Turner CH. Partitioning a daily mechanical stimulus into discrete loading bouts improves the osteogenic response to loading. Journal of Bone and Mineral Research 2000;**15**(8):1596-602.

251. Zaman G, Saxon LK, Sunters A, et al. Loading-related regulation of gene expression in bone in the contexts of estrogen deficiency, lack of estrogen receptor α and disuse. Bone 2010;**46**(3):628-42.

252. Lee K, Jessop H, Suswillo R, et al. Endocrinology: bone adaptation requires oestrogen receptor-α. Nature 2003;**424**(6947):389-89.

253. Kennedy OD, Herman BC, Laudier DM, et al. Activation of resorption in fatigue-loaded bone involves both apoptosis and active pro-osteoclastogenic signaling by distinct osteocyte populations. Bone 2012;**50**(5):1115-22.

254. Haapasalo H, Sievanen H, Kannus P, et al. Dimensions and estimated mechanical characteristics of the humerus after long-term tennis loading. Journal of Bone and Mineral Research 1996;**11**(6):864-72.

255. Huddleston AL, Rockwell D, Kulund DN, et al. Bone mass in lifetime tennis athletes. Jama 1980;**244**(10):1107-09.

256. Warden SJ, Bogenschutz ED, Smith HD, et al. Throwing induces substantial torsional adaptation within the midshaft humerus of male baseball players. Bone 2009;**45**(5):931-41.

257. Johnell O, Kanis JA. An estimate of the worldwide prevalence and disability associated with osteoporotic fractures. Osteoporos Int 2006;**17**(12):1726-33.

258. Dowthwaite J, Scerpella T. Distal radius geometry and skeletal strength indices after peripubertal artistic gymnastics. Osteoporosis international 2011;**22**(1):207-16.

259. Söderman K, Bergström E, Lorentzon R, et al. Bone mass and muscle strength in young female soccer players. Calcified tissue international 2000;**67**(4):297-303.

260. Robling AG, Hinant FM, Burr DB, et al. Improved bone structure and strength after long-term mechanical loading is greatest if loading is separated into short bouts. Journal of Bone and Mineral Research 2002;**17**(8):1545-54.

261. Fritton JC, Myers ER, Wright TM, et al. Loading induces site-specific increases in mineral content assessed by microcomputed tomography of the mouse tibia. Bone 2005;**36**(6):1030-8.

262. De Souza RL, Matsuura M, Eckstein F, et al. Non-invasive axial loading of mouse tibiae increases cortical bone formation and modifies trabecular organization: a new model to study cortical and cancellous compartments in a single loaded element. Bone 2005;**37**(6):810-18.

263. Fuchs RK, Bauer JJ, Snow CM. Jumping improves hip and lumbar spine bone mass in prepubescent children: a randomized controlled trial. Journal of Bone and Mineral Research 2001;**16**(1):148-56.

264. Warden S, Fuchs R, Turner C. Steps for targeting exercise towards the skeleton to increase bone strength. Europa medicophysica 2004;**40**(3):223-32.

265. Guadalupe-Grau A, Fuentes T, Guerra B, et al. Exercise and bone mass in adults. Sports Medicine 2009;**39**(6):439-68.

266. Winters KM, Snow CM. Detraining reverses positive effects of exercise on the musculoskeletal system in premenopausal women. Journal of Bone and Mineral Research 2000;**15**(12):2495-503.

267. Khan K, McKay H, Kannus PA, et al. *Physical activity and bone health*: Human Kinetics, 2001.

268. Nikander R, Sievänen H, Heinonen A, et al. Targeted exercise against osteoporosis: a systematic review and meta-analysis for optimising bone strength throughout life. BMC medicine 2010;**8**(1):47.

269. Kato T, Niwa M, Yamashita T, et al. Past sporting activity during growth induces greater bone mineral content and enhances bone geometry in young men and women. Journal of bone and mineral metabolism 2014:1-8.

270. Howe TE, Shea B, Dawson LJ, et al. Exercise for preventing and treating osteoporosis in postmenopausal women. The Cochrane Library 2011.

271. Moyer-Mileur L, Luetkemeier M, Boomer L, et al. Effect of physical activity on bone mineralization in premature infants. The Journal of pediatrics 1995;**127**(4):620-25.

272. Henwood MJ, Binkovitz L. Update on pediatric bone health. JAOA: Journal of the American Osteopathic Association 2009;**109**(1):5-12.

273. Nowlan NC, Sharpe J, Roddy KA, et al. Mechanobiology of embryonic skeletal development: insights from animal models. Birth Defects Research Part C: Embryo Today: Reviews 2010;**90**(3):203-13.

274. Wesstrom G, Bensch J, Schollin J. Congenital myotonic dystrophy. Acta Paediatrica 1986;**75**(5):849-54.

275. Rodríguez JI, Palacios J, García-Alix A, et al. Effects of immobilization on fetal bone development. A morphometric study in newborns with congenital neuromuscular diseases with intrauterine onset. Calcified tissue international 1988;**43**(6):335-39.

276. Roberts CD, Vogtle L, Stevenson RD. Effect of hemiplegia on skeletal maturation. The Journal of pediatrics 1994;**125**(5):824-28.

277. Nicole S, Diaz CC, Frugier T, et al. Spinal muscular atrophy: recent advances and future prospects. Muscle & nerve 2002;**26**(1):4-13.

278. Miller M, Hangartner TN. Temporary brittle bone disease: association with decreased fetal movement and osteopenia. Calcified tissue international 1999;**64**(2):137-43.

279. Miller ME. The bone disease of preterm birth: a biomechanical perspective. Pediatric research 2003;**53**(1):10-15.

280. Forwood MR, Burr DB. Physical activity and bone mass: exercises in futility? Bone and mineral 1993;**21**(2):89-112.

281. Cummings SR, Browner W, Black D, et al. Bone density at various sites for prediction of hip fractures. The Lancet 1993;**341**(8837):72-75.

282. Hernandez C, Beaupre G, Carter D. A theoretical analysis of the relative influences of peak BMD, age-related bone loss and menopause on the development of osteoporosis. Osteoporosis international 2003;**14**(10):843-47.

283. Warden SJ, Fuchs RK. Exercise and bone health: optimising bone structure during growth is key, but all is not in vain during ageing. British journal of sports medicine 2009;**43**(12):885-87.

284. Warden SJ, Hurst JA, Sanders MS, et al. Bone adaptation to a mechanical loading program significantly increases skeletal fatigue resistance. Journal of bone and mineral research 2005;**20**(5):809-16.

285. Bailey D, McKay H, Mirwald R, et al. A six-year longitudinal study of the relationship of physical activity to bone mineral accrual in growing children: the university of Saskatchewan bone mineral accrual study. Journal of Bone and Mineral Research 1999;**14**(10):1672-79.

286. Janz KF, Gilmore JM, Burns TL, et al. Physical activity augments bone mineral accrual in young children: The Iowa Bone Development study. The Journal of pediatrics 2006;**148**(6):793-99.

287. Tobias JH, Steer CD, Mattocks CG, et al. Habitual levels of physical activity influence bone mass in 11-year-old children from the United Kingdom: findings from a large population-based cohort. Journal of Bone and Mineral Research 2007;**22**(1):101-09.

288. Ducher G, Bass SL, Saxon L, et al. Effects of repetitive loading on the growth-induced changes in bone mass and cortical bone geometry: A 12-month study in pre/peri-and postmenarcheal tennis players. Journal of bone and mineral research 2011;**26**(6):1321-29.

289. Ducher G, Daly RM, Bass SL. Effects of repetitive loading on bone mass and geometry in young male tennis players: a quantitative study using MRI. Journal of bone and mineral research 2009;**24**(10):1686-92.

290. Bass S, Pearce G, Bradney M, et al. Exercise before puberty may confer residual benefits in bone density in adulthood: studies in active prepubertal and retired female gymnasts. Journal of Bone and Mineral Research 1998;**13**(3):500-07.

291. Matthews B, Bennell K, McKay H, et al. Dancing for bone health: a 3-year longitudinal study of bone mineral accrual across puberty in female non-elite dancers and controls. Osteoporosis international 2006;**17**(7):1043-54.

292. Rizzoli R, Bianchi ML, Garabédian M, et al. Maximizing bone mineral mass gain during growth for the prevention of fractures in the adolescents and the elderly. Bone 2010;**46**(2):294-305.

293. BONJOUR J-P, THEINTZ G, BUCHS B, et al. Critical Years and Stages of Puberty for Spinal and Femoral Bone Mass Accumulation during Adolescence*. The Journal of Clinical Endocrinology & Metabolism 1991;**73**(3):555-63.

294. Slemenda CW, Reister TK, Hui SL, et al. Influences on skeletal mineralization in children and adolescents: evidence for varying effects of sexual maturation and physical activity. The Journal of pediatrics 1994;**125**(2):201-07.

295. Fuchs RK, Snow CM. Gains in hip bone mass from high-impact training are maintained: a randomized controlled trial in children. The Journal of pediatrics 2002;**141**(3):357-62.

296. Gunter K, Baxter-Jones AD, Mirwald RL, et al. Impact Exercise Increases BMC During Growth: An 8-Year Longitudinal Study. Journal of Bone and Mineral Research 2008;**23**(7):986-93.

297. Kontulainen S, Kannus P, Pasanen M, et al. Does previous participation in high-impact training result in residual bone gain in growing girls? One year follow-up of a 9-month jumping intervention. International journal of sports medicine 2002;**23**(8):575-81.

298. Karlsson M, Linden C, Karlsson C, et al. Exercise during growth and bone mineral density and fractures in old age. The Lancet 2000;**355**(9202):469-70.

299. Seeman E. From density to structure: growing up and growing old on the surfaces of bone. Journal of bone and mineral research 1997;**12**(4):509-21.

300. MacKelvie KJ, Petit MA, Khan KM, et al. Bone mass and structure are enhanced following a 2-year randomized controlled trial of exercise in prepubertal boys. Bone 2004;**34**(4):755-64.

301. Macdonald HM, Kontulainen SA, Khan KM, et al. Is a school-based physical activity intervention effective for increasing tibial bone strength in boys and girls? Journal of bone and mineral research : the official journal of the American Society for Bone and Mineral Research 2007;**22**(3):434-46.

302. Janz KF, Gilmore JME, Levy SM, et al. Physical activity and femoral neck bone strength during childhood: the Iowa Bone Development Study. Bone 2007;**41**(2):216-22.

303. Janz KF, Burns TL, Levy SM, et al. Everyday activity predicts bone geometry in children: the iowa bone development study. Medicine and science in sports and exercise 2004;**36**(7):1124-31.

304. Farr JN, Blew RM, Lee VR, et al. Associations of physical activity duration, frequency, and load with volumetric BMD, geometry, and bone strength in young girls. Osteoporosis international 2011;**22**(5):1419-30.

305. Forwood MR, Baxter-Jones AD, Beck TJ, et al. Physical activity and strength of the femoral neck during the adolescent growth spurt: a longitudinal analysis. Bone 2006;**38**(4):576-83.

306. Bass SL, Saxon L, Daly R, et al. The effect of mechanical loading on the size and shape of bone in pre-, peri-, and postpubertal girls: a study in tennis players. Journal of Bone and Mineral Research 2002;**17**(12):2274-80.

307. Ward K, Roberts S, Adams J, et al. Bone geometry and density in the skeleton of pre-pubertal gymnasts and school children. Bone 2005;**36**(6):1012-18.

308. Ahlborg HG, Johnell O, Turner CH, et al. Bone loss and bone size after menopause. New England Journal of Medicine 2003;**349**(4):327-34.

309. Seeman E. Periosteal bone formation--a neglected determinant of bone strength. The New England journal of medicine 2003;**349**(4):320.

310. Warden S, Fuchs R, Castillo A, et al. Does exercise during growth influence osteoporotic fracture risk later in life? Journal of Musculoskeletal and Neuronal Interactions 2005;**5**(4):344.

311. Warden SJ, Fuchs RK, Castillo AB, et al. Exercise when young provides lifelong benefits to bone structure and strength. Journal of Bone and Mineral Research 2007;**22**(2):251-59.

312. Warden SJ, Galley MR, Hurd AL, et al. Cortical and Trabecular Bone Benefits of Mechanical Loading Are Maintained Long Term in Mice Independent of Ovariectomy. Journal of Bone and Mineral Research 2014;**29**(5):1131-40.

313. McKay H, MacLean L, Petit M, et al. "Bounce at the Bell": a novel program of short bouts of exercise improves proximal femur bone mass in early pubertal children. British journal of sports medicine 2005;**39**(8):521-26.

314. Zehnacker CH, Bemis-Dougherty A. Effect of weighted exercises on bone mineral density in post menopausal women a systematic review. Journal of Geriatric Physical Therapy 2007;**30**(2):79-88.

315. Grisso JA, Kelsey JL, Strom BL, et al. Risk factors for falls as a cause of hip fracture in women. New England Journal of Medicine 1991;**324**(19):1326-31.

316. Turner CH. Three rules for bone adaptation to mechanical stimuli. Bone 1998;**23**(5):399-407.

317. Sawakami K, Robling AG, Ai M, et al. The Wnt co-receptor LRP5 is essential for skeletal mechanotransduction but not for the anabolic bone response to parathyroid hormone treatment. J Biol Chem 2006;**281**(33):23698-711.

318. Robling AG, Burr DB, Turner CH. Skeletal loading in animals. J Musculoskelet Neuronal Interact 2001;**1**(3):249-62.

319. Stadelmann VA, Hocke J, Verhelle J, et al. 3D strain map of axially loaded mouse tibia: a numerical analysis validated by experimental measurements. Comput Methods Biomech Biomed Engin 2009;**12**(1):95-100.

320. Bonnet N, Standley KN, Bianchi EN, et al. The matricellular protein periostin is required for sost inhibition and the anabolic response to mechanical loading and physical activity. J Biol Chem 2009;**284**(51):35939.

321. Lynch ME, Main RP, Xu Q, et al. Cancellous bone adaptation to tibial compression is not sex dependent in growing mice. J Appl Physiol 2010;**109**(3):685-91.

322. Marenzana M, De Souza RL, Chenu C. Blockade of beta-adrenergic signaling does not influence the bone mechano-adaptive response in mice. Bone 2007;**41**(2):206-15.

323. Pierroz DD, Bonnet N, Bianchi EN, et al. Deletion of beta-adrenergic receptor 1, 2, or both leads to different bone phenotypes and response to mechanical stimulation. J Bone Miner Res 2012;**27**(6):1252-62.

324. Saxon LK, Galea G, Meakin L, et al. Estrogen receptors alpha and beta have different gender-dependent effects on the adaptive responses to load bearing in cancellous and cortical bone. Endocrinology 2012;**153**(5):2254-66.

325. Sugiyama T, Meakin LB, Galea GL, et al. Risedronate does not reduce mechanical loading-related increases in cortical and trabecular bone mass in mice. Bone 2011;**49**(1):133-9.

326. Sugiyama T, Saxon LK, Zaman G, et al. Mechanical loading enhances the anabolic effects of intermittent parathyroid hormone (1-34) on trabecular and cortical bone in mice. Bone 2008;**43**(2):238-48.

327. Sugiyama T, Meakin LB, Galea GL, et al. The cyclooxygenase-2 selective inhibitor NS-398 does not influence trabecular or cortical bone gain resulting from repeated mechanical loading in female mice. Osteoporos Int 2012.

328. Silva MJ, Brodt MD, Lynch MA, et al. Tibial loading increases osteogenic gene expression and cortical bone volume in mature and middle-aged mice. PLoS One 2012;**7**(4):e34980.

329. Grimston SK, Watkins MP, Brodt MD, et al. Enhanced periosteal and endocortical responses to axial tibial compression loading in conditional connexin43 deficient mice. PLoS One 2012;**7**(9):e44222.

330. Lynch ME, Main RP, Xu Q, et al. Tibial compression is anabolic in the adult mouse skeleton despite reduced responsiveness with aging. Bone 2011;**49**(3):439-46.

331. Lynch JA, Silva MJ. In vivo static creep loading of the rat forelimb reduces ulnar structural properties at time-zero and induces damage-dependent woven bone formation. Bone 2008;**42**(5):942-49.

332. Schmidt C, Priemel M, Kohler T, et al. Precision and accuracy of peripheral quantitative computed tomography (pQCT) in the mouse skeleton compared with

histology and microcomputed tomography (microCT). J Bone Miner Res 2003;**18**(8):1486-96.

333. Gere J, Timoshenko S. Mechanics of Materials. 2nd. Boston (MA): PWS-Kent 1984:492.

334. Stadelmann VA, Bonnet N, Pioletti DP. Combined effects of zoledronate and mechanical stimulation on bone adaptation in an axially loaded mouse tibia. Clin Biomech (Bristol, Avon) 2011;**26**(1):101-5.

335. Niziolek PJ, Warman ML, Robling AG. Mechanotransduction in bone tissue: The A214V and G171V mutations in Lrp5 enhance load-induced osteogenesis in a surface-selective manner. Bone 2012;**51**(3):459-65.

336. Fritton JC, Myers ER, Wright TM, et al. Bone mass is preserved and cancellous architecture altered due to cyclic loading of the mouse tibia after orchidectomy. J Bone Miner Res 2008;**23**(5):663-71.

337. Chow JW, Jagger CJ, Chambers TJ. Characterization of osteogenic response to mechanical stimulation in cancellous bone of rat caudal vertebrae. The American journal of physiology 1993;**265**(2 Pt 1):E340-7.

338. Poulet B, Hamilton RW, Shefelbine S, et al. Characterizing a novel and adjustable noninvasive murine joint loading model. Arthritis Rheum 2011;**63**(1):137-47.

339. Sheu Y, Zmuda JM, Boudreau RM, et al. Bone strength measured by peripheral quantitative computed tomography and the risk of nonvertebral fractures: the osteoporotic fractures in men (MrOS) study. J Bone Miner Res 2011;**26**(1):63-71.

340. Dennison EM, Jameson KA, Edwards MH, et al. Peripheral quantitative computed tomography measures are associated with adult fracture risk: The Hertfordshire Cohort Study. Bone 2014;**64**:13-7.

341. Ashe MC, Khan KM, Kontulainen SA, et al. Accuracy of pQCT for evaluating the aged human radius: an ashing, histomorphometry and failure load investigation. Osteoporos Int 2006;**17**(8):1241-51.

342. Duckham RL, Frank AW, Johnston JD, et al. Monitoring time interval for pQCT-derived bone outcomes in postmenopausal women. Osteoporos Int 2013;**24**(6):1917-22.

343. Giangregorio L, Lala D, Hummel K, et al. Measuring apparent trabecular density and bone structure using peripheral quantitative computed tomography at the tibia: precision in participants with and without spinal cord injury. J Clin Densitom 2013;**16**(2):139-46.

344. Grampp S, Lang P, Jergas M, et al. Assessment of the skeletal status by peripheral quantitative computed tomography of the forearm: short-term precision in vivo

and comparison to dual X-ray absorptiometry. J Bone Miner Res 1995;**10**(10):1566-76.

345. Groll O, Lochmuller EM, Bachmeier M, et al. Precision and intersite correlation of bone densitometry at the radius, tibia and femur with peripheral quantitative CT. Skeletal Radiol 1999;**28**(12):696-702.

346. Kontulainen SA, Johnston JD, Liu D, et al. Strength indices from pQCT imaging predict up to 85% of variance in bone failure properties at tibial epiphysis and diaphysis. J Musculoskelet Neuronal Interact 2008;**8**(4):401-9.

347. Liu D, Manske SL, Kontulainen SA, et al. Tibial geometry is associated with failure load ex vivo: a MRI, pQCT and DXA study. Osteoporos Int 2007;**18**(7):991-7.

348. Lochmuller EM, Lill CA, Kuhn V, et al. Radius bone strength in bending, compression, and falling and its correlation with clinical densitometry at multiple sites. J Bone Miner Res 2002;**17**(9):1629-38.

349. Louis O, Boulpaep F, Willnecker J, et al. Cortical mineral content of the radius assessed by peripheral QCT predicts compressive strength on biomechanical testing. Bone 1995;**16**(3):375-79.

350. Muller ME, Webber CE, Bouxsein ML. Predicting the failure load of the distal radius. Osteoporos Int 2003;**14**(4):345-52.

351. Rinaldi G, Wisniewski CA, Setty NG, et al. Peripheral quantitative computed tomography: optimization of reproducibility measures of bone density, geometry, and strength at the radius and tibia. J Clin Densitom 2011;**14**(3):367-73.

352. Sievänen H, Koskue V, Rauhio A, et al. Peripheral quantitative computed tomography in human long bones: evaluation of in vitro and in vivo precision. J Bone Miner Res 1998;**13**(5):871-82.

353. Swinford RR, Warden SJ. Factors affecting short-term precision of musculoskeletal measures using peripheral quantitative computed tomography (pQCT). Osteoporos Int 2010;**21**(11):1863-70.

354. Szabo KA, Webber CE, Gordon C, et al. Reproducibility of peripheral quantitative computed tomography measurements at the radius and tibia in healthy pre- and postmenopausal women. Canadian Association of Radiologists journal = Journal l'Association canadienne des radiologistes 2011;**62**(3):183-9.

355. Wilhelm G, Felsenberg D, Bogusch G, et al. Biomechanical examinations for validation of the Bone Strength-Strain Index SSI, calculated by peripheral quantitative computed tomography. In: Lyrithis GP, ed. Musculoskeletal Interactions. Athens: Hylonome 1999:105-11.

356. Schiessl H, Ferretti JL, Tysarczyk-Niemeyer G, et al. Noninvasive bone strength index as analyzed by peripheral quantitative computed tomography (pQCT). In: Schonau E, ed. Pediatric Osteology. Amsterdam: Elsevier, 1996:141-5.

357. Stratec. *XCT 3000 Manual Software Version 6.20*. Pforzheim, Germany: Stratec Medizintechnik GmbH.

358. Bogenschutz ED, Smith HD, Warden SJ. Mid-humerus adaptation in fast pitch softballers and the impact of throwing mechanics. Med Sci Sports Exerc 2011;**43**:1698-706.

359. Eser P, Hill B, Ducher G, et al. Skeletal benefits after long-term retirement in former elite female gymnasts. J Bone Miner Res 2009;**24**(12):1981-8.

360. Haapasalo H, Kontulainen S, Sievanen H, et al. Exercise-induced bone gain is due to enlargement in bone size without a change in volumetric bone density: a peripheral quantitative computed tomography study of the upper arms of male tennis players. Bone 2000;**27**(3):351-7.

361. Ireland A, Maden-Wilkinson T, Ganse B, et al. Effects of age and starting age upon side asymmetry in the arms of veteran tennis players: a cross-sectional study. Osteoporos Int 2014;**25**(4):1389-400.

362. Ireland A, Maden-Wilkinson T, McPhee J, et al. Upper limb muscle-bone asymmetries and bone adaptation in elite youth tennis players. Med Sci Sports Exerc 2013;**45**(9):1749-58.

363. Nikander R, Sievanen H, Uusi-Rasi K, et al. Loading modalities and bone structures at nonweight-bearing upper extremity and weight-bearing lower extremity: a pQCT study of adult female athletes. Bone 2006;**39**(4):886-94.

364. Shaw CN, Stock JT. Habitual throwing and swimming correspond with upper limb diaphyseal strength and shape in modern human athletes. Am J Phys Anthropol 2009;**140**(1):160-72.

365. Warden SJ. Extreme skeletal adaptation to mechanical loading. J Orthop Sports Phys Ther 2010;**40**(3):188.

366. Warden SJ, Bogenschutz ED, Smith HD, et al. Throwing induces substantial torsional adaptation within the midshaft humerus of male baseball players. Bone 2009;**45**(5):931-41.

367. Schoenau E, Neu CM, Rauch F, et al. The development of bone strength at the proximal radius during childhood and adolescence. J Clin Endocrinol Metab 2001;**86**(2):613-8.

368. Glüer C-C, Blake G, Lu Y, et al. Accurate assessment of precision errors: how to measure the reproducibility of bone densitometry techniques. Osteoporosis International 1995;**5**(4):262-70.

369. Baim S, Wilson CR, Lewiecki EM, et al. Precision assessment and radiation safety for dual-energy X-ray absorptiometry: position paper of the International Society for Clinical Densitometry. J Clin Densitom 2005;**8**(4):371-8.

370. Gluer CC. Monitoring skeletal changes by radiological techniques. J Bone Miner Res 1999;**14**(11):1952-62.

371. Glüer C-C, Blake G, Lu Y, et al. Accurate assessment of precision errors: how to measure the reproducibility of bone densitometry techniques. Osteoporos Int 1995;**5**:262-70.

372. Schousboe JT, Shepherd JA, Bilezikian JP, et al. Executive summary of the 2013 International Society for Clinical Densitometry Position Development Conference on bone densitometry. J Clin Densitom 2013;**16**(4):455-66.

373. Hudelmaier M, Kuhn V, Lochmuller EM, et al. Can geometry-based parameters from pQCT and material parameters from quantitative ultrasound (QUS) improve the prediction of radial bone strength over that by bone mass (DXA)? Osteoporos Int 2004;**15**(5):375-81.

374. Burr DB, Milgrom C, Fyhrie D, et al. In vivo measurement of human tibial strains during vigourous activity. Bone 1996;**18**:405-10.

375. Milgrom C, Finestone A, Simkin A, et al. In-vivo strain measurements to evaluate the strengthening potential of exercises on the tibial bone. J Bone Joint Surg Br 2000;**82**(4):591-4.

376. Taylor RE, Zheng C, Jackson RP, et al. The phenomenon of twisted growth: humeral torsion in dominant arms of high performance tennis players. Comput Methods Biomech Biomed Engin 2009;**12**:83-93.

377. Ogawa K, Yoshida A. Throwing fracture of the humeral shaft.: an analysis of 90 patients. Am J Sports Med 1998;**26**(2):242-6.

378. Whiteley RJ, Ginn KA, Nicholson LL, et al. Sports participation and humeral torsion. J Orthop Sports Phys Ther 2009;**39**(4):256-63.

379. Lind PM, Lind L, Larsson S, et al. Torsional testing and peripheral quantitative computed tomography in rat humerus. Bone 2001;**29**(3):265-70.

380. Sun L, Beller G, Felsenberg D. Quantification of bone mineral density precision according to repositioning errors in peripheral quantitative computed tomography (pQCT) at the radius and tibia. J Musculoskelet Neuronal Interact 2009;**9**(1):18-24.

381. Leslie WD, Moayyeri A, Manitoba Bone Density P. Minimum sample size requirements for bone density precision assessment produce inconsistency in clinical monitoring. Osteoporos Int 2006;**17**(11):1673-80.

382. Leslie WD, Moayyeri A, Sadatsafavi M, et al. A new approach for quantifying change and test precision in bone densitometry. J Clin Densitom 2007;**10**(4):365-9.

383. Nikander R, Sievänen H, Uusi-Rasi K, et al. Loading modalities and bone structures at nonweight-bearing upper extremity and weight-bearing lower extremity: a pQCT study of adult female athletes. Bone 2006;**39**(4):886-94.

384. Bramble DM, Lieberman DE. Endurance running and the evolution of Homo. Nature 2004;**432**(7015):345-52.

385. Heinonen A, Sievänen H, Kyröläinen H, et al. Mineral mass, size, and estimated mechanical strength of triple jumpers' lower limb. Bone 2001;**29**(3):279-85.

386. Warden SJ, Roosa SMM, Kersh ME, et al. Physical activity when young provides lifelong benefits to cortical bone size and strength in men. Proceedings of the National Academy of Sciences 2014;**111**(14):5337-42.

387. Ducher G, Tournaire N, Meddahi-Pellé A, et al. Short-term and long-term site-specific effects of tennis playing on trabecular and cortical bone at the distal radius. Journal of bone and mineral metabolism 2006;**24**(6):484-90.

388. Haapasalo H, Kannus P, Sievänen H, et al. Long-term unilateral loading and bone mineral density and content in female squash players. Calcified tissue international 1994;**54**(4):249-55.

389. Ireland A, Korhonen M, Heinonen A, et al. Side-to-side differences in bone strength in master jumpers and sprinters. J Musculoskelet Neuronal Interact 2011;**11**(4):298-305.

390. Young K, Sherk V, Bemben D. Inter-limb musculoskeletal differences in competitive ten-pin bowlers: a preliminary analysis. Journal of musculoskeletal & neuronal interactions 2011;**11**(1):21-26.

391. Coh M, Supej M. Biomechanical model of the take-off action in the high jump–A case study. New Studies in Athletics 2008;**23**(4):63-73.

392. Luhtanen P, Komi PV. Mechanical power and segmental contribution to force impulses in long jump take-off. European journal of applied physiology and occupational physiology 1979;**41**(4):267-74.

393. Mero A, Komi PV. Force-, EMG-, and elasticity-velocity relationships at submaximal, maximal and supramaximal running speeds in sprinters. European journal of applied physiology and occupational physiology 1986;**55**(5):553-61.

394. Muraki Y, Ae M, Koyama H, et al. Joint torque and power of the takeoff leg in the long jump. International Journal of Sport and Health Science 2008;**6**:21-32.

395. Swinford RR, Warden SJ. Factors affecting short-term precision of musculoskeletal measures using peripheral quantitative computed tomography (pQCT). Osteoporosis international 2010;**21**(11):1863-70.

396. Doube M, Kłosowski MM, Arganda-Carreras I, et al. BoneJ: Free and extensible bone image analysis in ImageJ. Bone 2010;**47**(6):1076-79.

397. Rantalainen T, Nikander R, Heinonen A, et al. An open source approach for regional cortical bone mineral density analysis. Journal of musculoskeletal & neuronal interactions 2011;**11**(3):243-48.

398. Warden SJ, Roosa SMM. Physical activity completed when young has residual bone benefits at 94 years of age: a within-subject controlled case study. Journal of musculoskeletal & neuronal interactions 2014;**14**(2):239.

399. Vico L, Zouch M, Amirouche A, et al. High-resolution peripheral quantitative computed tomography analysis at the distal radius and tibia discriminates patients with recent wrist and femoral neck fractures. Journal of bone and mineral research : the official journal of the American Society for Bone and Mineral Research 2008;**23**(11):1741-50.

400. Milgrom C, Finestone A, Levi Y, et al. Do high impact exercises produce higher tibial strains than running? British journal of sports medicine 2000;**34**(3):195-99.

401. Wilks DC, Winwood K, Gilliver S, et al. Bone mass and geometry of the tibia and the radius of master sprinters, middle and long distance runners, race-walkers and sedentary control participants: a pQCT study. Bone 2009;**45**(1):91-97.

402. Milgrom C, Finestone A, Segev S, et al. Are overground or treadmill runners more likely to sustain tibial stress fracture? British journal of sports medicine 2003;**37**(2):160-63.

403. Barrack MT, Rauh MJ, Nichols JF. Cross-sectional evidence of suppressed bone mineral accrual among female adolescent runners. Journal of Bone and Mineral Research 2010;**25**(8):1850-57.

404. MacKelvie K, Khan K, McKay H. Is there a critical period for bone response to weight-bearing exercise in children and adolescents? A systematic review. British journal of sports medicine 2002;**36**(4):250-57.

405. Heinonen A, Sievänen H, Kannus P, et al. High-impact exercise and bones of growing girls: a 9-month controlled trial. Osteoporosis International 2000;**11**(12):1010-17.

406. Witzke KA, Snow CM. Effects of plyometric jump training on bone mass in adolescent girls. Medicine and science in sports and exercise 2000;**32**(6):1051-57.

407. Fuchs RK, Weatherholt AM, Warden SJ. Progressive Skeletal Benefits of Exercise When Young. Medicine & Science in Sports & Exercise 2015.

408. Tanner JM. Growth at adolescence. 1962.

409. Weatherholt AM, Fuchs RK, Warden SJ. Cortical and trabecular bone adaptation to incremental load magnitudes using the mouse tibial axial compression loading model. Bone 2013;**52**(1):372-79.

410. Kontulainen S, Sievänen H, Kannus P, et al. Effect of Long-Term Impact-Loading on Mass, Size, and Estimated Strength of Humerus and Radius of Female Racquet-Sports Players: A Peripheral Quantitative Computed Tomography Study Between Young and Old Starters and Controls. Journal of Bone and Mineral Research 2002;**17**(12):2281-89.

411. Taylor R, Zheng C, Jackson R, et al. The phenomenon of twisted growth: Humeral torsion in dominant arms of high performance tennis players. Computer Methods in Biomechanics and Biomedical Engineering 2009;**12**(1):83-93.

412. Ashe MC, Liu-Ambrose T, Khan KM, et al. Optimizing results from pQCT: reliability of operator-dependent pQCT variables in cadavers and humans with low bone mass. J Clin Densitom 2005;**8**(3):335-40.

413. Turner C, Robling A. Exercises for improving bone strength. British journal of sports medicine 2005;**39**(4):188-89.

414. Burghardt AJ, Kazakia GJ, Ramachandran S, et al. Age-and gender-related differences in the geometric properties and biomechanical significance of intracortical porosity in the distal radius and tibia. Journal of Bone and Mineral Research 2010;**25**(5):983-93.

415. Haapasalo H, Kannus P, Sievänen H, et al. Effect of long-term unilateral activity on bone mineral density of female junior tennis players. Journal of Bone and Mineral Research 1998;**13**(2):310-19.

CURRICULUM VITAE

Alyssa M. Weatherholt

EDUCATION

Indiana University, Indianapolis, IN
- Doctor of Philosophy in Health and Rehabilitation Sciences, a concentration in Pathophysiology and Impairment, Minor in Nutrition (2015)

  Indiana University, Indianapolis, IN
- Master of Science in Physical Education, a concentration in Exercise Science (2009)

  University of Indianapolis, Indianapolis, IN
- Bachelor of Science in Physical Education, a concentration in Exercise Science; graduated *Cum Laude (*2007)

RESEARCH EXPERIENCE

Indiana University, Indianapolis, IN   **August 2008-August 2015**
The School of Health and Rehabilitation Sciences, Center for Translational Musculoskeletal Research, Graduate Research Assistant (2010-present)
- Performed anthropometric measurements (e.g. tibia, ulna, and femur length, hip and waist circumferences, waist and hip width) , pQCT scans, DXA scans, and Biodex (shoulder strength) measurements
- Recruited subjects for some of the studies in this lab
- Performed animal mechanical loading, strain gauging, tissue sampling and bone imaging (e.g. *ex-vivo* μCT, *in-vivo* pQCT & histomorphometry)
- Conducted vertical jump and force platform measurements

  The School of Health, Physical Education, and Recreation, Study Coordinator, KAATSU Training Lab (2008-2012)
- Recruited subjects, performed initial subject screenings, conducted all the pre, during, post training assessments (e.g. anthropometric measurements and pQCT scans), and scheduled training times with subjects and trainers

  The School of Health, Physical Education, and Recreation, Fibromyalgia Research, Fitness Specialist (*2009-2010)*
- Coordinated a schedule with subjects to meet with them at their home 2-3 times a week
- Trained and counseled subjects on how to perform stretches, lower body resistance training exercises or lower body resistance training exercises on vibration platform correctly

University of Indianapolis, Indianapolis, IN   January 2007-May 2007
The Department of Kinesiology, Human Performance Laboratory, *Research Assistant (Internship)*
- Collected data on physiological responses to firefighting using the vivometrics lifeshirt
- Assessed clinical population and athletes on their health (e.g. blood pressure, ECG, body composition, and aerobic capacity)

TEACHING EXPERIENCE

Franklin College, Franklin, IN   August 2015-Present
Department of Kinesiology, Visiting Assistant Professor
- **Instructor,** EXE 372: Exercise Physiology: The study of acute and chronic adaptations of the body's physiological systems to physical activity. Physiological foundations and the development of physiological fitness components will be discussed. A laboratory component is integrated into class session.
- **Instructor,** BIO110: Human Anatomy and Physiology: Develops a comprehensive understanding of the close inter-relationship between anatomy and physiology as seen in the human organism. Introduces students to the cell, which is the basic structural and functional unit of all organisms, and covers tissues, integument, skeleton, muscular and respiratory systems as an integrated unit. Includes lab.

University of Indianapolis, Indianapolis, IN   August 2014-August 2015
Department of Kinesiology, Associate Adjunct Faculty
- **Instructor**, KINS 190: Philosophical Foundations of Kinesiology and Health
This class introduces students to the discipline of kinesiology and various fields related to the discipline.
- **Instructor**, KINS 350: Exercise Physiology Lab
Laboratory activities related to the study of physiological changes that occur with acute and chronic exercise. Integration of cardiorespiratory, muscular, and biochemical responses and training adaptations are emphasized.
- **Instructor**, KINS 375: Resistance Training Assessment and Programming
This class provides principles of progressive resistance training, the various modes, and its application in physical conditioning to the competitive athlete, the physical education teacher, and various special populations.
- **Instructor**, KINS 245: Principles and Practices of Exercise Science
The class provides overview of the fundamental concepts concerning biological and mechanical aspects of human movement. Furthermore, the purpose is to improve the students' understanding of the scientific research process.
- **Advisor**, Exercise Science majors

Indiana University, Indianapolis, IN   August 2007-May 2009
The School of Health, Physical Education, and Recreation, Graduate Teacher Assistant
- **Instructor**, HPER E121: Conditioning and Weight Training

This class provided the basic principles of conditioning and weight training with emphasis on muscular strength, muscular endurance, flexibility and cardiorespiratory endurance.

- **Teaching Assistant**, HPER P215: Exercise Science
  A study of the scientific principles related to physical fitness and the practical application of principles to directing fitness programming in school, recreational, and corporate settings. Students were actively setting up, participating in, and evaluating personal fitness activities.
- **Teaching Assistant**, HPER P409: Exercise Physiology
  A survey of human physiology parameters as related to physical exercise, work and the development of physiological fitness factors.
- **Teaching Assistant**, HPER P419: Fitness Testing and Interpretation Lab
  This class provided the knowledge base and practical experiences in fitness testing, assessment, and exercise programming.
- **Teaching Assistant**, HPER P443: Internship in Physical Education Lab
  The penultimate capstone activity for the refinement of knowledge, skills, and program development for exercise science students.

CLINICAL EXPERIENCE

The YMCA at the Athenaeum, Indianapolis, IN   **September 2010-Present**
Personal Trainer
- Provides appropriate ongoing goal setting session(s) for each client to discuss lifestyle modifications
- Develops and conducts individualized exercise prescriptions and fitness assessments for members

NIFS, Indianapolis, IN   **February 2009-July 2010**
Special Populations Coordinator /Health Fitness Specialist
- Oversaw the Lifestyle RX program that focused on exercise as medicine for people with chronic diseases
- Developed and conducted individualized exercise prescriptions and fitness assessments to meet the needs of the clients' medical condition(s)
- Performed aerobic capacity tests and body composition tests on clients (Bod Pod & skinfold calipers)
- Oversaw a silent auction to award 25 scholarships a year to members who are in need of financial assistance
- Provided ongoing lifestyle modification education for the members
- Taught group exercise classes that included; active stretch ,core, and high intensity training
- Assisted in a fibromyalgia research study by conducting 6 minute walk tests and counseling the subjects on proper progression of aerobic exercise

The YMCA at the Athenaeum, Indianapolis, IN   **April 2007-January 2009** *Wellness Coach/Personal Trainer*

- Provided appropriate ongoing goal setting session(s) for each client to discuss lifestyle modifications
- Developed and conducted individualized exercise prescriptions and fitness assessments for members

CERTIFICATIONS

- ACSM's Exercise Physiologist Certification (2009-present)
- American Heart Association's Heartsaver CPR certification (2007-present)

MEMBERSHIPS

- American College of Sports Medicine (2009-present)

SERVICE

University of Indianapolis, Indianapolis, IN   **October 30, 2014**
Department of Kinesiology Career Information Day
- Presented my career path to freshman kinesiology majors
- Provided health and fitness career advice to freshman kinesiology majors

PRESENTATIONS

- Fuchs RK, **Weatherholt AM**, Warden SJ. Progressive Skeletal Benefits of Exercise When Young: 2319 Board# 66 May 29 11:00 AM-12:30 PM. Medicine & Science in Sports & Exercise 2015; 47:5.
- **Weatherholt AM**, Warden SJ. Jumping Athletes as a Model for Exploring Lower Extremity Skeletal Benefits of Exercise: 1513 Board # 306 May 28 8:00 AM-9:30 AM. Medicine & Science in Sports & Exercise 2015; 47:5.
- **Weatherholt AM**, Warden SJ. Exploring the Skeletal Benefits of Exercise during Growth Using Overhand Throwing Athletes as a Model: February 5, 1:00 PM-3:00 PM. CSM 2015 Annual Conference
- **Weatherholt A**, Fuchs R, Warden S. Overhand Throwing Athletes as a Model for Exploring the Skeletal Benefits of Exercise during Growth: September 15, 12:30 PM-2:30 PM. ASBMR 2014 Annual Conference
- **Weatherholt AM**, Greer SA, Ruark DL, Grider BJ, Mock MJ, Beekley MD, Mikesky A. Effects of KAATSU Training on Upper Extremity Size and Strength: Board #42 April 13 9:00 AM -12:00 AM. IUPUI Research Day 2012 Finalist.
- Mock MJ, **Weatherholt AM**, Greer SA, Ruark DL, Grider BJ, Urtel M, Beekley MD, Mikesky A. KAATSU Training: Perceptions and Compliance to an Upper Arm Exercise Program: Board # 39 April 13 9:00 AM-12:00 PM. IUPUI Research Day 2012.

- **Weatherholt AM**, Warden SJ. Tibial Loading in Mice Induces Dose-Response Cortical Bone Adaptation: 1267: Board# 3 June 1 9: 30 AM-11: 00 AM. Medicine & Science in Sports & Exercise 2011; 43: 244-245.
- Presented at the 2011 Annual American College of Sports Medicine Conference for the KAATSU Special Interest Group, presentation titled: "KAATSU training: Subject Perceptions and Training Responses".
- Presented at the 2010 Annual American College of Sports Medicine Conference for the KAATSU Special Interest Group, presentation titled: "KAATSU training: Subject Perceptions and Training Responses".

PUBLICATIONS

1. **Weatherholt AM**, Avin KG, Hurd AL, et al. Peripheral Quantitative Computed Tomography Predicts Humeral Diaphysis Torsional Mechanical Properties With Good Short-Term Precision. Journal of Clinical Densitometry 2014.
2. **Weatherholt A**, Beekley M, Greer S, Urtel M, Mikesky A. Modified Kaatsu Training: Adaptations and Subject Perceptions. Med Sci Sports Exerc 2013; 45: 952-961.
3. **Weatherholt AM**, Fuchs RK, Warden SJ. Cortical and trabecular bone adaptation to incremental load magnitudes using the mouse tibial axial compression loading model. Bone 2013; 52: 372-9.
4. **Weatherholt AM**, Fuchs RK, Warden SJ. Specialized connective tissue: bone, the structural framework of the upper extremity. J Hand Ther 2012; 25: 123-31.